



Kent Academic Repository

Connolly, Sean (2021) *Development of novel Donor-Acceptor Stenhouse Adducts with Unique Structures and Interesting Photochromic Properties.* Master of Science by Research (MScRes) thesis, University of Kent,.

Downloaded from

<https://kar.kent.ac.uk/90838/> The University of Kent's Academic Repository KAR

The version of record is available from

<https://doi.org/10.22024/UniKent/01.02.90838>

This document version

UNSPECIFIED

DOI for this version

Licence for this version

CC BY (Attribution)

Additional information

Versions of research works

Versions of Record

If this version is the version of record, it is the same as the published version available on the publisher's web site. Cite as the published version.

Author Accepted Manuscripts

If this document is identified as the Author Accepted Manuscript it is the version after peer review but before type setting, copy editing or publisher branding. Cite as Surname, Initial. (Year) 'Title of article'. To be published in *Title of Journal*, Volume and issue numbers [peer-reviewed accepted version]. Available at: DOI or URL (Accessed: date).

Enquiries

If you have questions about this document contact ResearchSupport@kent.ac.uk. Please include the URL of the record in KAR. If you believe that your, or a third party's rights have been compromised through this document please see our [Take Down policy](https://www.kent.ac.uk/guides/kar-the-kent-academic-repository#policies) (available from <https://www.kent.ac.uk/guides/kar-the-kent-academic-repository#policies>).

Development of Novel Donor-Acceptor Stenhouse Adducts with Unique Structures and Interesting Photochromic Properties

Sean William Connolly

Masters by Research

School of Physical Sciences

University of Kent

University of
Kent

Abstract

Donor-Acceptor Stenhouse Adduct (DASA) photo-switches have generated a lot of interest since they were first reported; various areas of research have taken advantage of simple synthesis and the desirable photochromic properties in designing novel systems with interesting applications. The work presented here describes the design and synthesis of novel DASA molecules and an analysis of their photochromic properties. The new systems present a unique structure that causes changes in the conformation of the cyclized DASA form due to an unreacted amino functionality. In addition, the photo-switching properties do not suffer from the concentration limitations exhibited by previously reported DASAs. UV-Vis spectroscopy is used to analyse the photo-switching properties of the DASAs and illustrate impressive switching efficiency, exhibiting >95% loss of absorption upon irradiation. The structure-property relationship is examined through single crystal X-ray diffraction data and computational modelling which reveal changes in the proton transfer steps of the photo-switching mechanism that could to explain the improved switching properties observed. A first look into the solid-state photoswitching potential of DASA molecules is also investigated with preliminary results discussed.

Acknowledgments

I would like to thank my supervisor Helena J. Shepherd for all the help and guidance throughout the duration of the project. I would also like to thank Simon Holder for his assistance as my secondary supervisor and providing the resources for the computational studies. I would also like to extend thanks to Rahul Tiwari, and Matt A. Lambie for their helpful discussion during the synthetic and analytical processes involved, and Andrew Morell for his assistance running some of the chromatography and mass spectrometry experiments. To the entire Shepherd group and members of the SISC research team at the University of Kent the advice and support received has been greatly appreciated.

Table of Contents

Abstract.....	I
Acknowledgments.....	II
Table of Contents.....	III
List of Abbreviations.....	V
Chapter 1. Introduction.....	1
1.1 Molecular Photo-switches and Photochromism.....	1
1.2 Donor-Acceptor Stenhouse Adducts.....	3
1.2.1 Photo-switching Mechanism.....	5
1.2.2 Solvent Effects.....	9
1.2.3 Solid-State Behaviour.....	10
1.3 DASA-Polymer Conjugates.....	10
1.3.1 Doping of DASAs into Polymer Matrices.....	10
1.3.2 Chemical Modification of Polymers with DASA Functionality.....	11
1.4 Light Controlled Actuation.....	14
1.5 Project Aims.....	18
Chapter 2. Design and Synthesis of Bi-Functional DASA Molecules.....	19
2.1 Introduction.....	19
2.2 Experimental.....	20
2.2.1 General Methods.....	20
2.2.2 Instrumentation.....	22
2.3 Results and Discussion.....	23
2.3.1 Attempted Synthesis of 1.....	23
2.3.2 Attempted Synthesis of 2.....	26
2.3.3 Attempted Synthesis of 3.....	27
2.3.4 HPLC Separation of 3 and 9.....	28
2.3.5 Attempted Synthesis of 4.....	29
2.3.6 Synthesis and UV-Vis spectroscopy of 5.....	29
2.3.7 Synthesis and UV-Vis spectroscopy of 6.....	32
2.4 Conclusions.....	34
Chapter 3. Photochromic Properties of Novel DASA Structures.....	35
3.1 Introduction.....	35
3.2 Experimental.....	36
3.2.1 General Methods.....	36
3.2.2 Instrumentation and Methodology.....	37
3.3 Results and Discussion.....	39
3.3.1 Synthesis of 7.....	39
3.3.2 Synthesis of 8.....	40
3.3.3 Photo-switching Efficiency of 7 and 8.....	41
3.3.4 Photo-switching Efficiency of 5.....	41
3.3.5 Switching Fatigue of 5.....	43
3.3.6 Structure Determination of 5 by X-ray Diffraction.....	44
3.3.7 Photo-switching Efficiency of 6.....	45

3.3.8	Switching Fatigue of 6.....	46
3.3.9	Computational Studies.....	47
3.4	Comparisons.....	48
3.5	Conclusions.....	51
Chapter 4 – Solid-State Behaviour.....		53
4.1	Introduction.....	53
4.2	Experimental.....	53
4.3	Results and Discussion.....	54
4.3.1	Single Crystals.....	54
4.3.1.1	DCM Solvate.....	54
4.3.1.2	H ₂ O Solvate.....	55
4.3.1.3	Un-solvated Form.....	56
4.3.2	Powdered Samples.....	57
4.4	Conclusions.....	60
Experimental Chapter.....		61
5.1	Synthesis.....	61
5.2	UV-Vis Spectroscopy.....	63
5.3	Instrumentation.....	64
References.....		66
Appendix 1. ¹H NMR Spectra.....		71
Appendix 2. Single Crystal X-ray Diffraction Data.....		76
Appendix 3. UV-Vis Spectroscopy.....		80
Appendix 4. (Aza-)Piancatelli Rearrangement and Iso Nazarov Reaction.....		89

List of Abbreviations

Abs	Absorbance
Abs _{max}	Maximum Absorbance
Abs _{DEQ}	Absorbance at dark equilibrium
B-int	Barbituric acid - furfural intermediate
CHCl ₃	Chloroform
°C	Degrees celsius
Cu	Copper
d	Doublet (NMR)
dd	Double doublet (NMR)
DAE	Diarylethene
DASA	Donor-Acceptor Stenhouse Adduct
DCM	Dichloromethane
DFT	Density Functional Theory
DMSO	Dimethyl sulfoxide
FT-IR	Fourier transform Infrared
H	Proton
HPLC	High performance liquid chromatography
HTPB	Hydroxyl terminated poly-butadiene
IR	Infrared
K	Kelvin
K α	K-Alpha
K ₂ CO ₃	Potassium carbonate
LC-MS	Liquid chromatography-Mass pectroscopy
m	Multiplet (NMR)
M	Molarity (mol dm ⁻³)
min	minutes
M-Int	Meldrum's acid - furfural intermediate
MHz	Megahertz
mm	Milli-metre
mM	millimolar
N	Nitrogen
nm	Nano-metre
NMR	Nuclear magnetic resonance
PMA	Poly methacrylate
PMMA	Poly methyl methacrylate
PSS	Photo-stationary state
PXRD	Powder X-ray diffraction
PZ	Piperazine
s	Singlet (NMR)
t	Triplet (NMR)

TBP	4,4-trimethylene Bis-piperidine
T _g	Glass transition temperature
THF	Tetrahydro furan
UV	Ultra violet
UV-Vis	Ultra violet – visible
W	Watts
XRD	X-ray diffraction
Å	Angstrom
μL	Micro-litre
μm	Micro-metre
λ	Wavelength
%PSS	Percentage conversion at the PSS
%DEQ	Percentage uncyclized at dark equilibrium
Δ	Heat

Chapter 1 – Introduction

1.1 Molecular photo-switches and photochromism

Photochromism is described as a light induced reversible transformation of a chemical species between electronically or structurally different isomers, accompanied by a colour change.¹⁻³ As well as the two isomers of a photochromic species having different absorption spectra, there are a number of other physiochemical properties which may differ; such as the refractive index, dielectric constant/polarity or structure.³ Photochromism was first described in 1867 by Fritzsche upon noticing that an orange solution of tetracene would bleach under sunlight and recolour in darkness.⁴ Later in 1899, Marckwald described two solid compounds, β -tetrachloro- α -ketonaphthalene (Figure 1) and anhydrous quinoquinoline hydrochloride, which became coloured when exposed to light and decolourised in the dark.⁵ The term “phototrophy” was used to describe the process initially with photochromism being suggested in 1950 by Hirshberg.⁶ Photochromes which interconvert between two stable isomers using light energy have been further given the name “molecular photo-switches”.⁷

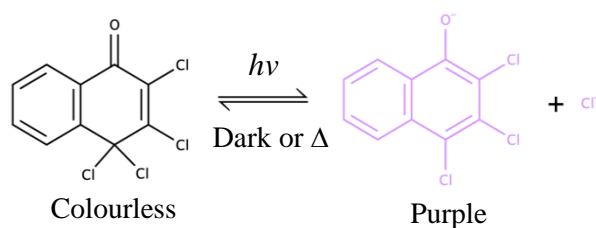


Figure 1. Photochemical reaction of β -tetrachloro- α -ketonaphthalene.

Photo-switches may be classified as either, P-type or T-type. For P-type photo-switches both the forward and backward reactions are photochemical transformations between thermodynamically stable isomers, whereas T-type switches are thermally reversible.^{1a} Another important descriptor of photochromes is whether they are traditional photochromes, that become coloured upon irradiation such as with β -tetrachloro- α -ketonaphthalene shown above, or negative photochromes which decolourise upon irradiation.^{1b}

Photochromism was not extensively explored until the mid 20th century as many of the earlier photochromes were quick to fatigue, meaning over time the molecules ability to convert between forms would gradually reduce until no or very little change was observed. Also, spectroscopic measurements were only then improving to the point where the species could be fully characterised.⁸ Development of fatigue-resistant compounds such as spirooxazines/spiropyrans (Figure 2) led to applications including photo-responsive ophthalmic

lenses in the 1980s.^{1,2} The leuco form of Spirooxazines/Spiropyrans is colourless and they photoisomerise to their coloured form via a C-O bond cleavage, seen in Figure 2a. Another fatigue-resistant class of photo-switches are the azobenzenes, which are thermally stable as the trans-isomer and upon irradiation with UV light undergo a trans-cis isomerisation to the cis-isomer, Figure 2b, after which the trans-form can be recovered in the dark.⁹ Azobenzenes have very attractive properties as photo-switches including high quantum yields, minimal photo-bleaching, a dramatic shape and a change in dipole.¹⁰ Furthermore, the picosecond timescale of the isomerisation¹¹ and the thermodynamically stable trans-isomer being present >99.9% at equilibrium in the dark at room temperature,¹² and their ease of synthesis make them some of the most widely studied photochromic molecules.

Stilbenes are another photochromic species with photochemistry similar to azobenzenes,¹³

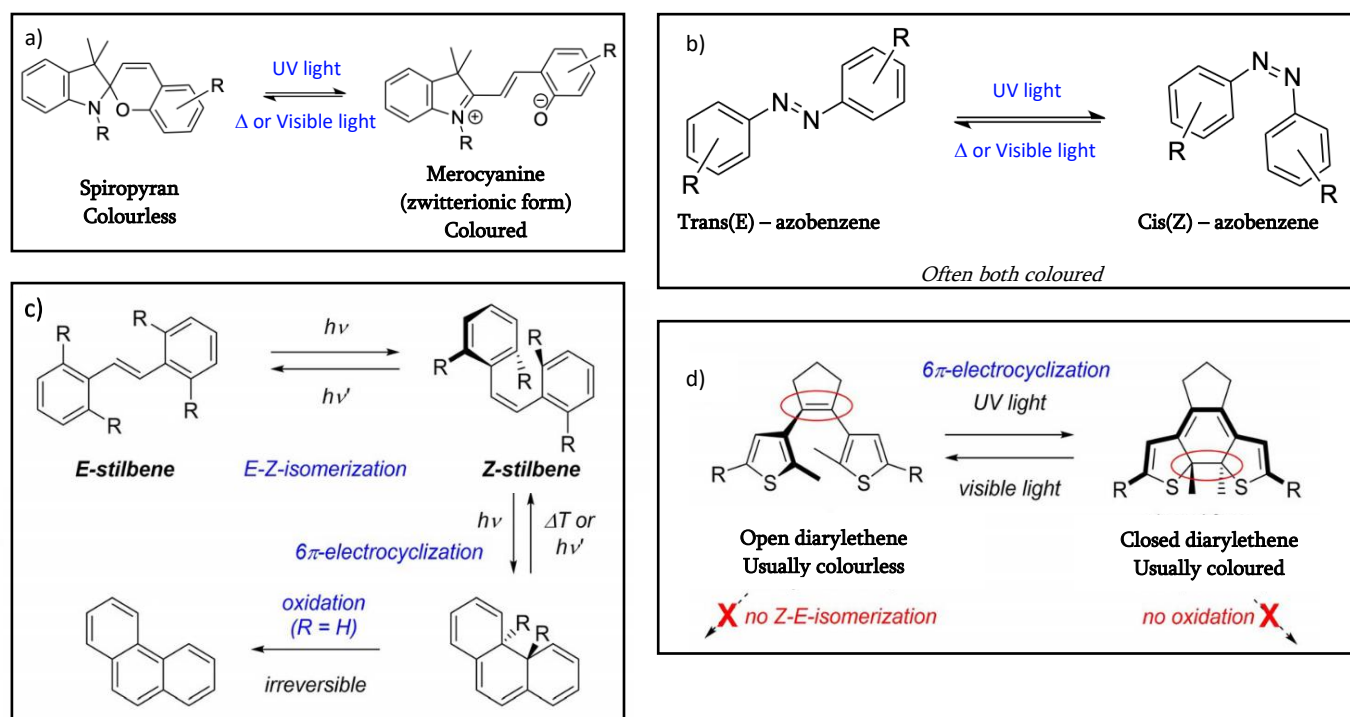


Figure 2. a) Thermally reversible photoisomerisation reaction of spiropyrans which gives the coloured merocyanine form. b) Thermally reversible trans-cis photoisomerisation reaction of azobenzenes. c) Photoisomerisation reaction of stilbenes followed by the often observed cyclization and irreversible oxidation. d). Photoisomerisation reaction of diarylethenes, where both isomers are thermally stable and no oxidation occurs. Adapted with permission from ref. 13. Copyright © 2019, Wiley.

however they can undergo a cyclization and subsequent irreversible oxidation (dehydrogenation) reaction in the presence of air, Figure 2c, eliminating their photo-switching capability.¹⁴ Replacement of the phenyl rings of stilbene with thiophene rings, first introduced by Kellogg¹⁵ in 1967 and further explored in 1999¹⁴ led to the development of the class of photo-switches known as diarylethenes (DAEs). DAEs perform a thermally irreversible photo-isomerisation unlike the spiro- and azobenzene photo-switches, making them P-type photo-switches, therefore the reverse

process is initiated with a second wavelength of light. The photoinduced 6π -electrocyclization and cycloreversion reactions occur due to UV and visible light irradiation respectively, shown in Figure 2d. A variety of other classes of photochromic molecules have been studied; indigoids,³⁷ acylhydrazones,^{17,18} fulgides,^{19,20} all exhibit some form of photochromism.

1.2 Donor-Acceptor Stenhouse Adducts

Donor-acceptor Stenhouse adducts (DASAs) are a new class of molecular photo-switch, first described by the Read de Alaniz research group in 2014.²¹ The acceptor group consists of a heterocyclic carbon acid, initially Barbituric or Meldrum's acid, shown in Figure 3. After activation through a ring opening reaction with furfural (Figure 3a), the activated furfural intermediate compound is formed. Then the donor, any nucleophilic secondary amine is added to the intermediate leading to the formation of DASAs.²²

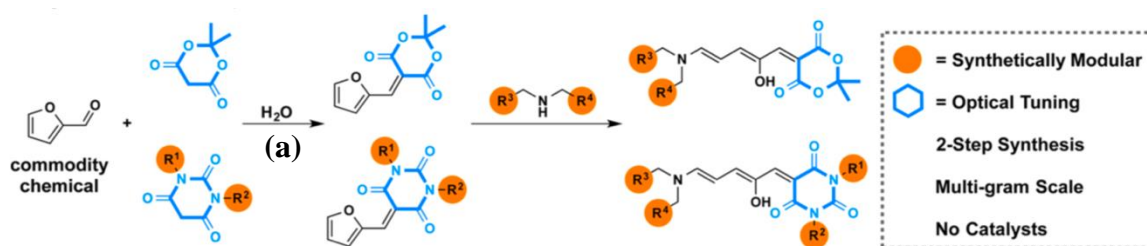


Figure 3. Schematic displaying simple and modular synthesis of DASAs, adapted with permission from ref. 22. Copyright © 2014, American Chemical Society.

DASAs express T-type negative photochromism and undergo photo-switching upon irradiation with visible light. Furthermore, DASAs undergo a notable change in polarity as they isomerise, from a hydrophobic elongated conformation where the donor and acceptor are connected via a triene moiety (**X**), into a hydrophilic compact molecule where the triene becomes a cyclopentanone (**Y**). This isomerisation is also clearly visible in solution as a change from coloured to colourless as expected with negative photochromes, seen in Figure 4 in addition to a typical absorption spectrum observed of DASA molecules. The absorption band in the 500 – 600 nm region is due to the absorption from the conjugation within the triene moiety, when photoisomerisation occurs and the conjugation is lost, the absorption decreases. These characteristics open the possibility for a variety of applications for DASAs in chemistry, engineering and biomedicine. Simple, fast and modular preparation,²² (Figure 3), has aided in many applications already being explored, including drug delivery,²³ chemosensing²⁴ and temperature sensing.^{24,25}

The first generation of DASAs^{21,22} are defined as those prepared using alkyl secondary amines. First generation DASAs exhibit the largest change in polarity due to the coloured or “open”

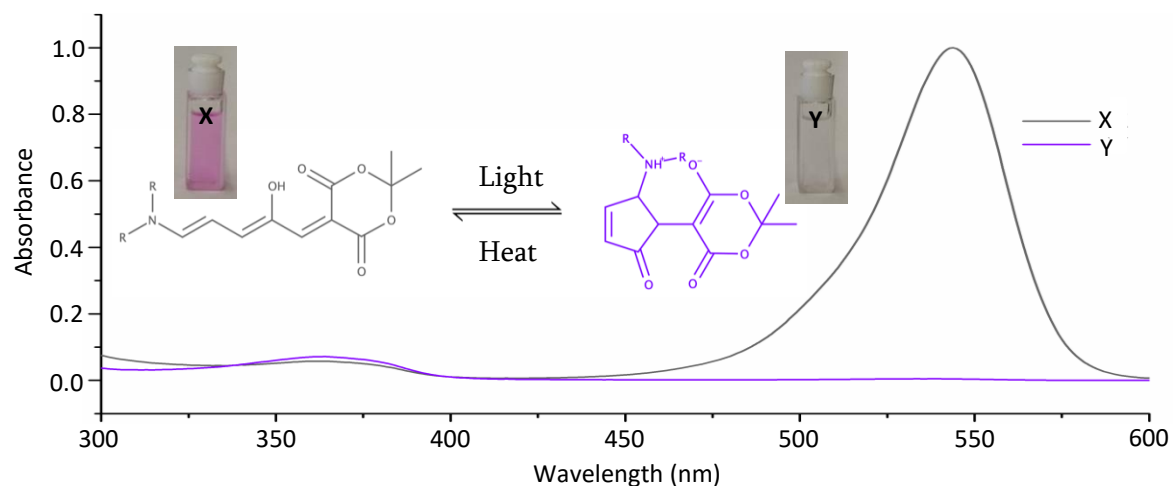


Figure 4. Typical absorption spectra for DASAs, reaction scheme for photoisomerisation, and colour change of 1st gen DASAs.

form existing as a neutral molecule while the colourless or “cyclized” form is a zwitterion, shown in Figure 4, this also results in a change in the hydrophobic/hydrophilic nature of the molecules. While this characteristic has been shown to give impressive possibilities for application,²⁶⁻²⁸ it also means that the photo-switching is irreversible in polar solvents such as methanol²³ and water^{23,29}. In contrast, the process is reversible in some non-polar and aromatic solvents for some first generation DASAs, depending on the amine used in synthesis, see section on solvent effects for more detail.

A second generation of DASAs were later introduced in 2016,^{30,31} employing the use of aniline based donors. The use of the cyclic donors causes both the open and cyclized isomers to be neutral molecules, no longer forming a zwitterion in the cyclized state. The aniline based donors also caused a bathochromic shift in the absorption of the DASAs, allowing for near infrared activation which is advantageous regarding biomedical application. The shift in absorption has been

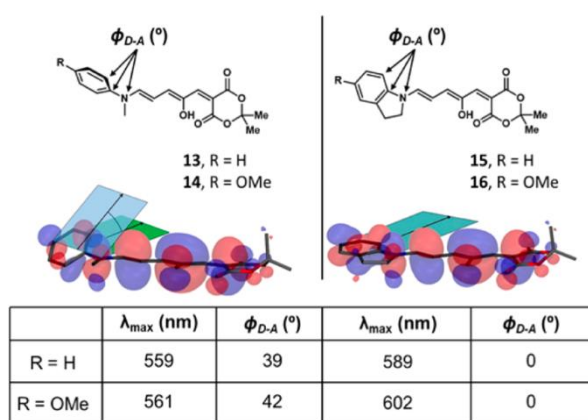


Figure 5. DFT models showing the effect of aniline based donors, and enhanced effect with electron donating substituents and cyclic amines, adapted with permission from ref. 30. Copyright© 2016, American Chemical Society.

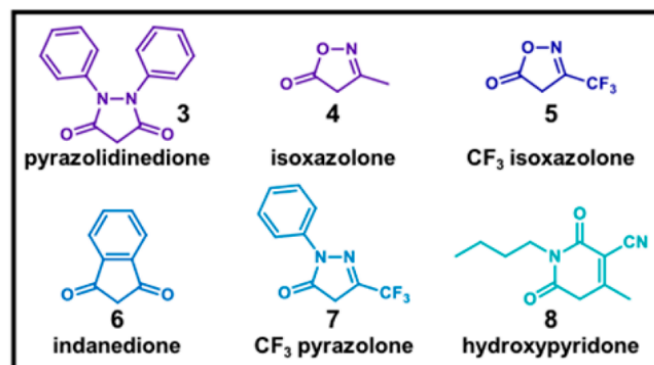


Figure 6. New carbon acid acceptor molecules reprinted with permission from ref. 32. Copyright© 2018, American Chemical Society.

attributed to homoconjugation between the donor and acceptor groups. This bathochromic shift can be extended further through the use of indoline based donors, and even more so with electron donating substituents. DFT calculations show how the planar nature of the indoline donors enforce planarity between the aromatic moieties and the triene, enhancing the conjugation,³⁰ shown in Figure 5. The second generation DASAs also display improved reversibility in solution when compared to the first generation, even in some polar solvents such as acetonitrile.³¹

Most recently in 2018 a third generation of DASAs were introduced,³² where a new set of the carbon acid acceptor groups were identified, shown in Figure 6. These materials showed improvements in the efficiency, reversibility, thermal equilibrium and a further bathochromic shift in absorbance, adding an extra level of tunability to the DASA family of photo-switches.

1.2.1 Photo-switching mechanism

Knowledge of the photoisomerization mechanism of a set of photochromic species is vital in understanding how the molecules will behave in different environments, whether it be in solution, as a solid, or contained within in polymer matrix. The first review of DASAs³³ from Feringa and co-workers highlights some of the initial work^{29,34-36} on understanding the isomerisation process and the intermediate compounds observed. However, these efforts only described fully the initial photo-induced step, with less detail of the cyclization steps. Only recently has the full pathway been analysed in-depth revealing the true complexity of the system.³⁷

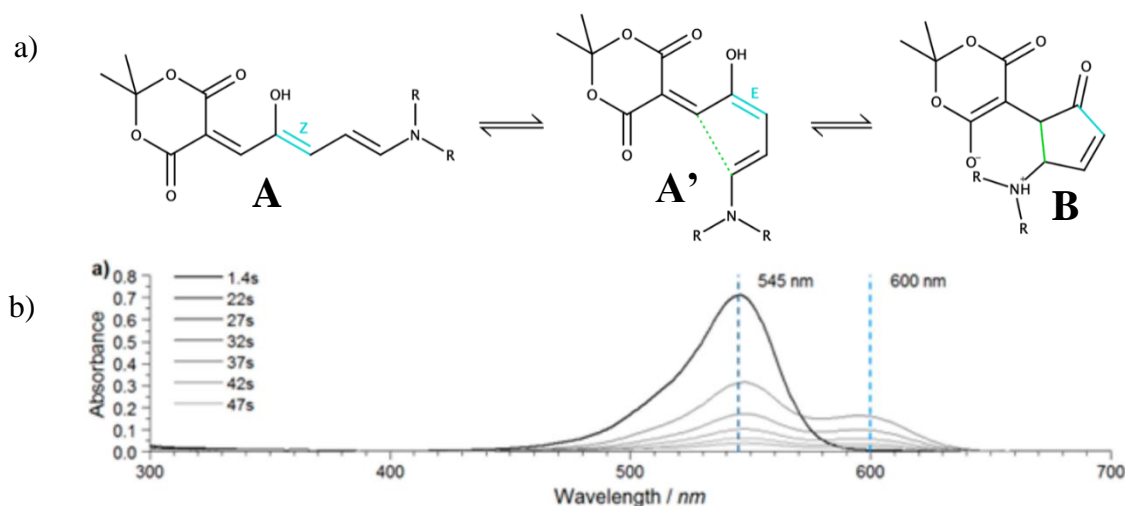


Figure 7. a) Initially suggested isomerisation pathway for DASAs. b) Absorption spectra of diethyl amine/Meldrum's acid DASA illustrating the loss in absorbance with irradiation, reprinted with permission from ref. 29. Copyright © 2016, American Chemical Society.

Although the open and cyclized conformations were known from X-ray crystallography data published in 2014,^{21,22} first attempts to properly define the pathway between these were not

suggested until 2016.²⁹ Through considering possible reaction mechanisms with analogy to the (Aza) Piancatelli rearrangement³⁸ and the iso-Nazarov reaction³⁹ (see appendix 4) the light induced Z – E isomerisation around the C₂ – C₃ bond, followed by a thermally allowed 4 π -electrocyclization was determined, shown in Figure 7a, and the focus was on isolating and characterising the intermediate **A'**.²⁹

UV/Vis spectroscopy revealed that with irradiation the absorption band at 545 nm would begin to diminish and a “transient band” in the absorption spectrum at 600 nm would appear and then begin to disappear as irradiation continued, Figures 7b, 8a. Lowering the temperature to 253 K removed the pathway for the cyclization and resulted in the stabilisation of the absorbance at 600 nm, shown in Figure 8b. It was concluded that this data supported the existence of **A'** and that its formation was due to the initial Z – E isomerisation caused by irradiation from visible light.²⁹

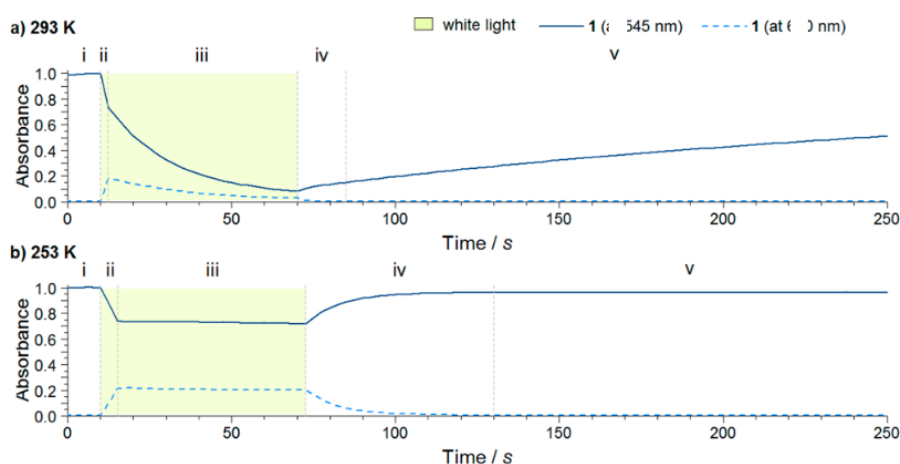


Figure 8. Graphs displaying the time dependent changes in absorbance of bands corresponding to **A** (545 nm) and **A'** (600 nm) and 293 (a) and 253 K (b). reprinted with permission from ref. 29. Copyright© 2016, American Chemical Society.

Later work in 2017, using time resolved UV/Vis and IR spectroscopy added another intermediate between **A** and **A'** to the mechanism as it was noted that the Z – E isomerisation alone would not facilitate the formation of the intermediate **A'**, which is needed for a successful cyclization to **B**.³⁴ It was confirmed that the molecule found to be accumulating at lower

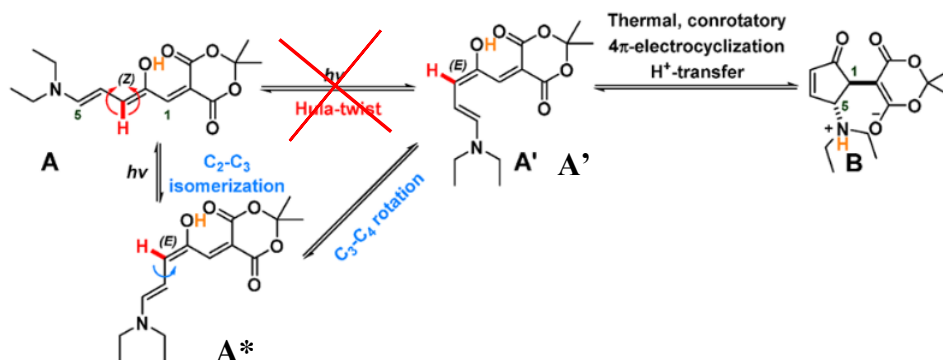


Figure 9. Second isomerisation pathway suggested. Reprinted with permission from ref. 34. Copyright© 2017, American Chemical Society.

temperatures was the intermediate **A*** and so an additional bond rotation was added to the thermally driven steps of the mechanism as shown in Figure 9.

In contrast a more recent gas phase study from 2018 using a “charge-tagged” DASA, shown in Figure 10, and tandem ion mobility mass spectroscopy coupled with laser excitation⁴⁰ found evidence that the second step, from **A*** to **A'**, could also be photoinduced. The results showed that

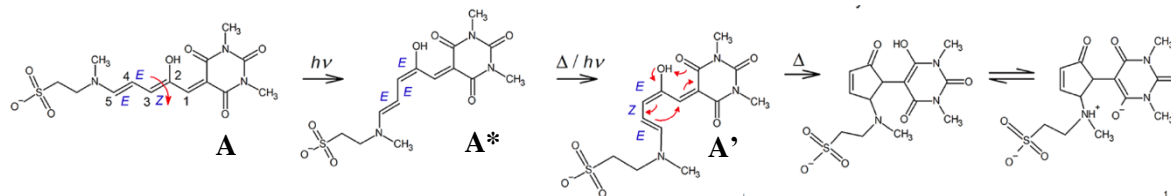


Figure 10. Suggested isomerisation mechanism for a charge tagged DASA in the gas phase. Reprinted with permission from ref. 40. Copyright © 2018, American Chemical Society.

after formation of intermediate **A*** a second photon is absorbed, causing further isomerisation that leads to the 4π -electrocyclization. This may only be the case in the gas phase as it is in disagreement with previous work suggesting that only the initial step is photo-induced. They state that this could be down to the intrinsic differences of the different DASA molecules studied and the fundamental differences between solution and gas phase. Interactions between the solvent and the potential energy surfaces of the excited species may limit a “one-way photocyclization reaction” even though the results of the gas phase study suggested this is possible.⁴⁰

The importance of the hydroxyl group was investigated and confirmed later in 2018.³⁵ Using a combination of in-situ ¹H NMR, time resolved spectroscopy and DFT calculations to analyse a DASA and an analogue lacking the hydroxyl group; it was shown that the intramolecular hydrogen

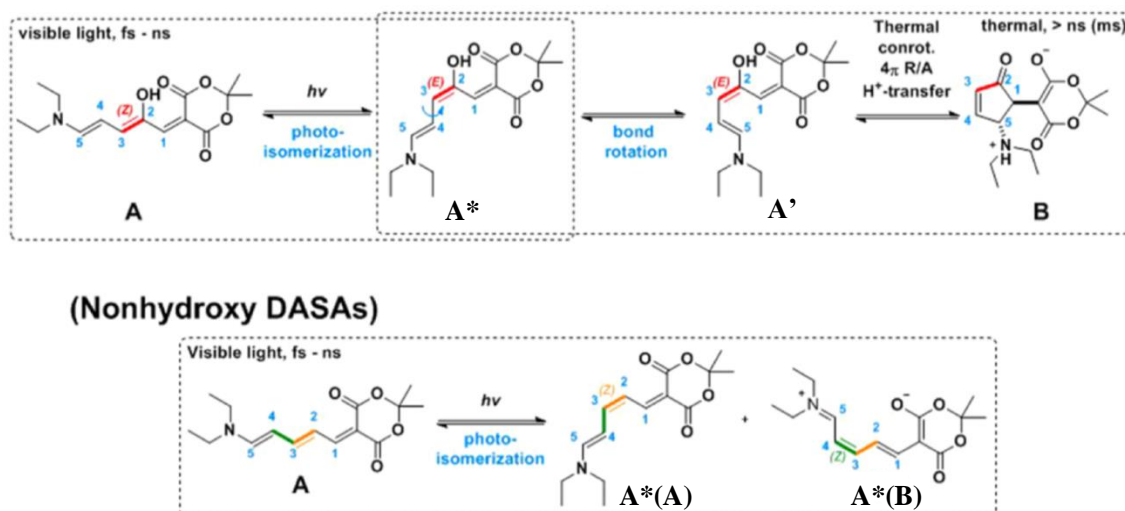


Figure 11. Comparison of mechanisms of DASA and analogue lacking the hydroxyl group. Adapted with permission from ref. 35. Copyright © 2018, American Chemical Society.

bonding interaction between the carbonyl moiety of the acceptor and the hydroxyl is vital in

ensuring the thermal cyclization occurs. The interaction ensures that intermediate **A*** is obtained instead of a mixture of **A*(A)** and **A*(B)**, shown in Figure 11.

The hydroxyl group appears to “pre-select” the C₂ – C₃ bond for the initial photo-isomerization, likely due to the elongation and decrease in electron density of that specific bond.³⁵ This would weaken the bond raising its energy and making excitation here the most energetically favourable. **A*(A)** and **A*(B)** were also found to accumulate in photo-accumulation experiments. Furthermore, the hydroxyl group plays a second vital role in polarizing the triene, which allows the cyclization to occur between C₁ and C₅.³⁵ It does this through a proton transfer to the carbonyl group as shown in Figure 12.

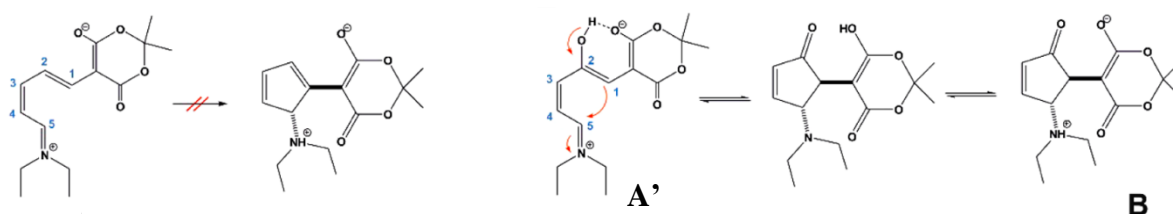


Figure 12. Schematic displaying polarisation and proton transfer mediated via hydroxyl group and lack of phenomenon in the hydroxyl lacking analogue. Adapted with permission from ref. 35. Copyright© 2018, American Chemical Society.

Since the publication of the review paper,³³ a more complete understanding of the thermally driven part of the mechanism has been reported. Rapid-scan FT-IR spectroscopy was used in combination with kinetic modelling and quantum chemical calculations to obtain an idea of the true complexity of the switching pathway³⁷. All possible thermal interconversions were considered, shown in Figure 13. Notably the EZZ isomer was found to be consistently formed in the mechanism for second generation DASAs, unlike the first generation where the EZZ isomer is not formed. The importance of the thermally driven stages was outlined, showing that even though

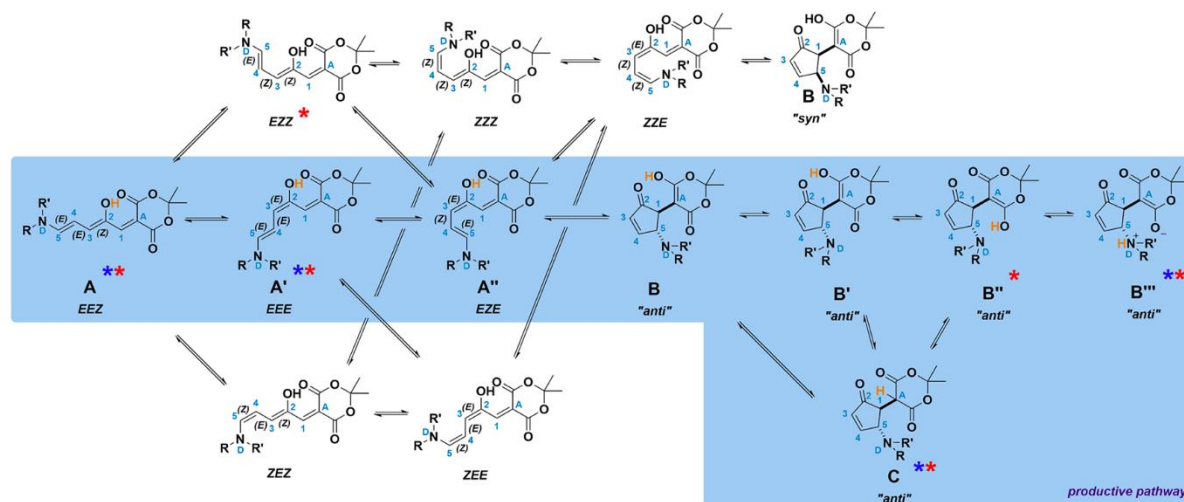


Figure 13. All possible intermediates possible through thermal interconversions for DASA molecules. Reprinted with permission from ref. 37. Copyright© 2019, American Chemical Society.

the initial photo-induced step is crucial in beginning the process the overall behaviour is thermally controlled. Moreover, the thermally allowed steps are rate-limiting and essential for the cyclization and proton transfer, proving very important in understanding and manipulating DASA photo-switching.³⁷

1.2.2 Solvent Effects

Solvent effects are of important consideration for DASAs as the photo-switching properties including switching rate, reversibility and where the thermodynamic equilibrium between the open and cyclized forms sits are solvent dependent. The first generation DASAs in particular show highly solvent dependent properties.^{21,22} In polar solvents such as methanol and water irreversible photo-bleaching to the cyclized isomer is observed both in the presence and exclusion of light whereas in chlorinated solvents insignificant photoisomerisation occurred.²² This is due to the structural changes the molecules undergo during photoisomerisation forming a zwitterion in the colourless, cyclized form. Aromatic solvents such as benzene and toluene were found to be the most appropriate for complete reversible switching.^{21,22} The rate of switching has also been shown to be solvent dependent; in toluene rapid photoisomerisation was recorded while other solvents the process is much slower.^{29,36} Second generation DASAs also experience solvent dependent switching rates,³⁶ although do not suffer as much in terms of reversibility as both the open and cyclized forms are neutral molecules. Dissimilar to the first generation where the formation of the zwitterion is commented on as the primary reason for the considerable solvent effects.^{22,41}

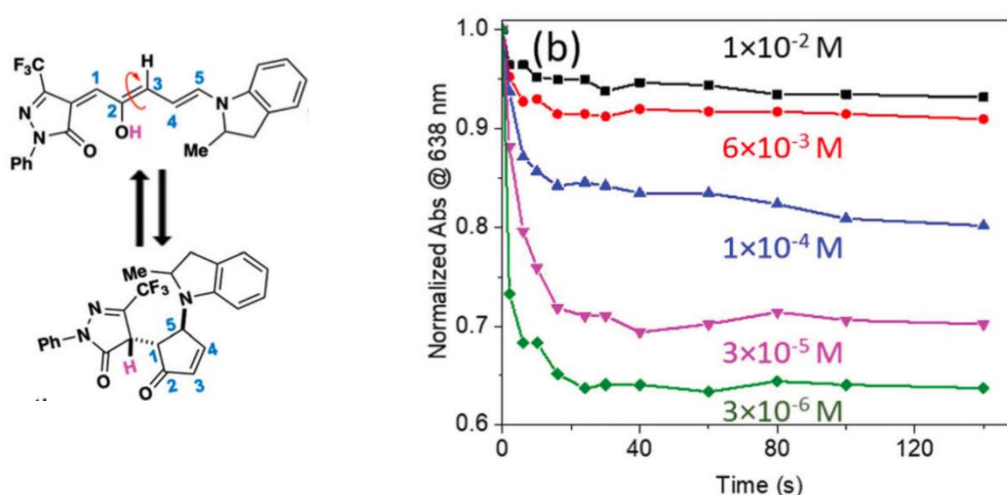


Figure 14. a) Schematic of the photoisomerisation of a third generation DASA used to study the concentration dependence. b) UV-Vis spectroscopy data showing the decrease in absorbance over time at a range of concentrations for the DASA shown in the figure. Reproduced from ref. 42. with permission from The Royal Society of Chemistry

Another effect seen involving the solvent is the “unusual concentration dependence” of the photo-switching properties of DASAs. A recent report highlights the concentration dependent behaviour showing that as photochrome concentration increases the extent of photo-switching decreases, as shown by Figure 14. Although the report only included data for the third generation DASA shown, in the concluding remarks the phenomenon was described as a general effect, shared by various DASA derivatives in range of solvents and solid environments.⁴² Later we present data on the exploration of the effect of specific amines on the reported concentration dependent nature.

1.2.3 Solid-state behaviour

As previously noted, crystal structures were characterised and published in the initial work on the 1st generation of DASAs, a variety of structures with different donors and acceptors having been crystallised.^{21,22,31} To date, no evidence for solid-state photo switching has been reported. Over a 2 year period of observations no solid-state photochromism was recorded²² and neat films have shown no changes in colour to indicate any switching.^{31,42} This is unlike other photochromes, some of which do exhibit solid-state switching.⁴³⁻⁴⁵ DASAs dispersed in polymer matrices have been shown to keep their some of their photo-switching properties, which will be explored later. There is also an example of adsorption of DASAs onto the surfaces of nanoparticles followed by irreversible switching in suspension.⁴⁶

1.3 DASA-Polymer Composites

1.3.1 Doping of DASAs into Polymer Matrices

The early work done to help understand the fundamentals of DASA photo-switching quickly led to some very interesting DASA-polymer composite materials, this continues to be the case with frequent additions to the literature.^{25,30,47-50} The review from Feringa and co-workers³³ features several efforts where DASAs and polymers have been combined with impressive success.^{25,30,47-50} Early evidence of DASAs switching ability within polymer matrixes was described in 2016 by Read de Alaniz and co-workers, where two second-generation DASAs were simply suspended in polymethyl methacrylate (PMMA) films³⁰ and wavelength selective reversible photo-switching was displayed in drop cast films, shown in Figure 15.

Given the thermal reversibility of DASAs, temperature mapping has also been investigated using a DASA with a dioctyl amine donor, that was homogeneously embedded within a hydroxyl-terminated polybutadiene elastomer (HTPB).²⁵ The resultant material allowed for

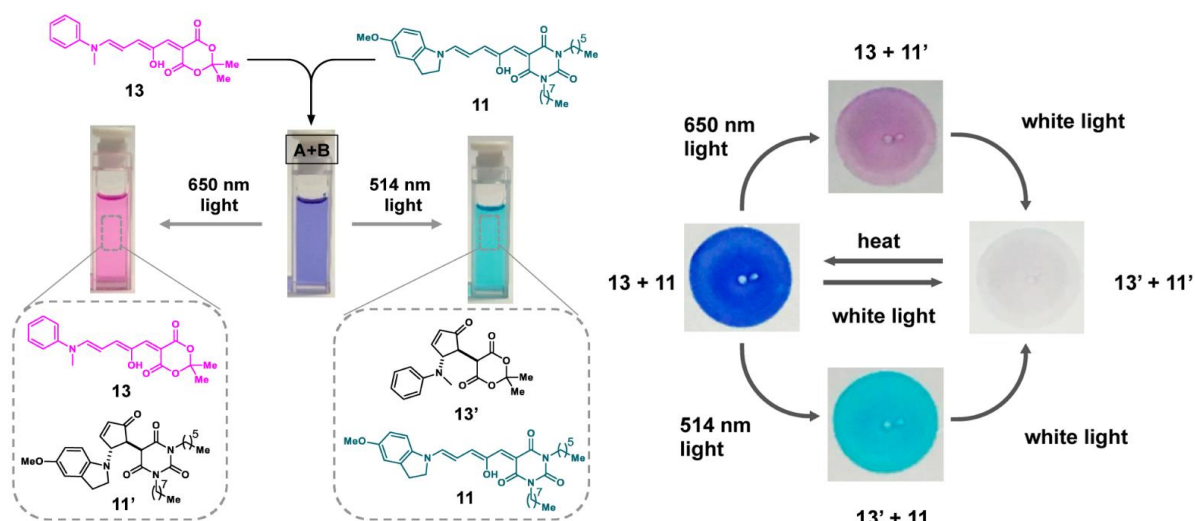


Figure 15. Wavelength selective reversible photo-switching of PMMA films containing two DASA compounds. Adapted with permission from ref. 30. Copyright© 2016, American Chemical Society.

reversible switching of the embedded DASAs, shown in Figure 16(a), and recolouration was temperature dependant. The sensitivity of the recolouration to temperature enabled highly accurate local temperature mapping within the elastomer. While visibly identifiable, near-field scanning optical microscopy allowed for temperature changes from ballistic entries into the material to be mapped at a high resolution, shown in Figure 16(b).

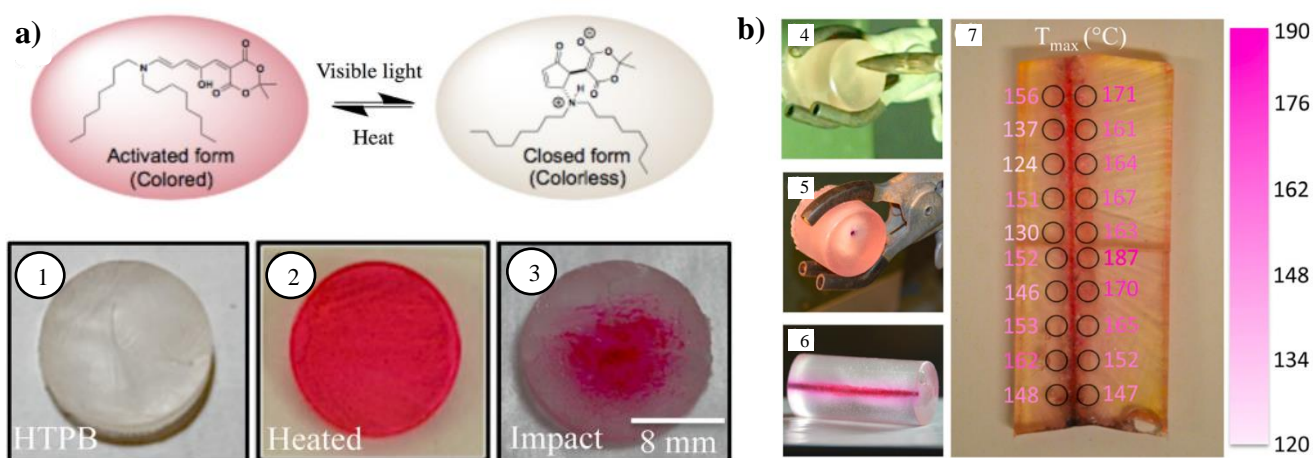


Figure 16. Showing temperature mapping of HTPB elastomer embedded with DASA. a) DASA species used. 1) irradiated sample 2) heated sample 3) Colour change from impact. b) Temperature mapping after ballistic impact. 4) Before impact. 5/6) After penetration with bullet 7) Accurate temperature mapping of cut segment. Adapted with permission from ref. 25. Copyright© 2016, Applied Physics Letters.

1.3.2 Chemical Modification of Polymers with DASA Functionality

In addition to doping of DASA molecules into polymer matrices, DASAs have also been covalently attached to polymers as side-chains or “pendants” on the polymer back bone.⁴⁸ In 2017 Read de Alaniz and co-workers presented work functionalising a variety of polymers, polymethacrylate (PMA), poly-ethyl methacrylate (PEMA), poly-propyl methacrylate (PPMA), and

poly-butyl methacrylate (PBMA), with DASAs as pendants. Cyclic and non-cyclic amines were first added to the polymer backbones followed by reactions with an excess of the furfural intermediates yielding a library of DASA-polymer conjugates. Thin films of polymers with first generation DASA pendants switched irreversibly whereas the second-generation variants showed reversible switching, displayed in Figure 17.

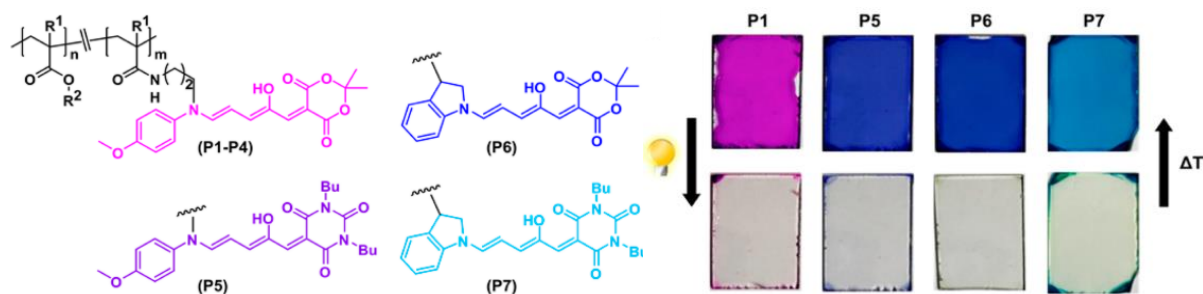


Figure 17. Structures of DASA-polymer conjugates and spin-coated thin films prior to and post irradiation with visible light. Adapted with permission from ref. 48. Copyright® 2017, American Chemical Society.

The glass transition temperature (T_g) was also shown to have an effect on photo-switching. Testing the reversibility of the switching of thin films showed that the T_g has a dramatic effect on the thermal reversion. Above the T_g films would return to the coloured state but not below, suggesting the glassy state “traps” the colourless cyclized form, inhibiting thermal isomerisation back to the coloured form,⁴⁸ shown in Figure 18. This information is vital for the design of future DASA-polymer conjugates in order to maintain reversible switching.

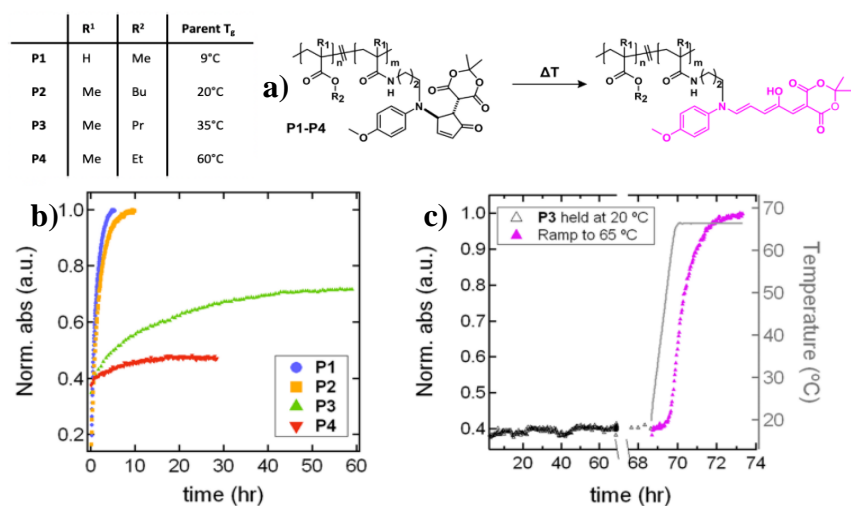


Figure 18. a) Diagram displaying structure and photo-switching of P1-P4. b) Thermal reversion of P1-P4 at 40°C. c) Heating through T_g (20°C) for P3 showing increase in absorbance upon heating. Adapted with permission from ref. 48. Copyright® 2017, American Chemical Society.

Photo-patterning of a polymer surface was also explored quickly after DASAs emerged, through an amino-functionalised polycarbonate foil which was further functionalised with DASA by addition of the Meldrum’s acid furfural intermediate forming surface bound DASAs.⁴⁹ Using a mask and visible light irradiation, highly accurate photopatterning of the surface was achieved, shown in

Figure 19, the highlighted simplicity of the process makes DASAs a facile option for polymer surface photopatterning.

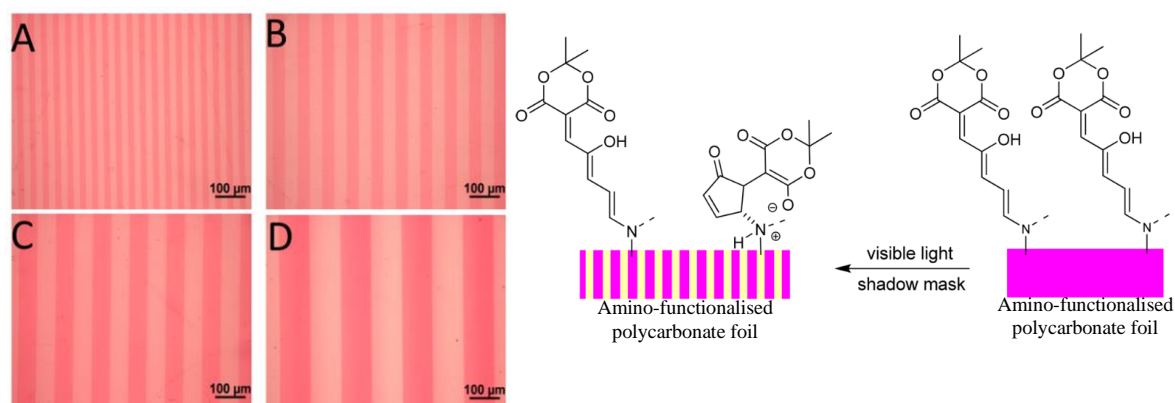


Figure 19. Irreversible visible light photopatterning of amino-functionalised polycarbonate through bound DASAs. (A-D) Show high level of accuracy attainable. Adapted with permission from ref. 49. Copyright © 2015, American Chemical Society.

A recent addition to the literature takes a different approach to functionalising a polymer with DASAs directly onto the backbone. Instead of reacting the furfural intermediates with an amino-functionalised polymer, monomers containing the activated furfural intermediate were created and used to synthesise co-polymers, which when exposed to amines would form DASA moieties as side chains.²⁴ Whilst giving the opportunity for a large variety of DASA-polymer conjugates to be made by simply varying the amine used, the copolymers also serve as excellent chemo-sensors for amines, shown in Figure 20a,b,c. This is also the first example of DASAs being used for amine sensing in an aqueous environment. In the same work they presented colourless

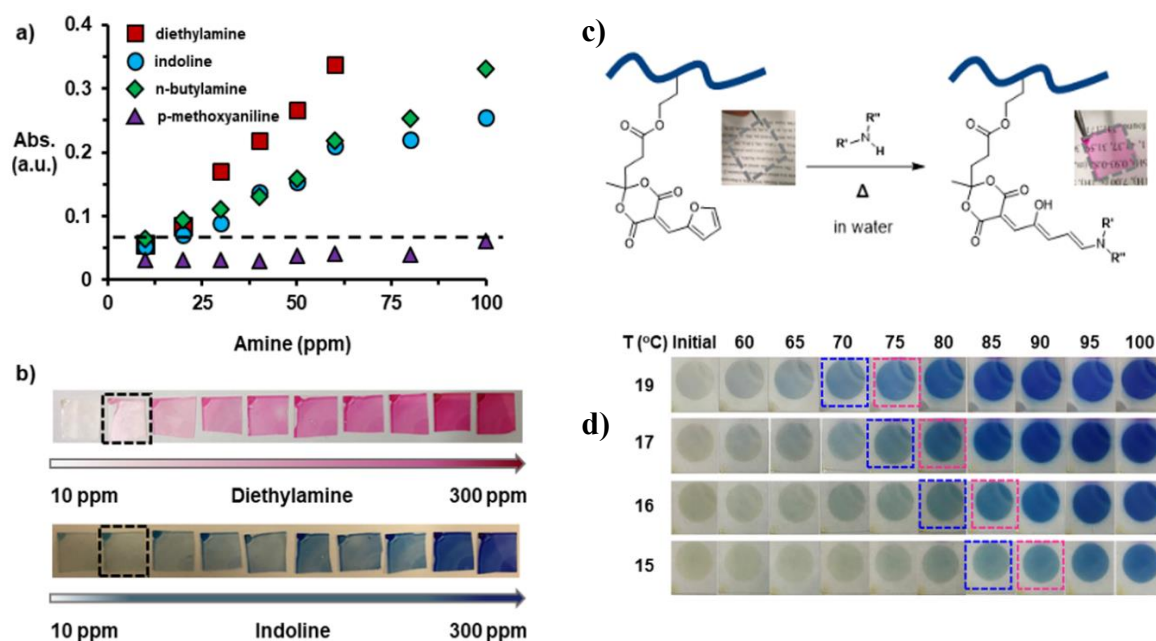


Figure 20. a) UV/Vis absorbance data at λ_{max} for polymer films exposed to aqueous amine solution at 75 °C. b) images of films post exposure to aqueous solutions. Dotted lines indicate limit of detection. c) General reaction for detection of amines/ DASA-polymer conjugate formation. d) Images displaying films exposure different temperatures. Adapted with permission from ref. 24. Copyright © 2019, American Chemical Society.

films, which were found to be stable at 0 °C for a month, and could also be used as highly accurate temperature sensors with differences ≥ 5 °C being visible to the naked eye, displayed in Figure 20d.

DASA-Polymer conjugates have also entered the area of nano-materials, in the form of polymersome “nano-reactors”.²⁸ Block co-polymers functionalised with DASAs formed polymersome membranes, which were impenetrable by small molecules unless irradiated with visible light. Once loaded with enzymes, the polymersomes acted as “nano-reactors” allowing for reactions to occur within and for products to be released, selectively under illumination, Figure 21. Not only does this have impressive potential in nano-scale reaction control, but also in pharmaceuticals for accurate and controlled drug delivery. Other work involving nanoparticles include light induced changes in the wettability of a surface taking advantage of the change in polarity and hydrophobic to hydrophilic nature of DASAs.^{26,27}

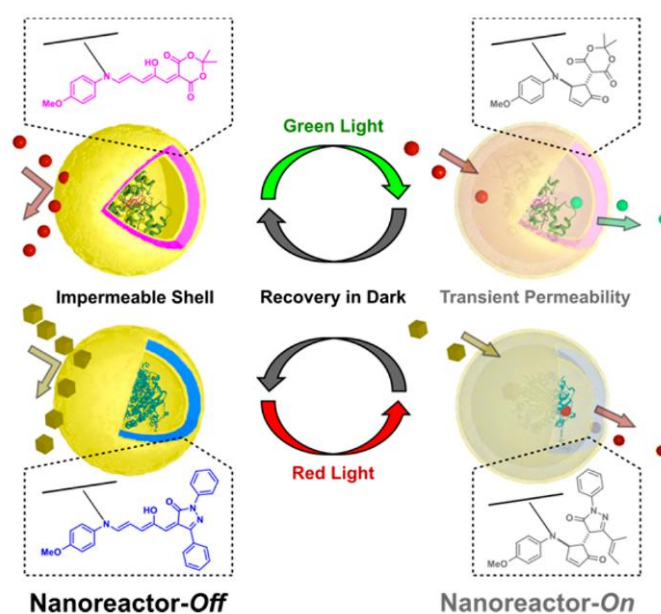


Figure 21. Two different DASA functionalised polymersome nano-reactors. Visible light irradiation opens the membrane for access to the encapsulated enzymes for reactions to take place. Reprinted with permission from ref. 28. Copyright © 2018, American Chemical Society.

1.4 Light controlled actuation

In addition to colour changes, the changes in molecular structure that some photochromes exhibit, such as the notable change to DASAs structure upon photo-switching, is a property that can be exploited for application. One example is displayed above with the nano-reactors where the structural change induces a change in the polymersome structure allowing molecules to enter. Another possible application is in the area of soft-robotics, where materials capable of actuation like motion are highly sought after, the molecular scale structural change can be used to generate

strain within a material leading to a macroscopic scale motion. Such materials could replace heavy mechanical parts with lightweight, flexible and cheap parts. Furthermore, the need for electronically powered components can be eliminated by using photochromes which respond to light as stimuli, light is also easily produced and controlled whilst having little effect on the system illuminated. Molecular photo-switches have already shown great potential in achieving light controlled motion, a number of examples can be found in the literature illustrating this.^{53-59, 62-64} Some of the work to date incorporates a few of the photochromes mentioned in section 1.1. Other materials which have shown some success in this area are hydrogels,^{51,52} and liquid crystal based polymer materials.⁵³⁻⁵⁶ Azobenzenes have been used a number of times to generate light activated motion in flexible polymer materials.⁵³⁻⁵⁹ For example liquid crystal monomers with azobenzene cores were used to generate films which acted as belts on a motor signifying the first plastic motor driven by light⁵⁷, shown in Figure 22. Azobenzene-based Crosslinked Liquid Crystal Polymers

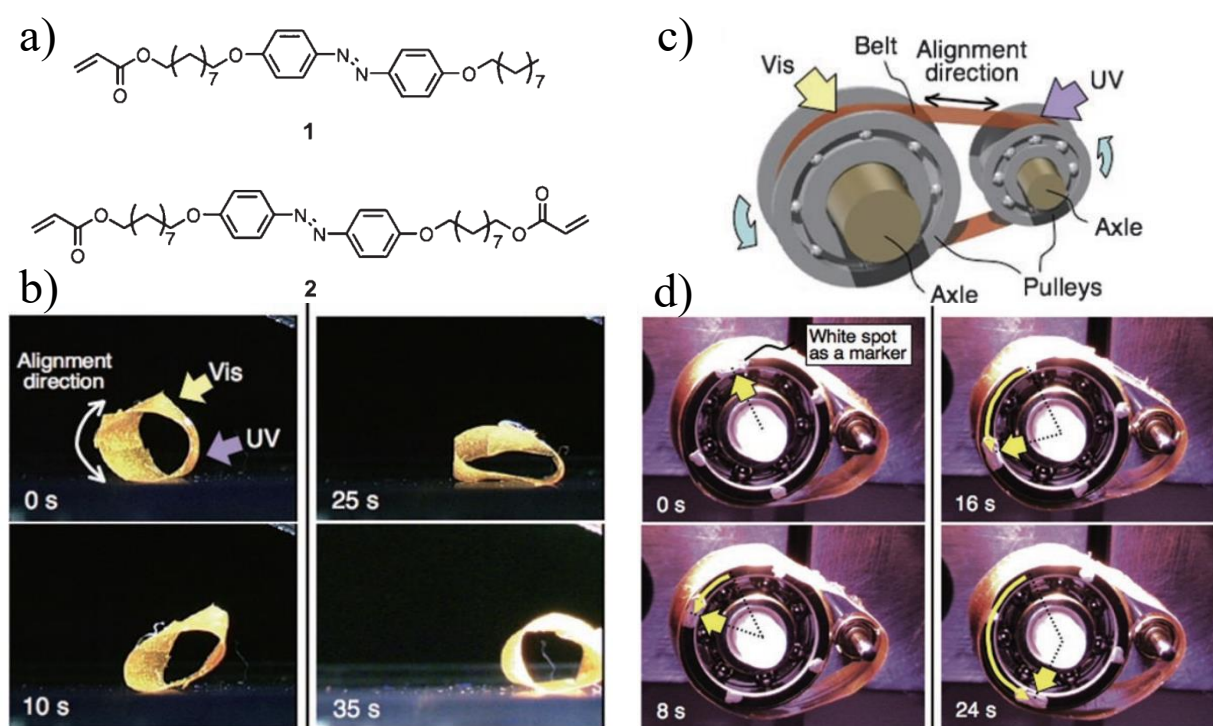


Figure 22. a) Chemical structures of the Azobenzene liquid crystal monomer (1) and diacrylate (2) used for the films. b) Series of images displaying the rolling motion of the film induced by Vis and UV light. c) Schematic for the design of the plastic light driven motor. d) Images of the motor working rotation. Reprinted with permission from ref. 57. Copyright© 2008, Wiley.

(CLCPs) have shown to be capable of light controlled actuation with a number of successes being published to date.^{60,61} Most notably an azobenzene together with a liquid crystal monomer and crosslinker were used to make thin films which when illuminated presented motion akin to a Venus fly-trap,⁵³ described as an “artificial fly-trap” shown in Figure 23.

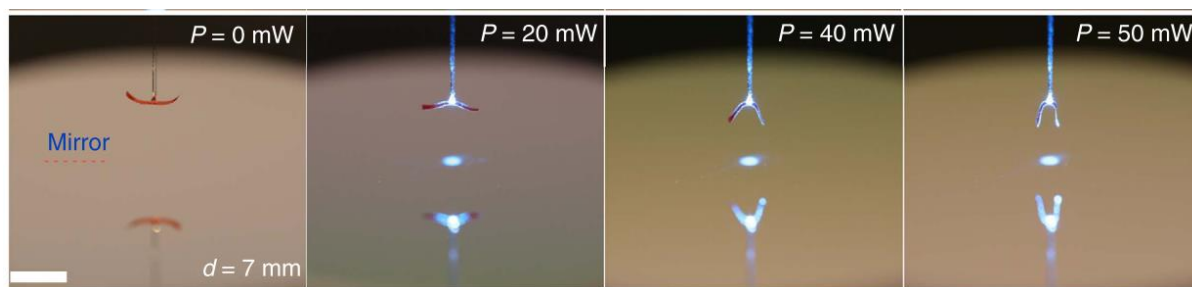


Figure 23. Series of images showing the Venus fly-trap like motion of a CLCP thin film containing 2 mol % of an azobenzene with increasing light intensity. Reprinted with permissions from ref 53. Open access, Springer Nature.

Although much of the work on light controlled actuating polymers involves azobenzene photo-switches other photochromes have been used in similar ways. Thin films consisting of poly methyl methacrylate (PMMA) doped with a spiroxazine were shown to change the radius of the curve of the films surface with UV- irradiation.⁶² Hydrazones have also shown potential in the area, liquid crystal polymer hosts doped with specially designed hydrazones exhibited large deformations and reversible shape changes when UV light was applied⁶³ as shown in Figure 24. Figure 24 also displays how the direction of the bend was dependent on the wavelength of light used to irradiate the samples.

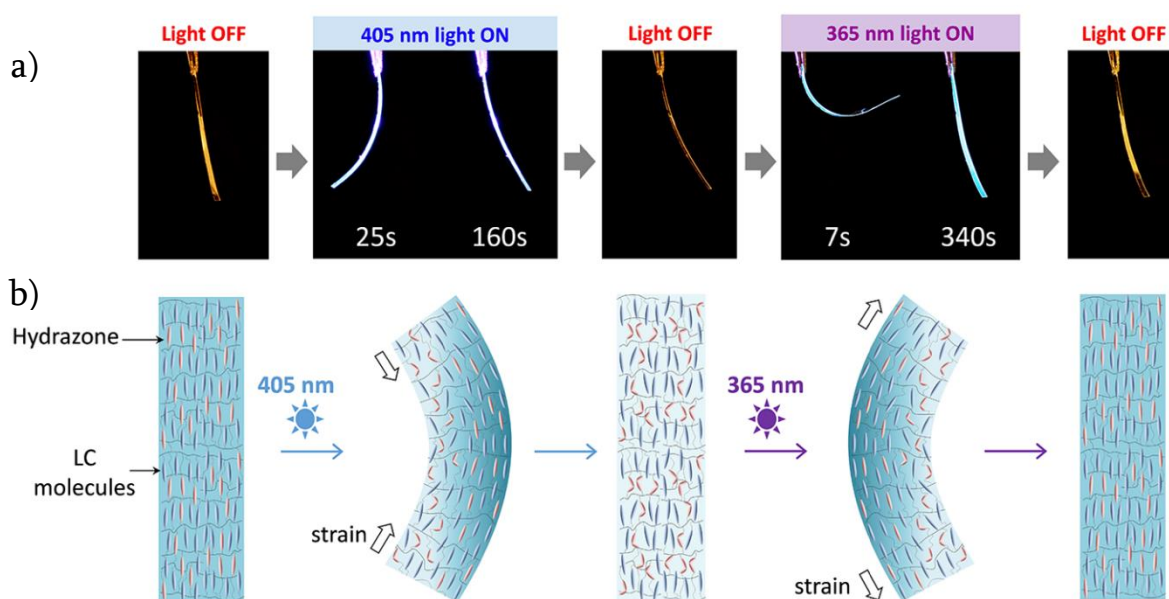


Figure 24. a) Photo-induced actuation of polymer films doped with designed hydrazones. c) Representation of the structure and shape change. Reprinted with permission from ref. 63. Copyright© 2004, Society of Photo-Optical Instrumentation Engineers

Light controlled actuation is also not exclusive to non-crystalline materials, some single crystals have also performed reversible motion caused by photochemical reactions. Single crystals of diarylethenes can bend upon irradiation even bearing more than their own mass, as shown in Figure 25. This motion has been explained through the accumulation of cyclization reactions of the

molecules within the lattice resulting in an anisotropic expansion (volume change) at the site of irradiation resulting in a bend away from the light source.⁶⁴

Smart materials with light controlled actuation properties could advance areas including specialist medical equipment, drug delivery, soft robotics and engineering with the promise of precise motion control of lightweight flexible materials through the use of light. Currently the motion of the majority of such materials is triggered by UV light instead of visible, and in the case of hydrogels they almost exclusively work submerged in water. UV activation is more difficult and more expensive to produce than visible light, and is also damaging to biological material,³³ eliminating the possibility for UV controlled actuators in biomedical applications.

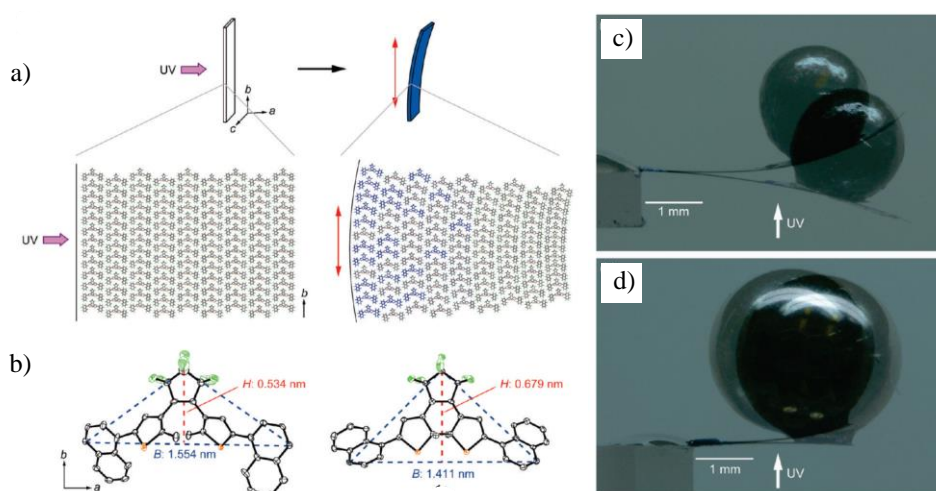


Figure 25. a) Schematic diagram showing of the photo-induced bending, where blue molecules represent cyclised molecules within the crystal. b) ORTEP drawings of the uncyclized and cyclised molecules. c) UV induced motion of single crystal carrying a 2 mm lead ball, 46.77 mg. d) UV induced motion of single crystal carrying a 3 mm steel ball, 110.45 mg. Adapted with permission from ref. 64. Copyright © 2010, American Chemical Society.

Work in the Shepherd group focuses on designing and optimising switchable molecular materials for use in smart technologies. This includes the use of DASAs to produce actuating materials that respond to visible light.

DASAs are controlled by visible light and heat and have been shown to perform in aqueous, non-aqueous/organic, and solvent-less environments, whilst also being negative photochromes, eliminating any issues associated with light penetration into the interior of a material. The simple tuneability through fast and modular synthesis of DASA molecules further increases the potential for application in areas including soft robotics and biomedicine.

Previous work in the Shepherd group has involved incorporating DASA molecules into polymers through doping, and covalent attachment to the polymer back bone.⁶⁵ Investigations involving doping DASAs into both polystyrene and PDMS revealed that there appears to be a maximum concentration of doped DASA of c.a. 1wt%, beyond which point no photoisomerisation

is observed. Higher concentrations are an inactive, due to self-association of DASA molecules into crystallites within the polymer matrix. This poor loading is problematic for application in actuation as high strain is required to generate motion, necessitating a high loading of the active component. As such doping was abandoned as a strategy for incorporation of DASAs into polymer composites for actuating applications.

Similarly, with covalently bonded DASA-polymer conjugates there appears to be a relationship between concentration and photo-switching efficiency. Covalently attaching DASAs to a copolymer backbone consisting of polymethacrylate and piperazine functionalised polystyrene based monomers saw a decrease in the ability to photoisomerise as concentrations of DASA onto the backbone increased, this was found both in solution and in the solid-state.⁶⁵

1.5 Project Aims

The aims of this work are to investigate the fundamental aspects of proximity and concentration of DASA moieties, and their effect on the efficiency of photoisomerisation. The proximity of DASA moieties will be investigated through attempting to synthesise bi-functional symmetric DASA molecules. Such molecules could be the basis for DASA-polymer conjugates where the DASAs act as cross-linking units.

The clear relationship between concentration and the efficiency of DASA photo-switching is examined through analysis of mono-substituted analogues of the bi-functional DiDASAs, which are compared to published DASA structures investigating the effect of concentration. Any unusual photochemical properties are investigated for novel synthesised materials and compared with known systems. Finally, preliminary results on the possible solid-state photo-switching of DASAs are investigated.

Chapter 2

2.1 Introduction

Polymers doped with DASA molecules so far have only been reported to contain low percentages of DASAs, at higher concentrations they form crystallites which do not photoisomerise.⁶⁵ The concentrations at which this occurs are too low to generate enough strain within the material to cause any actuation. Polymers synthesised with covalently attached DASA pendants have also not displayed any actuator properties to date, and exhibit similar concentration limitations. One route with potential to overcome this would be to design polymers with DASA molecules included in the back bone, or for DASA moieties to act as crosslinking units. As previously noted, a recent publication investigated the unusual concentration dependence of DASA molecules, highlighting that in both solid and liquid media there is a clear inhibition of the photo-switching as the photochrome concentration increases.¹⁶ It was suggested that proximity of DASAs causing a disruption to the cyclization steps were the cause of the phenomenon, through long-range Coulombic interactions that may interfere with the thermally allowed electrocyclization stages of the isomerisation, mentioned in section 1.2.1.

In order to investigate the effect of the proximity of the DASA functionality on photo-switching ability, a series of symmetrical bifunctionalised molecules were designed. As shown in Figure 26 four molecules were designed, with either the Meldrum's acid or

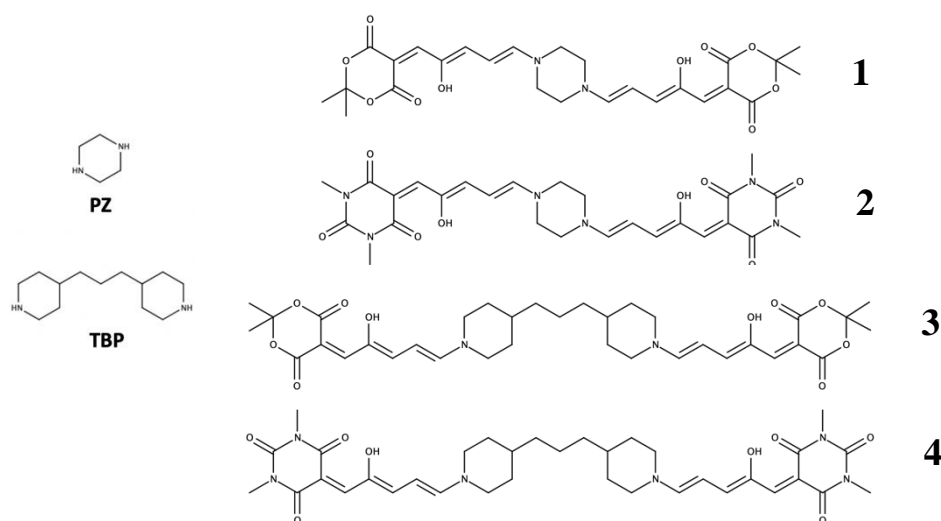


Figure 26. Structures of **PZ** and **TBP** in addition to the molecules designed to investigate the effect of DASA-DASA proximity on photo-switching properties.

Barbituric acid as the acceptor molecules. The separation between the switching units was also varied through the use of structurally similar di-amines for the donor moiety, piperazine (**PZ**) and 4,4'-Trimethylenebispiperdine (**TBP**). The difference in the N-N distance on either donor was designed to probe how the proximity of the switching moieties affects the photo-switching properties. Furthermore, these structures also serve as preliminary tests as to whether similar symmetrical bifunctional DASA could be used as effective cross-linking units.

In the original design and synthesis of DASA molecules⁶⁶ by S. Helmy, similar bi-functional structures were presented, employing both di-amines and bi-functional acceptor structures. S. Helmy reported that the bi-functional Meldrum's acid groups were too rigid and impeded complete switching and the barbituric variants warranted further investigation. The di-amines derivatives were presented without any characterisation and a only brief mention of the photo-switching properties commenting on whether complete photo-switching was observed. It was concluded that the di-amines with more conformational freedom allowed for complete switching whereas the more rigid structures did not, but no more information was given.

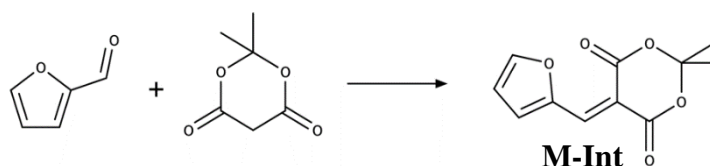
2.2 Experimental

2.2.1 General methods. Unless stated otherwise all reactions were performed in oven dried glassware in an atmosphere of air using reagent or analytical grade solvents. All reagents obtained from commercial suppliers were used as received. Reaction temperatures were controlled through automated heating plates with oil or aluminium bead baths, and unless explicitly stated reaction were performed at room temperature (approximately 23 °C). Vacuum drying was done using either a Büchner set up or vacuum oven.

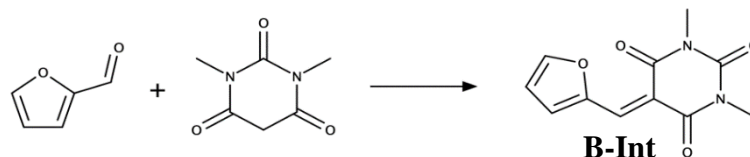
Procedure A. Furfural activated intermediate (1 equiv) was dissolved in minimal THF, to this solution the amine (0.5 equiv) dissolved in minimal THF was added. The reaction mixture was stirred at room temperature for no less than 2 h, followed by cooling to <0 °C for 20 min by placing in the freezer. The mixture was then filtered and the resultant solid was washed with ether to remove any excess reagents and further dried under vacuum.

Procedure B. Piperazine (0.298 mmol, 0.0258 g) and **M-Int** (1 mmol, 0.222 g) were dissolved in a solution of THF (4 mL) and methanol (1 mL). Added to this was a solution of K_2CO_3 (0.003 mmol, 0.0042 g) in water (0.3 mL), methanol (0.5 mL), and THF (0.1 mL). The mixture was left to stir at room temperature (23 °C) for 20 h, followed by cooling to <0 °C for 20 min by placing in the freezer. The mixture was then filtered and the resultant solid was washed with ether to remove any excess reagents and further dried under vacuum.

Furfural activated Intermediates



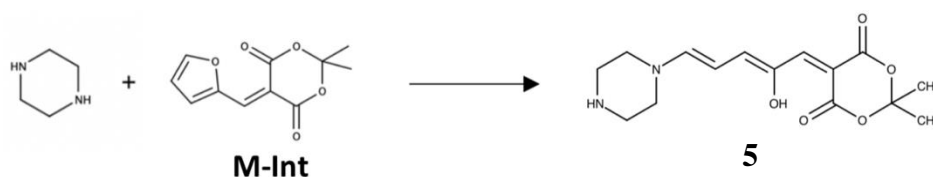
5-[(furan-2-yl)methylidene]-2,2-dimethyl-1,3-dioxane-4,6-dione (M-Int). M-Int was prepared according to the literature procedure². 2,2-Dimethyl-1,3-dioxane-4,6-dione (10 mmol, 1.44 g) and furfural (10 mmol, 0.961 g) were mixed in water (30 mL) followed by heating to 75 °C and stirring for 2 hours. The solid obtained was filtered, vacuum dried and dissolved in dichloromethane (30 mL) followed by washing sequentially with saturated $NaHSO_3$ (30 mL), water (30 mL), $NaHCO_3$ (30 mL), and brine solution (30 mL). The organic layer was then dried over $MgSO_4$, filtered, and the solvent removed via rotary evaporation.



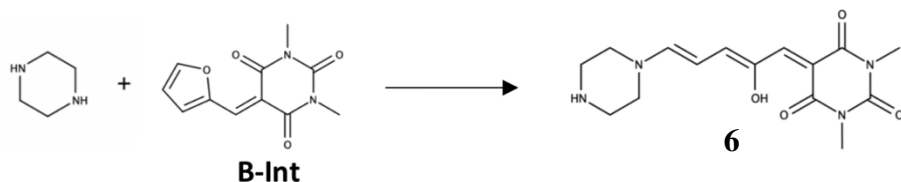
5-[(cyclopenta-1,3-dien-1-yl)methylidene]-1,3-dimethyl-1,3-diazinane-2,4,6-trione (B-Int). 1,3-Dimethylbarbituric acid (10 mmol 1.56 g) and furfural (10 mmol, 0.961 g) were mixed in water (40 mL) and stirred for 12 hours at room temperature. The solid obtained was filtered, vacuum dried and dissolved in dichloromethane (60 mL) followed by washing sequentially with saturated $NaHSO_3$ (30 mL), water (30 mL), $NaHCO_3$ (30 mL), and brine solution (30 mL). The organic layer was then dried over $MgSO_4$, filtered, and the solvent removed via rotary evaporation.

Compounds 1, 2, 3, 4. The attempted synthesis of **1**, **2**, **3**, and **4** all followed procedure A. Reaction temperatures, durations and reagent ratios were varied across multiple reactions, the details of which will be discussed in the results and discussion.

Compounds 5 and 6



5-[(2Z,4E)-2-hydroxy-5-(piperazin-1-yl)penta-2,4-dien-1-ylidene]-2,2-dimethyl-1,3-dioxane-4,6- (5). Meldrum's acid intermediate **M-int** (0.555 g, 2.497 mmol) was dissolved in THF (5 mL). To this solution piperazine (0.189 g, 2.194 mmol) dissolved in THF (5 mL) was added. The reaction mixture was stirred for 2 h, followed by cooling to 0 °C for 20 min. The mixture was filtered and the resultant solid was washed with diethyl ether and further dried under vacuum yielding a dark purple powder (0.583 g, 86%).



5-[(2Z,4E)-2-hydroxy-5-(piperazin-1-yl)penta-2,4-dien-1-ylidene]-1,3-dimethyl-1,3-diazinane-2,4,6-trione (6). Barbituric acid intermediate **B-int** (0.234 g, 1.0 mmol) was dissolved in THF (15 mL). To this solution piperazine (0.069 g, 0.801 mmol) dissolved in THF (5 mL) was added. The reaction mixture was stirred at room temperature (23 °C) for 17 h, followed by cooling to 0 °C for 20 min. The mixture was filtered and the resultant solid was washed with diethyl ether and further dried under vacuum yielding a purple powder (0.078 g, 25%).

2.2.2 Instrumentation

High performance liquid chromatography (HPLC)

HPLC was performed using an Agilent technology 1260 Infinity HPLC. Reverse phase HPLC was run using a gradient eluent starting at 98% water and 2% methanol (0.1% NH₃) ramping up to 50% methanol. Temperature was controlled at 23 °C and flow rate of 4 mL/min was maintained. 50 µL injections were injected from a 3.6 mg/mL solution. An Agilent 5 Prep-C₁₈, 50 x 10 mm column was used.

¹H NMR spectroscopy

¹H NMR spectra was recorded using a 600 MHz five channel Bruker Avance III. Unless stated otherwise spectra were recorded at room temperature (approximately 20 °C).

Liquid Chromatography - Mass spectroscopy (LC-MS)

LC-MS was performed using the Thermo Scientific Dionex UltiMate 3000 HPLC and Thermo MSQ Plus Quadrupole Mass Spectrometer. Reverse phase HPLC was run using an isocratic eluent of 50% H₂O and 50% methanol (0.1% NH₃). The column used was a Thermo Acclaim RSLC 120 C₁₈, 3 μm, 3.0 x 75 mm. Negative ion electrospray ionisation was used for the mass spectroscopy.

UV-Vis absorption spectroscopy

The UV-Vis absorption spectra were recorded using a Shimadzu UV-1800 spectrometer. Each spectrum recorded was over a range of 400 – 650 nm. The samples were irradiated from all directions using a 50 W, 650 K, full spectrum LED flood light, illuminating a container lined with reflective mylar sheeting, room temperature was maintained by allowing a current of air to flow through the container. Samples were continuously irradiated in between each measurement and sequential measurements of the UV-Vis absorbance were taken until no notable changes in the spectra were observed, at which point the thermal reversion was recorded through the same procedure, heating samples in a dark oven at 50 °C. In-situ irradiation of samples was not possible due to the apparatus available, as the illumination would interfere with the incident beams and detector of the spectrometer. Therefore samples were quickly moved from the illumination container to the spectrometer to take measurements and placed back inside once the measurement was finished, the scan rate of the spectrometer was increased to the max in order to limit the time samples were left unirradiated. Similarly, when performing the thermal reversion measurements samples were moved between the oven and spectrometer, wrapped in foil to avoid light contamination while transporting.

2.3 Results and Discussion

2.3.1 Attempted Synthesis of Compound 1. The synthesis of **1** was attempted following procedure **A**. Upon addition of the piperazine (**PZ**) the solution became bright pink followed by darkening to a deep purple over time. This distinct colour change indicated the formation of a **DASA**. The resultant product was a previously unreported mono-substituted piperazine **DASA (5)** as identified by the ¹H NMR spectrum shown in Figure 27. Analysis of the spectrum determined that only mono-substitution onto the piperazine had occurred, indicated by the peaks at 2.7 and 3.08 ppm, which correspond with the hydrogen environments around the **PZ** ring, in addition the

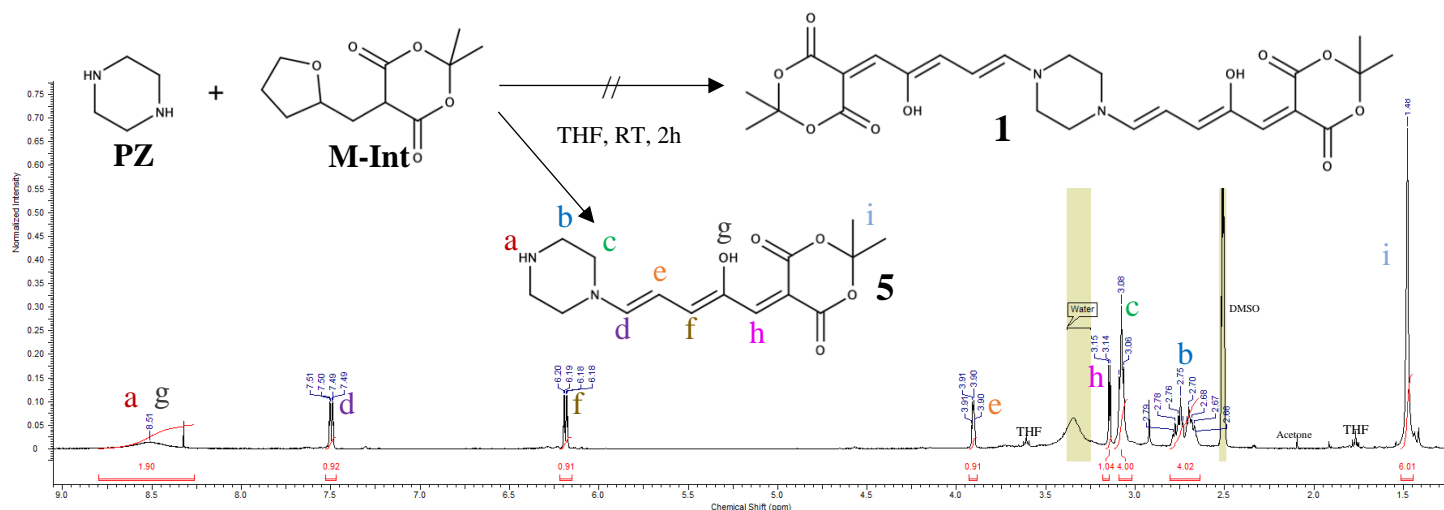


Figure 27. ^1H NMR spectrum in d^6 -DMSO of products from initial attempts to synthesise compound **1**, reacting **M-Int** with **PZ**, under the conditions described in procedure A. The peak at ≈ 2.85 ppm was an unidentifiable peak that did not appear always.

broad singlet at 8.5 ppm which is representative of the unreacted amine. The peaks at 3.1, 3.9, 6.2 and 7.4 ppm are indicative of the characteristic triene moiety of DASA molecules. Variations to the reactant ratios, reaction temperatures and durations were attempted but the same results were attained through these adjustments.

Catalysts were employed in attempts to achieve di-substitution onto the piperazine including pyridine, and potassium carbonate (K_2CO_3). Reactions attempted using pyridine as a catalyst and following procedure A produced the same results as when no catalysis was used. The reactions using K_2CO_3 as a catalyst following procedure B resulted in a mixture of the mono-

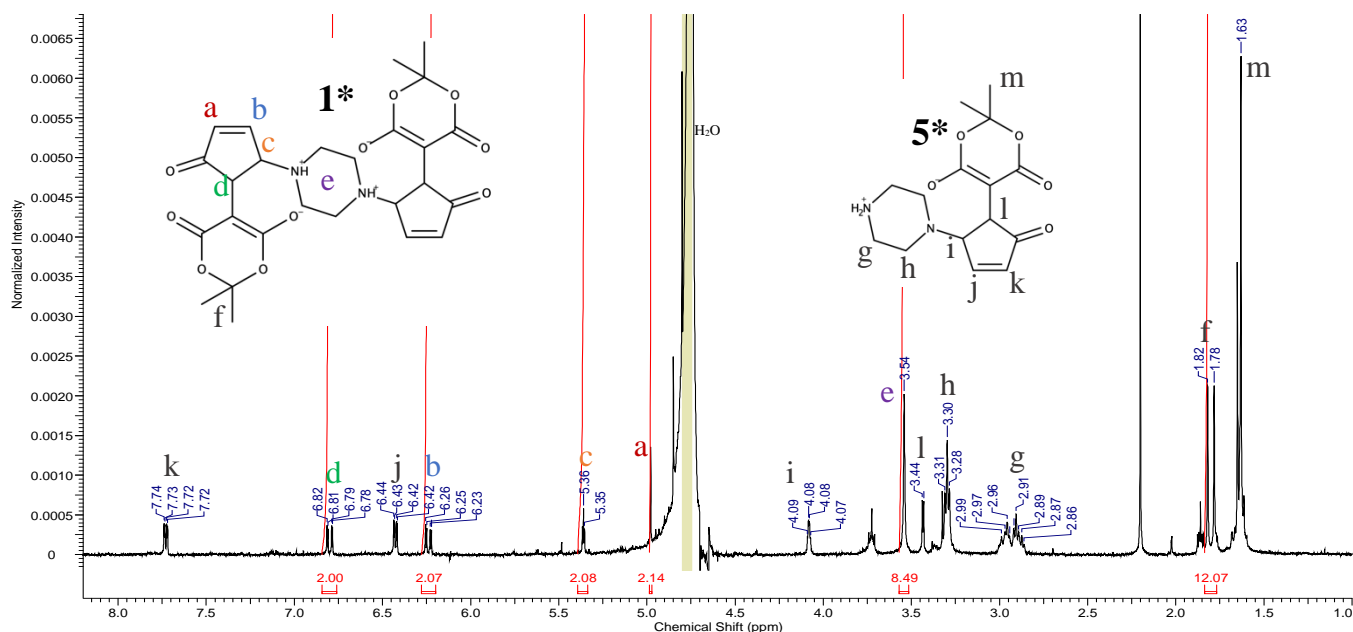


Figure 28. ^1H NMR spectrum in D_2O of the products from the reaction between **M-Int** and **PZ** using K_2CO_3 as a catalyst. The * Symbol is used to denote the cyclized isomers of the DASA molecules **1** and **5**.

substituted (**5**) and di-substituted (**1**) products in approximately a 50:50 ratio, as identified by the ^1H NMR spectra shown in Figure 28. A singlet was identified for the eight hydrogen atoms on the di-substituted piperazine at 3.54 ppm indicating a di-substituted piperazine product.

Due to previous work,⁶² and the high reactivity of **M-Int** with secondary amines in addition to the rapid colour change of the reaction mixture it was assumed that di-substitution onto **PZ** would occur. Although as the results indicate, under these conditions only mono-substitution on to **PZ** was possible yielding **5**. The additional attempts made to synthesise **1**, varied the reaction temperatures, durations and stoichiometry in order to induce di-substitution on **PZ**. Reaction durations up to 3 days, heating under reflux in THF and ratios between **M-Int** and **PZ** up to 10:1 all had no effect on the results, consistently producing **5**. Figure 29 exhibits stacked ^1H NMR spectra of the products obtained through selected reaction conditions, as shown these physical changes to the reaction conditions caused no desirable changes to the products obtained.

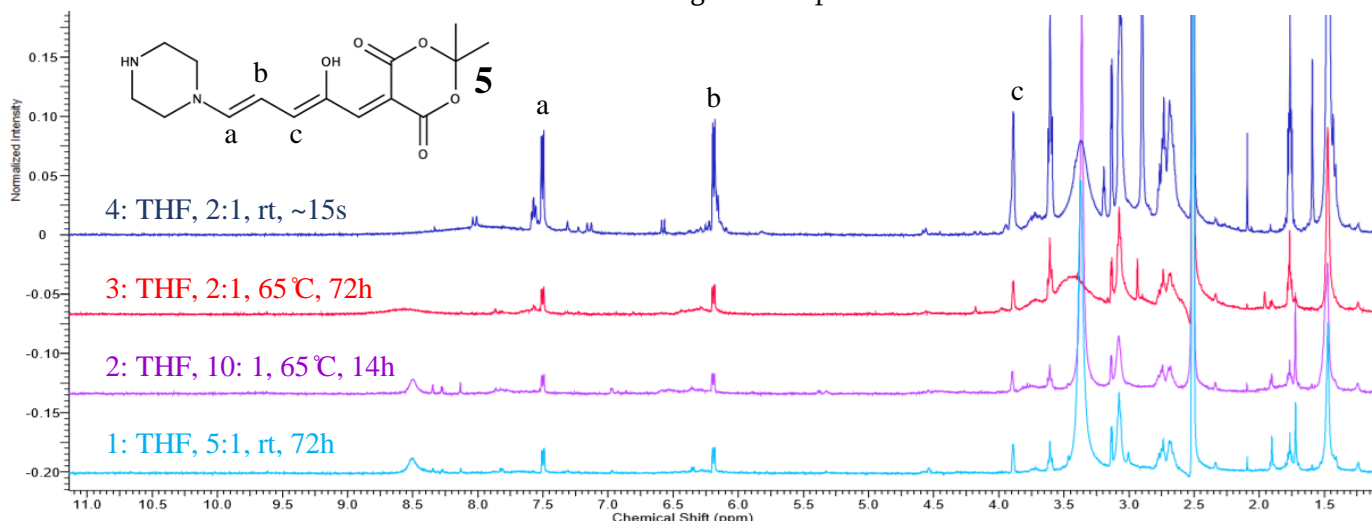


Figure 29. ^1H NMR spectra in d^6 -DMSO for the products from reactions between **M-Int** and **PZ** with varied conditions.

As the energy barrier of the reaction pathway leading to di-substitution could not be overcome through physical changes to the conditions, catalysts were employed to increase the nucleophilicity of the amines in efforts to push the reaction forward to form the di-substituted product. Use of pyridine as a catalyst caused no changes to the products obtained, this is likely due to lower $\text{p}K_b$ value of piperazine (4.19) compared to pyridine (8.77). The lower basicity of pyridine meant it could not increase the nucleophilicity of the piperazine and push the reaction forward. Conversely, the use of K_2CO_3 resulted in some evidence of the di-substituted product being formed. The ^1H NMR spectrum of the products obtained from reactions using K_2CO_3 showed the familiar spectrum of the mono-substituted **PZ** DASA **5**, in addition to a second set of peaks, visible in the spectrum in Figure 28 and highlighted in Figure 30. Through analysis of the spectrum the new

peaks were identified as the desired di-substituted product **1**. However, after repeated attempts to adjust the reaction conditions, **DASA 1** could not be produced in isolation. Inability to isolate **1** meant no investigation into the switching properties of could be carried out, moreover the solid material which gave the spectrum in Figure 28 was only soluble in water and so the testing the switching properties may not have been possible even if isolated due to the propensity of water to favour the cyclized form.³³

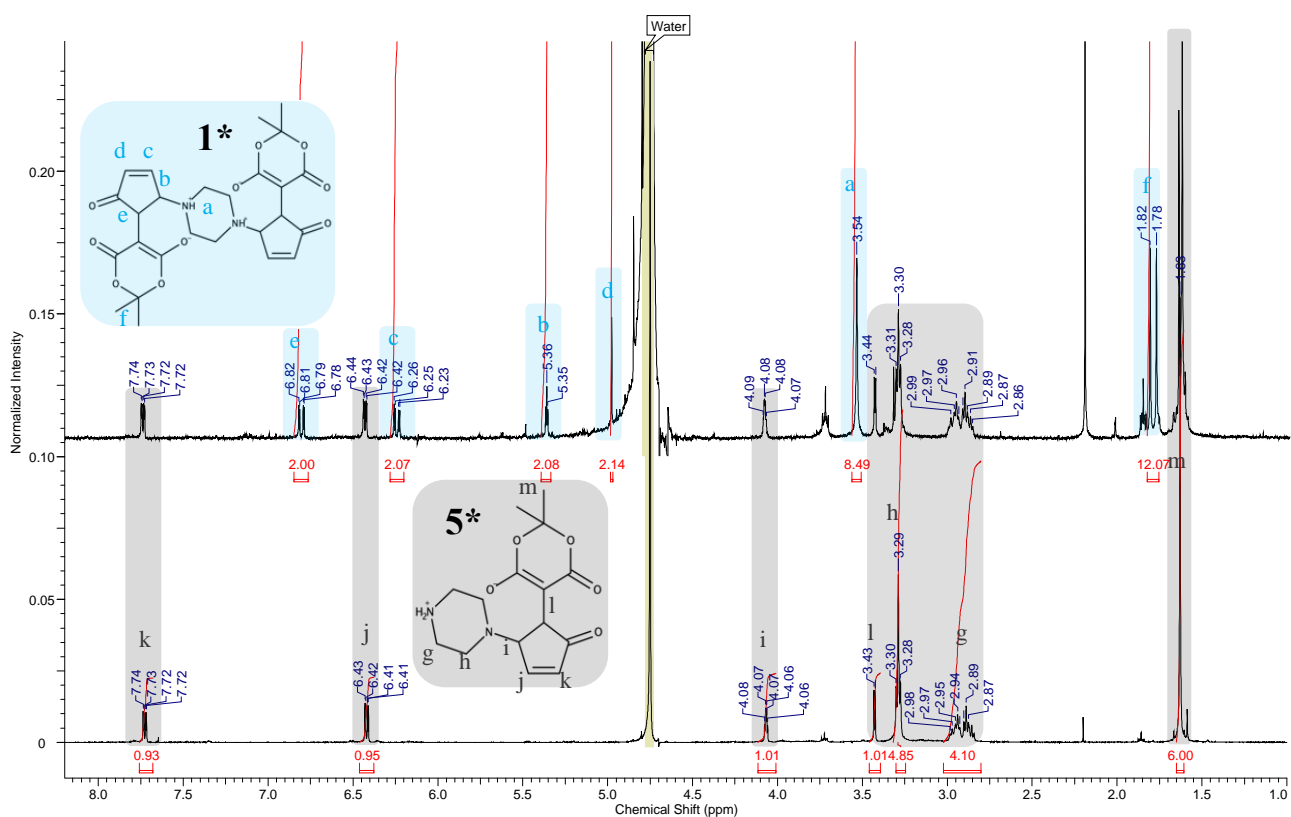


Figure 30. Stacked ^1H NMR spectra in D_2O of products from the reaction with K_2CO_3 catalyst (top), and of compound **5** (bottom) highlighting the mixture of **1** and **5** obtained from reactions with K_2CO_3 .

2.3.2 Attempted Synthesis of Compound 2. The attempted synthesis of **2** through the reaction of **B-Int** with **PZ** following procedure **A**, the conditions published for the synthesis of **DASA** molecules.² The reaction resulted in a colour change from yellow to purple in solution but upon cooling and filtering the reaction mixture it was not possible to isolate a solid product. Increased reaction times resulted in compound (**6**), the mono-substituted piperazine product, as identified by the ^1H NMR spectrum shown in Figure 31. The peaks at 2.72 and 3.06 ppm that correspond with the two hydrogen environments on the **PZ** ring, and the broad singlet at 8.46 ppm, which is representative of the unreacted amine, indicated that mono-substitution had occurred. Further variations to the reaction times and temperatures yielded no changes to the resultant products, and there were no catalysed reactions attempted. No further efforts were made to

synthesise **2**, and therefore no investigation into the switching properties of **2** could be performed.

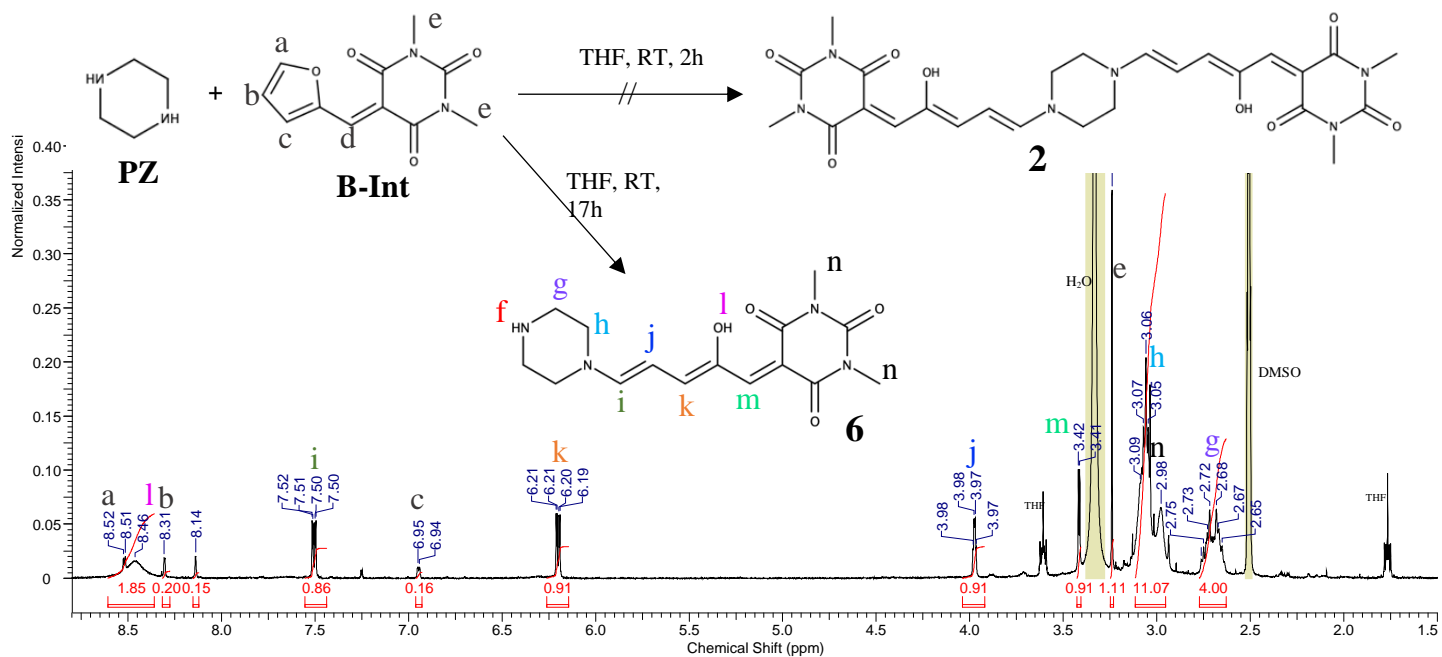


Figure 31. ^1H NMR spectrum in d^6 -DMSO of products from initial attempts to synthesise compound **2**, reacting **B-Int** with **PZ**, under the conditions described in procedure A. Some peaks remained unidentified, assumed to be unwanted impurities.

2.3.3 Attempted Synthesis of Compound 3. The synthesis of **3** was attempted through the reaction of **M-Int** with **TBP** following procedure **A**, this resulted in a mixture of the mono-substituted (**3**) and di-substituted (**9**) products as identified by the mass spectrometry data presented in Figure 32, in combination with ^1H NMR spectroscopy. Complete characterisation of the ^1H NMR spectrum was complicated by the presence of both molecules **9** and **3** in solution with multiple overlapping signals, as show in Figure 33. Variations to the reaction conditions including temperature, duration and stoichiometry did not cause any changes to the results achieved. The use of catalysts, pyridine and K_2CO_3 had no effect on the products obtained.

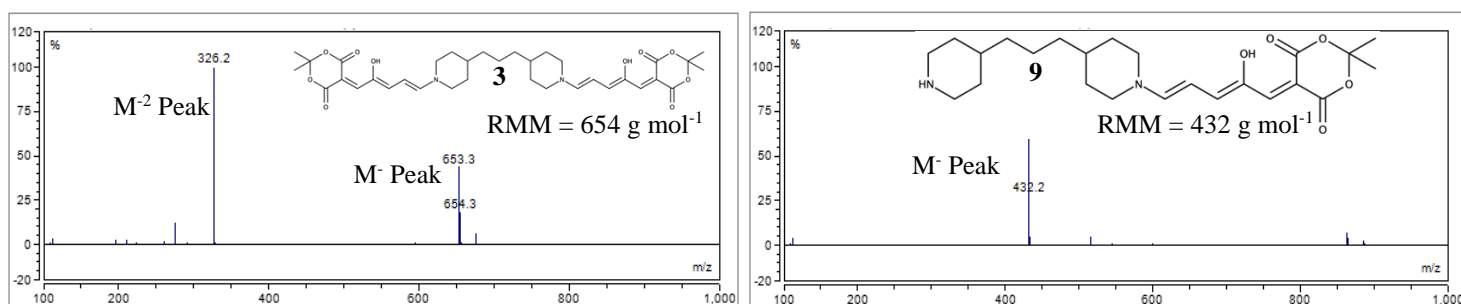


Figure 32. Mass spectra of separate fractions containing compound **3** (left) and compound **7** (right) after HPLC separation.

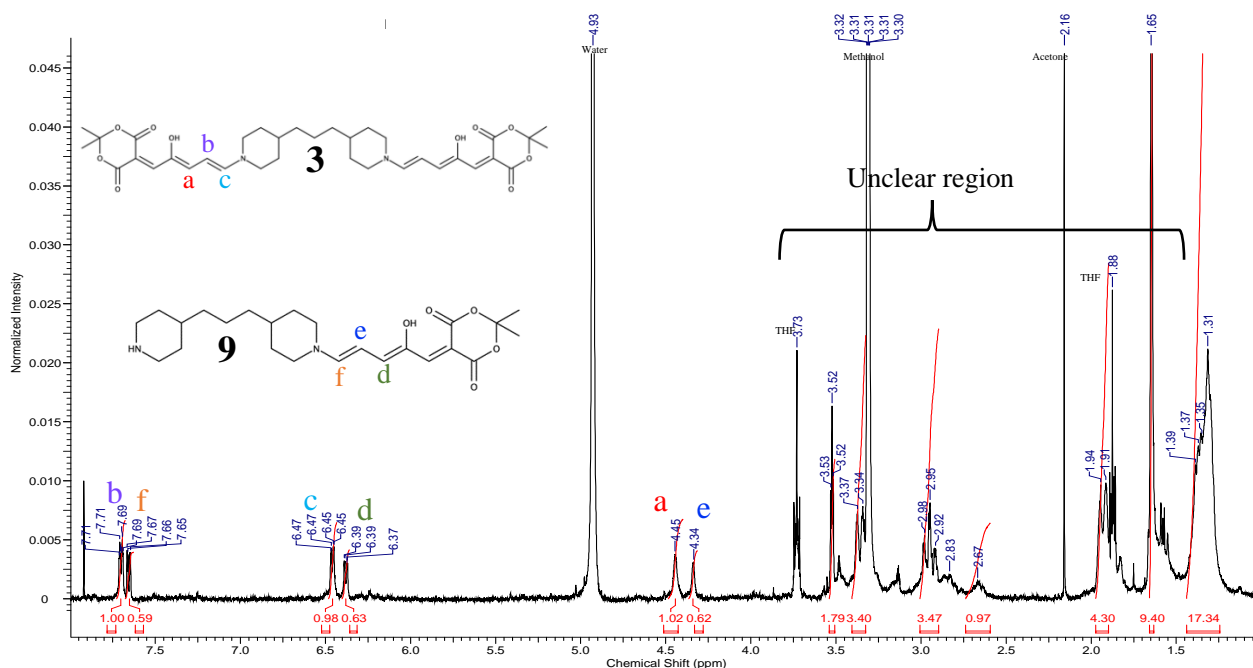


Figure 33. ^1H NMR spectrum in d_4 -Methanol of the product obtained from reactions between *M-Int* and *TBP* in attempts to synthesise **3**. The spectrum shows all visible peaks, NH and OH peaks were not observed, assumed to be in fast exchange with the solvent.

The complications involving the ^1H NMR spectrum obtained meant only the region between 4 and 8 ppm gave any distinct information about the products. It was clear that two species were present from the offset couples of peaks in the mentioned region, shown in Figure 33. One could mistake these peaks as being representative of the open and cyclized DASA forms in equilibrium as this is found for various first generation DASAs, but this was not the case here. There would be an additional one or two sets of peaks in region between 4 and 8 ppm, representative of the cyclopentanone ring on the cyclized forms of **3** and **9**, but this was not found. Based on the results from attempting to synthesise **1** and **2**, the speculation was that both the mono- and di-substituted variants would be present and from the investigation using LC-MS it was confirmed that the desired product **3** and the mono-substituted variant **9** were both present, shown by Figure 32. Furthermore, varying the reactions conditions through the same amendments to process **A** as when attempting to synthesise DASA **1** yielded no changes in the products formed, moreover the use of the same catalysts, pyridine and K_2CO_3 seemed to have little or no effect on the reaction. Therefore attempts to isolate either DASA **3** or **9** through synthetic means was abandoned.

2.3.4 HPLC Separation of **3 and **9**.** As the isolation of **9** was not possible through synthetic means, HPLC was employed in attempts to separate **3** and **9** so that the photo-switching properties

of each could be examined, and the structures fully characterised. Separation was possible indicated by the clear differentiated peaks in the HPLC chromatograph, shown in Figure 34. The fractions collected were then confirmed to be **3** and **9** through subsequent LC-MS analysis. However, difficulties with solubility of the products in the HPLC medium, limiting injections to solutions

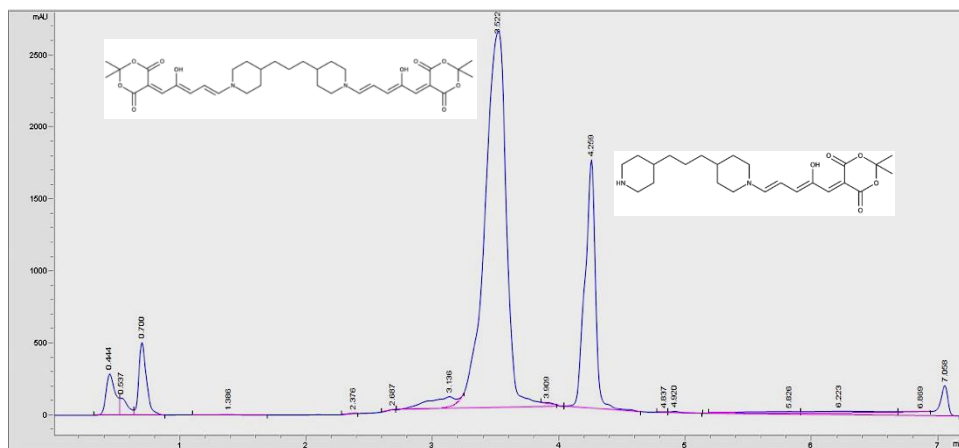


Figure 34. HPLC Chromatograph of the separation of **3** and **9**, showing distinct separated peaks.

with up to ≈ 20 mg per mL, followed by further solubility issues after removal of the HPLC solvent caused a loss of product and consequently led to the inability to test the photochromic properties, despite repeated attempts. This is thought to be due to DASAs instability to both the basic conditions of the mobile phase and the environment inside the separating column, in agreement with previous comments on DASAs limited stability to column chromatography.⁷

2.3.5 Attempted Synthesis of DASA 4. Synthesis of **4** was initially attempted through procedure **A**, following the conditions published for the synthesis of DASA molecules.² As the results presented, the reactions between **B-Int** and **TBP** yielded no useful product. With extended reaction times some product was formed, however upon collection very low quantities were obtained, and solubility issues hindered characterisation through ¹H NMR spectroscopy. Even if characterised the solubility issues would not allow for testing of the photochromic properties. Therefore, due to the difficulties yielding qualitative amounts of product and the solubility issues no further pursuits were made in the synthesis of **4**.

2.3.6 Synthesis and UV-Vis Absorption Spectroscopy of Compound 5. The synthesis of **5** was attempted through **M-Int** with **PZ** following the procedure described in the experimental section for **5**, which resulted in the desired mono-substituted piperazine product **5** in isolation, as

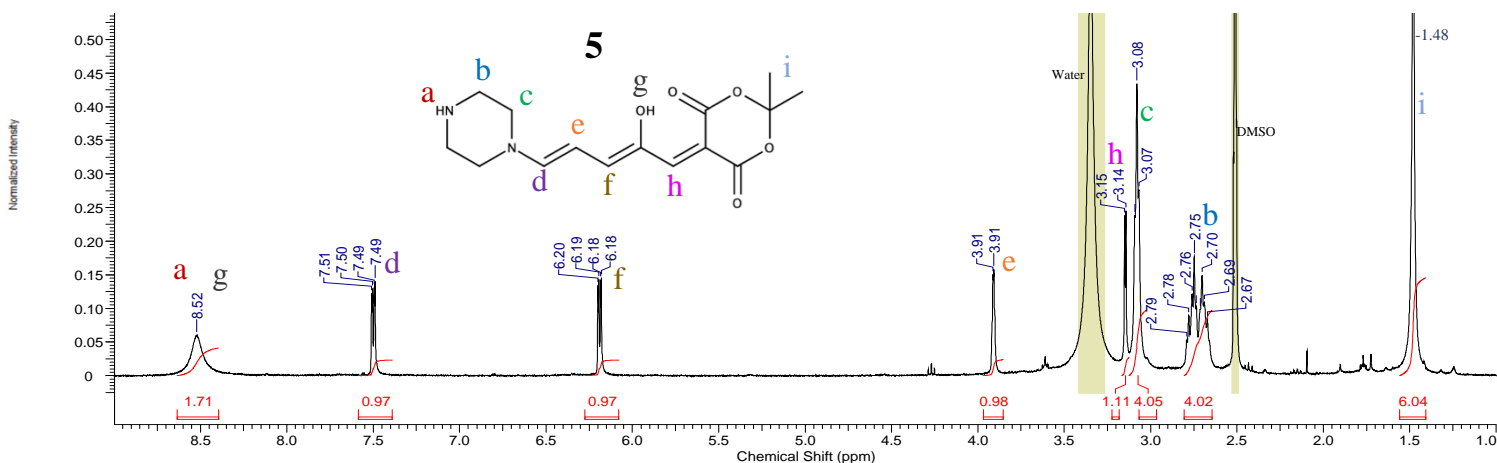


Figure 35. ^1H NMR spectrum of **5** in d^6 -DMSO.

shown by the ^1H NMR spectrum in Figure 35. Reaction conditions were optimised for synthesising **5** from the attempts to synthesise DASA **1**.

The photochromic properties of DASA **5** were analysed through UV-Vis spectroscopy. The results showed that **5** exhibits near complete and reversible photo-switching in chloroform as shown in Figure 36. In toluene and chlorobenzene complete photoisomerisation occurs but the thermal reversion was incomplete with full recovery of the absorbance not possible, see appendix 3. Consistent with other first generation DASAs, **5** undergoes the cyclization reaction in methanol even in the dark and UV-Vis measurements in appendix 3.11 illustrate this. The results of further testing the photo-switching properties in chloroform showed that **5** undergoes complete, reversible photo-switching at varying concentrations up to 2×10^{-4} M with rapid photoisomerisation rates, the full details of which are discussed in chapter 3. UV-Vis spectroscopy was also used to test the

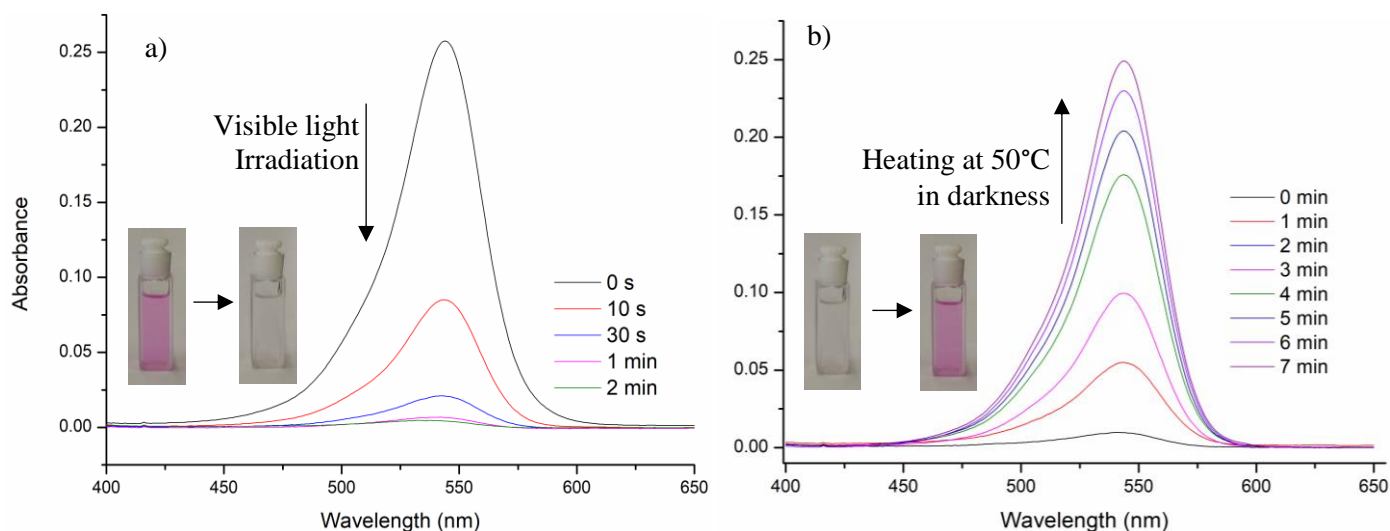


Figure 36. a) UV-Vis spectra of **5** in a 1×10^{-5} M chloroform solution indicating photoisomerisation in under 2 minutes of irradiation. B) UV-Vis spectra of **5** in a 1×10^{-5} M chloroform solution displaying complete thermal reversion in 7 minutes of heating at 50°C in the dark.

stability of **DASA 5**; measuring the absorption spectra of a single sample on two occasions 27 days apart, after being kept in a dark cupboard at room temperature, revealed no decrease in the absorbance recorded as shown by Figure 37.

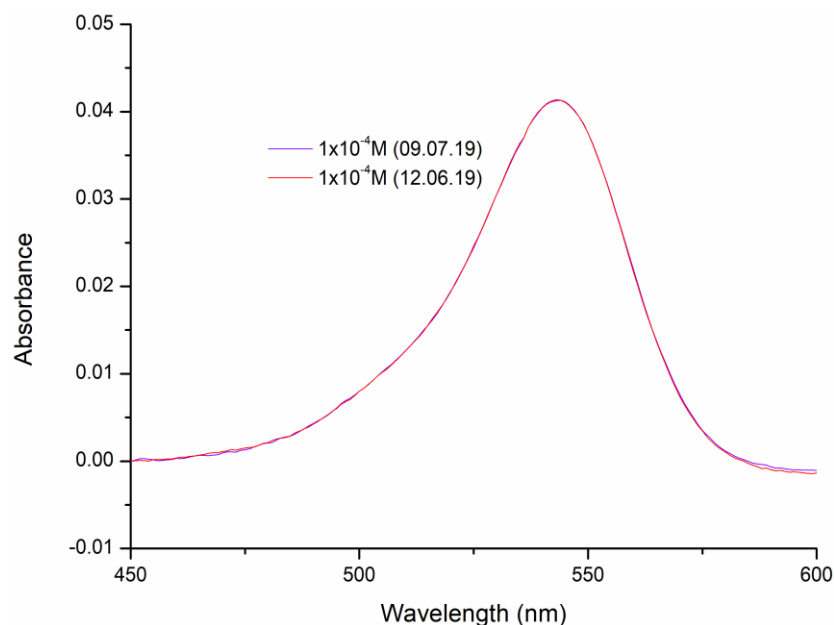


Figure 37. UV-Vis spectra of a 1×10^{-4} M solution of **5** in chloroform, 27 days apart.

Although attempts to isolate **DASA 1** were unsuccessful, the endeavour led to the synthesis of the previously unreported **DASA 5**. Minor adjustments to the reaction conditions in procedure **A** allowed for the isolation of **5** in good yields. The ^1H NMR spectra of the open and cyclized forms can be seen in Figures 35 and 30 respectively. As noted, DASAs have been reported to breakdown in the presence of excess amine, due to nucleophilic additions on the triene chain producing side products.^{3,4} Therefore the new **DASA** structure prompted further investigation due to the unreacted amine present on the **PZ** donor moiety, combined with apparent stability. Investigating the stability of **DASA 5** showed that the unreacted amine did not appear to impact the stability, as displayed by Figure 37, no changes in the absorption spectrum were observed over the period of a 27 days indicating no breakdown had occurred over that period.

The photo-switching properties were impressive with rapid, complete and reversible photo-switching in chloroform as shown by Figure 36. The complete photoisomerisation at a variety of concentrations up to 2×10^{-4} M, which is the solubility limit in chloroform, suggests that **5** does not suffer from the concentration dependence reported to negatively affect **DASA** photo-switching,¹⁶ a more in-depth look into the details of the photo-switching properties is presented in chapter 3.

2.3.7 Synthesis and UV-Vis Absorption Spectroscopy of Compound 6. The synthesis of **6** was attempted through reacting **B-Int** with **PZ** following the procedure described in the experimental section. This resulted in the desired mono-substituted piperazine product **6**, as shown by the ^1H NMR spectrum in Figure 38. Reaction conditions were optimised for synthesising **6** from attempts to synthesise **2** and although low yields were recorded, isolated samples of **6** were obtained. No experiments were performed to directly investigate the stability of **6**, however observing solid samples of **6** over a period of weeks in bench top conditions found that decolouration would occur. Synthesised samples turned from a purple to brown powder and correspondingly the ^1H NMR spectra gained additional peaks, shown in Figure 40, and the peak integral ratios were changed, indicating break down and the formation of side products.

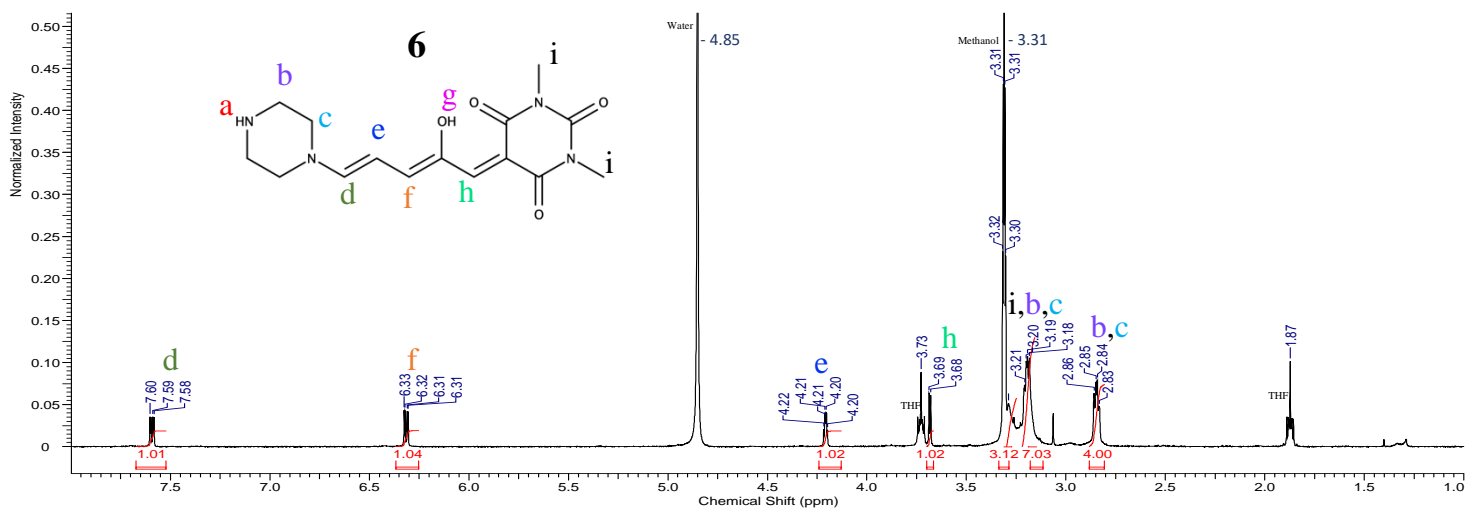


Figure 38. ^1H NMR spectrum of **6** in d_4 -Methanol. Peaks **a** and **g** were not observed, the protons were assumed to be in fast exchange with the solvent.

The photochromic properties of DASA **6** were analysed through UV-Vis spectroscopy. The results show that **6** exhibits near complete photo-switching and partial reversibility in chloroform shown in Figure 39, although a minor decrease to the recovered absorbance was observed. This fatigue was continually observed with repeated switching cycles. Complete photoisomerisation was observed at concentrations up to 1 mM in chloroform, the full details of which are discussed in Chapter 3 (see section 3.3.7). DASA **6** also showed rapid reversible photo-switching in chlorobenzene shown in appendix 3.12, although some fatigue was observed upon repeated cycles as shown in appendix 3.14. No data was recorded for the switching properties of **6** in any other solvents.

Although synthesis of **2** was unsuccessful the attempts led to the synthesis of previously unreported DASA **6**. Increasing reaction times of procedure **A** was necessary as the reaction between **B-Int** and **PZ** is slow, which allowed for the isolation of **6** as shown by the spectrum in

Figure 38, the NH and OH peaks are absent due to fast exchange with the solvent, methanol was used due to the increased solubility of **6** in methanol. The initial thorough investigation of DASAs²² by Read de Alaniz reported no reaction between **B-Int** and morpholine or phenyl piperazine illustrating the low reactivity between **B-Int** and heterocyclic compounds with two non-carbon atoms; this could explain the low yields achieved for **6**.

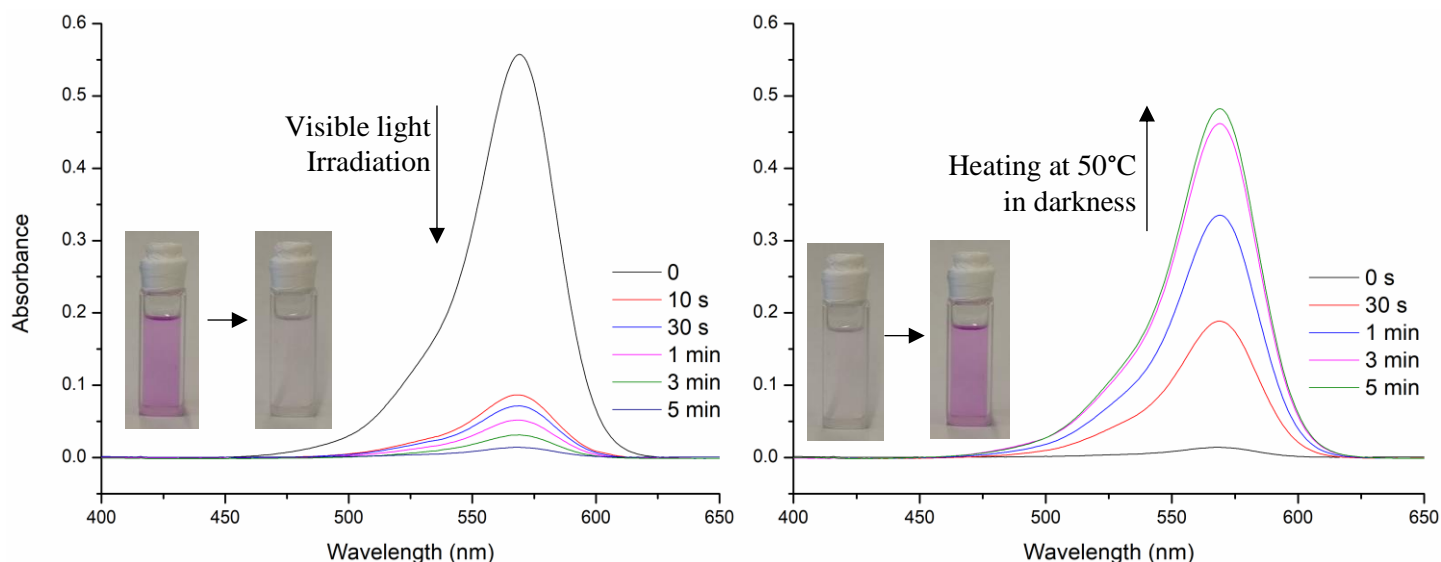


Figure 39. a) UV-Vis spectra of **6** in a 1×10^{-5} M chloroform solution indicating photoisomerisation in under 5 minutes of irradiation. b) UV-Vis spectra of **6** in a 1×10^{-5} M chloroform solution displaying thermal reversion in 5 minutes of heating at 50°C in the dark.

The structure of **6** only differs from **5** in the acceptor moiety, therefore for the same reasons as discussed for **5**, the unreacted amine present on the **PZ** ring warranted further investigation into the properties of **6**. Though the stability of **6** was not directly investigated, as mentioned the powder was observed to break down over time. Reactions produced a vibrant purple powder which would gradually become brown over time, the ^1H NMR spectra of the browned powder contained additional peaks not representative the structure of **6**, shown in the spectrum in Figure 40, recorded 2 months after synthesis. The mechanism of the breakdown was not investigated further.

The photo-switching properties of **6** were similar to **5** with rapid and near complete photoisomerisation in chloroform, although in contrast to **5** the thermal reversion was incomplete as the absorbance was not fully recovered upon heating in the absence of light. However, the $>95\%$ photoisomerisation observed for **6** up to 1 mM/ 1×10^{-3} M suggests that there is no clear inhibition to the photoisomerisation of **6** as photochrome concentration increases. A more in-depth investigation into the photo-switching properties of **6** through comparisons with **5** and other analogous DASA molecules is presented and discussed in chapter 3, further exploring the reported concentration dependent photo-switching of DASAs.

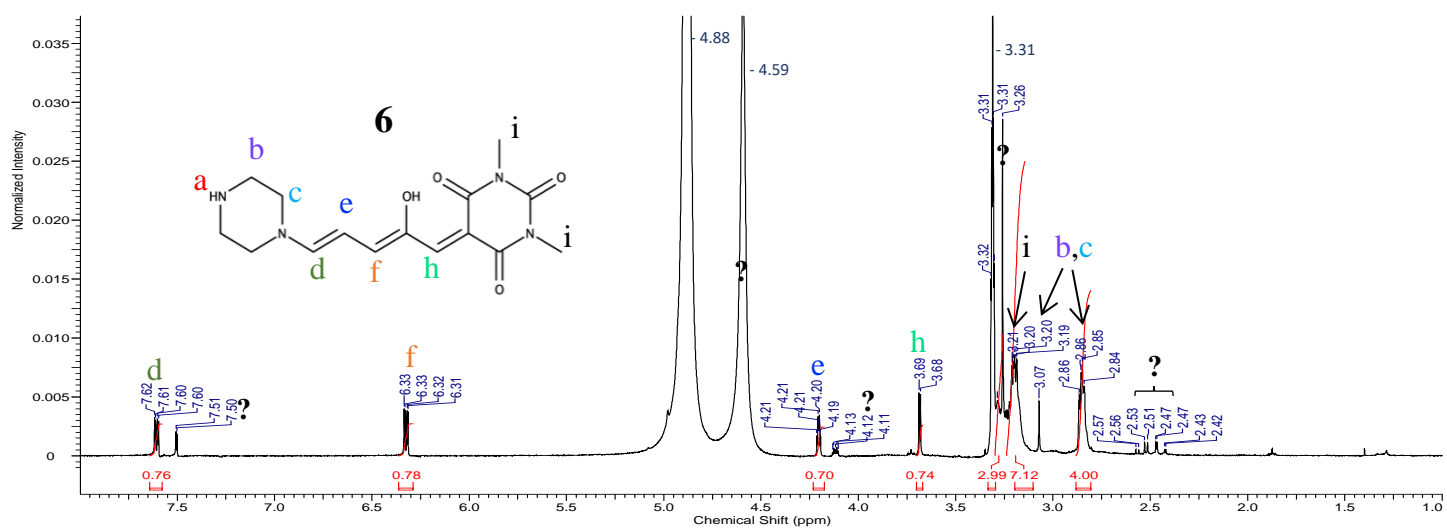


Figure 40. ^1H NMR spectrum in d_4 -methanol of **6** after the powder discoloured from purple to brown.

The photo-switching properties of **6** were similar to **5** with rapid and near complete photoisomerisation in chloroform, although in contrast to **5** the thermal reversion was incomplete as the absorbance was not fully recovered upon heating in the absence of light. However, the >95% photoisomerisation observed for **6** up to 1 mM/ 1×10^{-3} M suggests that there is no clear inhibition to the photoisomerisation of **6** as photochrome concentration increases. A more in-depth investigation into the photo-switching properties of **6** through comparisons with **5** and other analogous DASA molecules is presented and discussed in chapter 3, further exploring the reported concentration dependent photo-switching of DASAs.

2.4 Conclusions

The synthesis of isolated bi-functional symmetric DASAs was unsuccessful, reactions between the activated furfural intermediates (**M-Int** and **B-Int**) and the selected di-amine donors (**PZ** and **TBP**) resulted in either the mono-substituted product alone or mixtures of the mono- and di-substituted products. Efforts to modify reaction conditions or separate the variants in order to isolate the di-substituted molecules were not met with success. Only the mono-substituted piperazine DASAs **5** and **6** could be synthesised in isolation.

The results suggest that DASAs will not easily form in such close proximity, the di-amines appear to lose their nucleophilicity to some extent when they are close together. It would appear that once the first nucleophilic substitution has occurred, the energy barrier for the second substitution is much greater. Considering that under the conditions of procedure **A** there was

evidence of DASA **3** forming, but not DASA **1** there must be a relationship between the distance between the reacting amines and the change in the in the energy barrier between the first and second substitutions.

The desired products were not synthesised and isolated and the photochromic properties of the bi-functional DASA molecules could not be tested. However, previously unreported DASAs **5** and **6** were obtained and structures observed via ¹H NMR. Both molecules show impressive photo-switching properties in chloroform when confirmed to other 1st generation DASAs. Most interestingly, neither DASA shows signs that their photo-switching properties are affected by photochrome concentration in the way that has been previously reported for DASAs.¹⁶ The results of an in-depth analysis and comparison of the photochromic properties of DASAs **5** and **6** is presented and discussed in chapter 3.

Chapter 3

3.1 Introduction

The novel structures of DASAs **5** and **6** differ from any other DASA reported to date due to the unreacted amine present on the molecule. How this structural and chemical difference affects the photo-switching properties is investigated herein.

The efficiency of a photo-switch is measured based on the proportion of isomerised molecules in the photostationary state (PSS), and how fast this point is reached. The PSS can be described as the stable state at which the absorption of light induces no further isomerisation between the two states under consistent conditions.⁶⁷ Other than the intrinsic efficiency of the photo-switch, the primary factors affecting where this stable equilibrium will be reached are the temperature and solvent. For DASA molecules there appears to also be a relationship between the PSS and the concentration, where higher concentrations limit the number of molecules which can undergo photoisomerisation from the coloured to the colourless form.¹⁶ As noted in section 1.4 studies on a single DASA molecule showed that both in solution and embedded within polymer matrices DASAs photo-switching efficiency is dependent on concentration.¹⁶ Other photochromes such as spiropyrans and diarylethenes see no concentration dependence with even the crystalline forms exhibiting some photochromism.⁶⁸⁻⁷¹ The highly attractive photo-switching properties of DASAs makes determining the source of the concentration dependence, or a method to overcome

it, vital so that new DASAs that can perform effectively at any concentration can be designed and synthesised.

Molecules **5** and **6**, which were synthesised in chapter 2 are shown in Figure 41. They are previously unreported DASA structures which exhibit impressive photochromic properties and initial photo-switching experiments show differences to the previously published DASAs, **7** and **8** (Fig. 41) – hence the unreacted amine must have a significant effect. In order to further investigate the effect of the unreacted amine on the photo-switching, **7** and **8** were synthesised for comparison of the properties and to demonstrate the effect of the structural difference. The aim is to further characterise the photo-switching behaviour of previously undiscovered **5** and **6** and compare select switching properties with previously published DASAs **7** and **8**, to illustrate the effect the unreacted amine has on the photochromism.

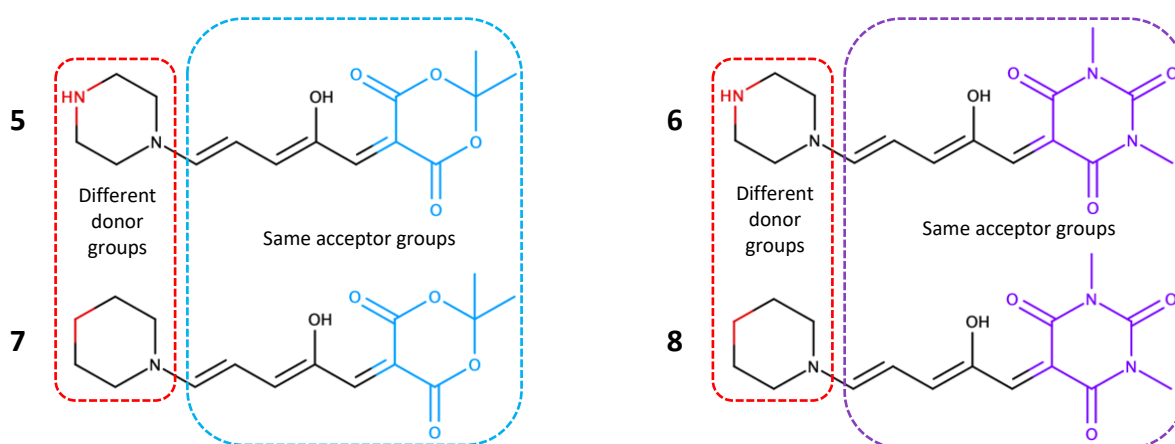
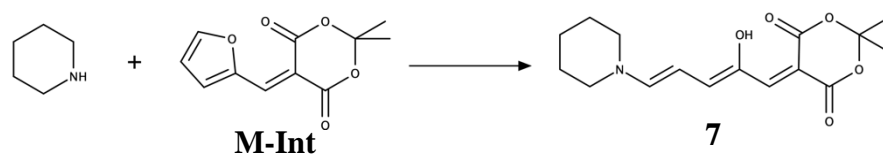


Figure 41. Diagram illustrating the structural similarities and differences between DASAs **5** and **7** (left) and **6** and **8** (right).

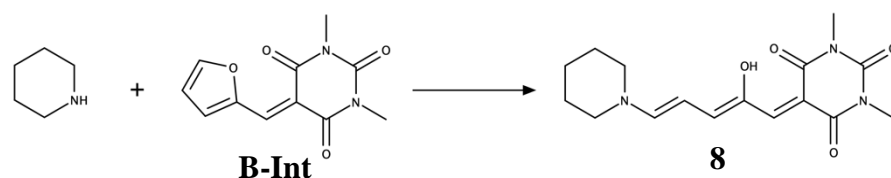
3.2 Experimental

3.2.1 General methods. Unless stated otherwise all reactions were performed in oven dried glassware in an atmosphere of air using reagent or analytical grade solvents. All reagents obtained from commercial suppliers were used as received. Reaction temperatures were controlled through automated heating plates with oil or aluminium bead baths, and unless explicitly stated reaction were performed at room temperature (approximately 23 °C). Vacuum drying was done using either a Büchner set up or vacuum oven The procedure for the synthesis of DASAs **5**, **6** and the activated furfural intermediate compounds **M-Int** and **B-Int** is presented in chapter 2.

Compounds 7 and 8.



5-[(2Z,4E)-2-hydroxy-5-(piperidin-1-yl)penta-2,4-dien-1-ylidene]-2,2-dimethyl-1,3-dioxane-4,6-dione (**7**). Compound **7** was prepared according to the literature procedure.² Meldrum's acid intermediate **M-int** (0.299 g, 1.35 mmol) was dissolved in THF (5 mL) and left to stir. Piperidine (0.111 g, 1.30 mmol) was added via micropipette, the reaction was left to stir at room temperature (23 °C) for 1 h followed by cooling to 0 °C for 20 min. The mixture was filtered and the resultant solid was washed with diethyl ether and further dried under vacuum yielding a red powder (0.331 g, 1.07 mmol, 82.3%).



5-[(2Z,4E)-2-hydroxy-5-(piperidin-1-yl)penta-2,4-dien-1-ylidene]-1,3-dimethyl-1,3-diazinane-2,4,6-trione (**8**). Compound **8** was prepared according to the literature procedure. Barbituric acid intermediate **B-int** (0.299 g, 1.28 mmol) was dissolved in THF (20 mL). To this solution piperidine (0.109 g, 1.28 mmol) was added via micropipette. The reaction mixture was stirred at room temperature (23 °C) for 2.5 h, followed by cooling to 0 °C for 20 min. The mixture was filtered and the resultant solid was washed with diethyl ether and further dried under vacuum yielding a purple powder (0.221 g, 0.692 mmol, 46.9%).

3.2.2 Instrumentation and Methodology

UV-Vis Absorption spectroscopy

General methods. The UV-Vis absorption spectra were recorded using a Shimadzu UV-1800 spectrometer. Each spectrum recorded was over a range of 400 – 650 nm. The samples were irradiated from all directions using a 50 W, 650 K, full spectrum LED flood light, illuminating a container lined with reflective mylar sheeting, room temperature was maintained by allowing a current of air to flow through the container. Samples were continuously irradiated in between each measurement and sequential measurements of the UV-Vis absorbance were taken until no notable

changes in the spectra were observed, at which point the thermal reversion was recorded through the same procedure, heating samples in a dark oven at 50 °C. In-situ irradiation of samples was not possible due to the apparatus available, as the illumination would interfere with the incident beams and detector of the spectrometer. Therefore samples were quickly moved from the illumination container to the spectrometer to take measurements and placed back inside once the measurement was finished, the scan rate of the spectrometer was increased to the max in order to limit the time samples were left unirradiated. Similarly, when performing the thermal reversion measurements samples were moved between the oven and spectrometer, wrapped in foil to avoid light contamination while transporting.

Unless stated otherwise, samples were first dissolved in DMSO to create a 0.01 M solution, this was then diluted with chloroform to the concentrations needed.

Determination of the %PSS. The %PSS is defined as the percentage of molecules that have undergone photo-switching to the cyclized form at the photo-stationary state (PSS). Determination of the PSS was achieved through constant irradiation of samples and sequential measurement of the UV-Vis absorbance until no notable changes in the spectra were observed, at which point the PSS was assumed to have been reached. The %PSS was then calculated through equation 1 using the maximum recorded absorbance (Abs_{max}), and the absorbance value measured at the PSS (Abs_{PSS}). It is assumed that the Abs_{max} represents the absorbance value for a solution containing 100% open, coloured isomers. Abs_{max} was determined by heating samples in an oven at 50 °C in the absence of any light, measuring the absorbance until no further increase was observed.

$$\%PSS = 100 - \frac{Abs_{PSS}}{Abs_{max}} \times 100\% \quad (\text{Equation 1})$$

Determination of the %DEQ. Determining the where the dark equilibrium between the open, coloured form and the cyclized, colourless form exists was accomplished through allowing samples to equilibrate in the dark and sequentially measuring the UV-Vis absorbance. Once no notable changes in the spectra were observed, giving Abs_{DEQ} , the dark equilibrium was assumed to have been reached. Then, under the assumption that the Abs_{max} represents the absorbance of a solution consisting of 100% open, coloured isomers the percentage of open, uncyclized molecules at the dark equilibrium (%DEQ) could be estimated through equation 2.

$$\%DEQ = \frac{Abs_{DEQ}}{Abs_{max}} \times 100\% \quad (\text{Equation 2})$$

Cycling Studies. In order to investigate the potential for fatigue and decreased efficiency on repeated photoisomerisation, repeated cycles were performed. Cycling the photoisomerisation process was done by alternating between irradiation and heating multiple times in series. Absorbance readings were measured over the same range of wavelengths as stated previously and taken throughout irradiation until no changes in the spectrum were observed. Then samples were placed into an oven at 50 °C in the absence of light and the process was repeated for multiple cycles. Minor fluctuations in the Abs_{max} occurred due to small changes in the oven temperatures from opening and closing the door. The absorbance value at λ_{max} was used to plot data.

Single crystal X-ray diffraction. Crystallographic structure determination was performed using the SuperNova, Dual, Atlas S2 diffractometer, using Cu radiation (λ 1.5406 Å). Crystals were kept at 100 K during data collection. Using Olex2,⁷² the structure was solved with the ShelXT⁷³ structure solution program using Direct Methods and refined with the ShelXL⁷⁴ refinement package using Least Squares minimisation.

Computational experiments. The initial minimum energy conformations of all molecules were assessed following conformational searches and energy minimisations using the intrinsic molecular dynamics MM2 force field intrinsic to Chem3D, v15.0 (Perkin Elmer). All final conformations were modelled at the semi-empirical PM7 level (in CHCl₃, e=4.81, COSMO) using MOPAC 2016⁷⁵ through the MOPAC Interface with Chem3D, v15.0 (Perkin Elmer).

3.3. Results and Discussion

3.3.1. Synthesis of 7. The reactions between **M-Int** and piperazine led to the formation of product **7** being formed, as indicated by the ¹H NMR spectrum Figure 43 and appendices 1.5 and 1.6. Good yields were achieved, and the structure was further confirmed through X-ray diffraction seen in Figure 42.

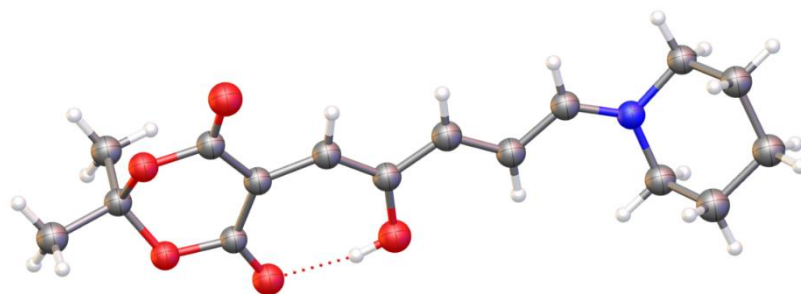


Figure 42. Crystal structure of DASA 7, as the coloured, uncyclized form.

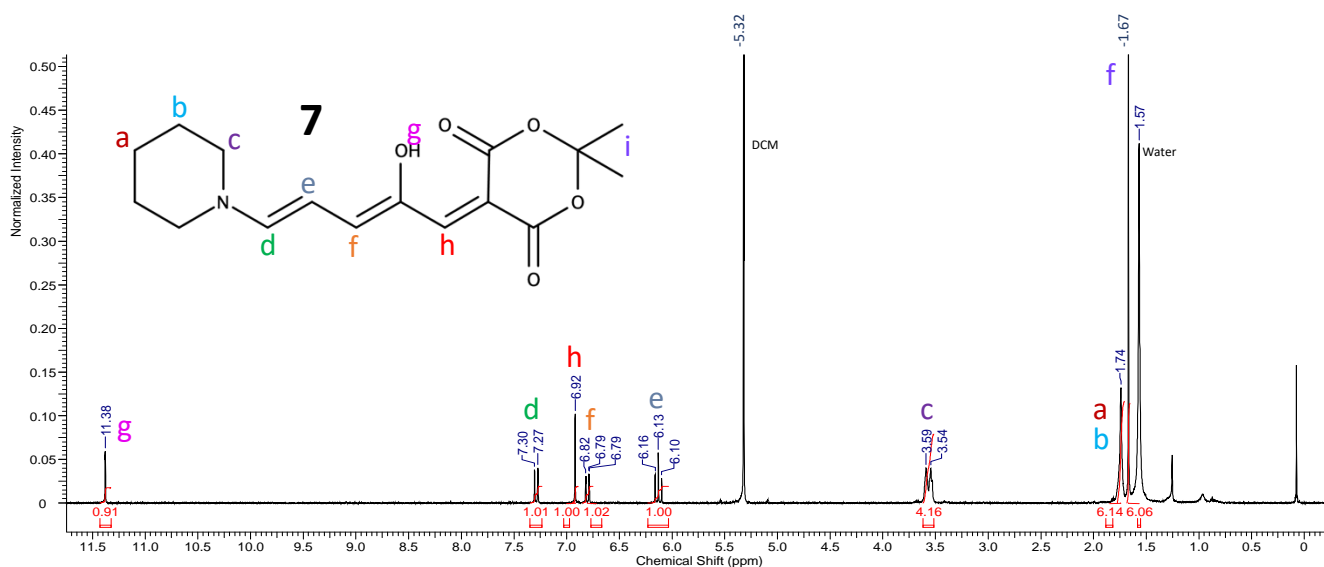


Figure 43. ^1H NMR Spectrum in CD_2Cl_2 of compound **7**, the coloured uncyclized form.

3.3.2 Synthesis of 8. The reactions between **B-Int** and piperazine resulted in the formation of desired product **8** being formed, as indicated by the ^1H NMR spectrum in Figure 44a and appendices 1.3 and 1.4. Good yields were achieved, and the structure was further confirmed through X-ray diffraction seen in Figure 44b.

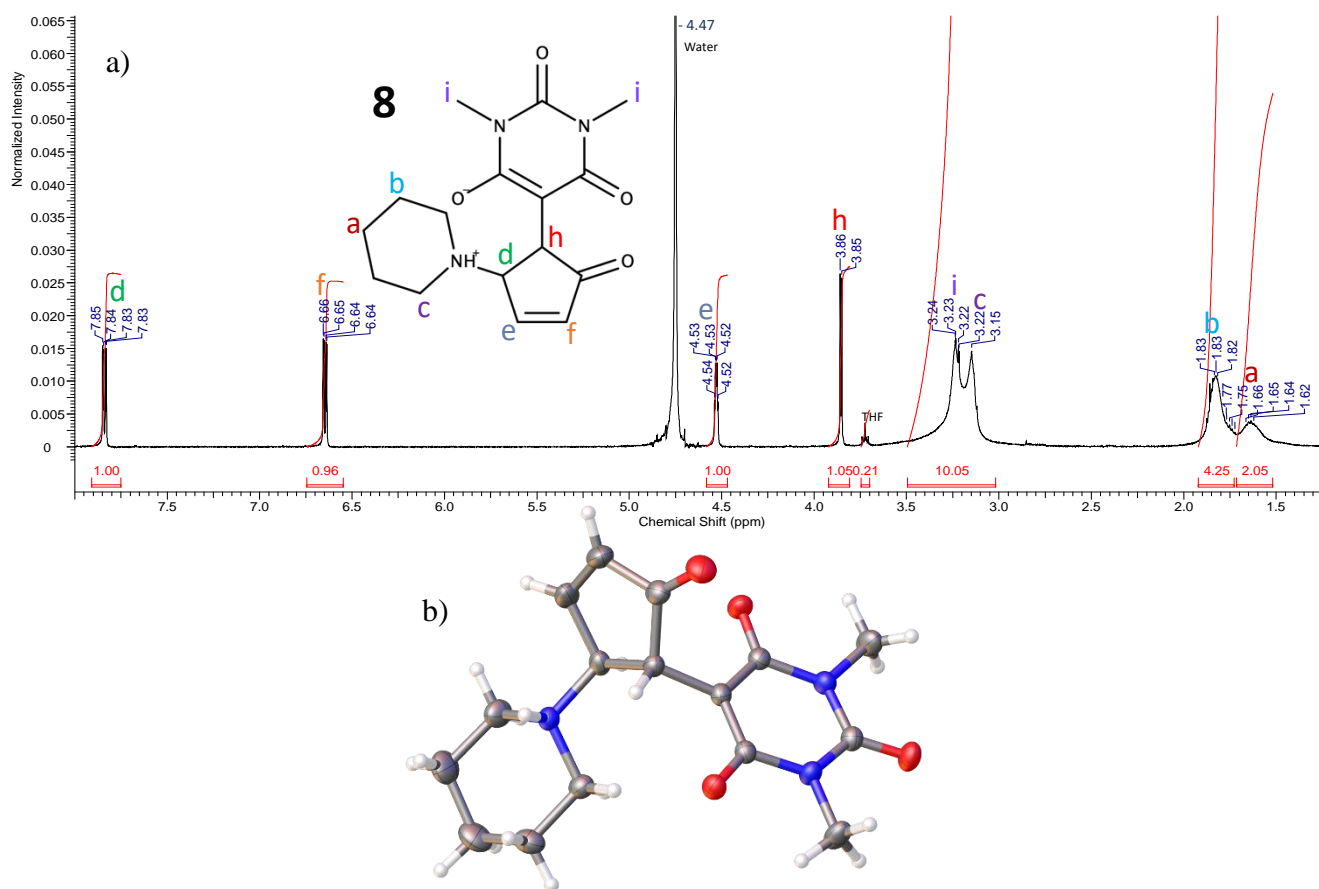
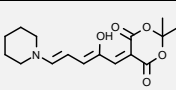
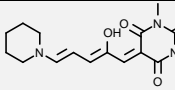


Figure 44. a) ^1H NMR Spectrum in D_2O of compound **8**, the colourless, cyclized form. b) Crystal structure of DASA **8**, as the colourless, cyclized form

3.3.3 Photo-switching efficiency of 7 and 8. The photo-switching efficiency of **7** and **8** was only measured in terms of the %PSS in chloroform. The results of the investigation into the switching of **7** and **8** is displayed in Table 1. The highest %PSS observed for either molecules was <90% and for both molecules there was an observed decrease in the %PSS as photochrome concentration increased. Furthermore, the rate of the photoisomerisation also decreased as concentrations increased, shown in Figures 45, 55. The thermal reversion properties were not investigated for DASAs **7** and **8**. The results reveal that the photoisomerisation behaviour of **7** and **8** is consistent with previously published DASAs in that there is an inhibition to photo-switching in terms of both the %PSS and the rate of switching with increasing photochrome concentration.

Table 1 – showing %PSS data for **7** and **8**, at concentrations between 5×10^{-6} and 2×10^{-4} M in CHCl_3 .

	 7	 8
5×10^{-6} M	87.5%	66.4%
1×10^{-5} M	89.1%	61.0%
1×10^{-4} M	85.4%	49.5%
2×10^{-4} M	65.6%	17.2%

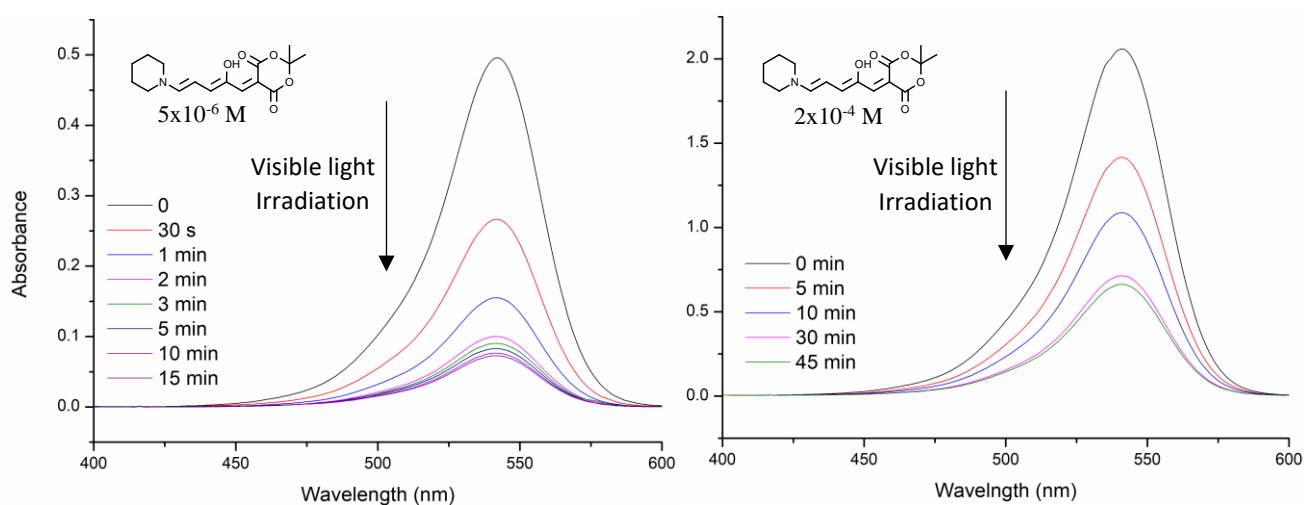


Figure 45. UV-Vis Absorption spectra of **7** in chloroform at concentrations of 5×10^{-6} M (left) and 2×10^{-4} M (right).

3.3.4 Photo-switching efficiency of 5. The photo-switching efficiency of **5** was investigated through measuring both the %PSS and %DEQ. The calculated results of the UV-Vis spectroscopy are displayed in Table 2. The %PSS was >99% at each concentration tested showing the impressive photo-switching efficiency of DASA **5**. Determination of the dark equilibrium resulted in %DEQ values >89% at the lower concentrations tested, however at 2×10^{-4} M the %DEQ value dropped considerably, this is thought to have been due to experimental error, as the lid of the UV-Vis

spectrometer may have been accidentally opened between readings. The rate of switching was also rapid, visually the colour change from coloured to near colourless happens within 1 minute in chloroform. Figure 46 exhibits the fast and near complete (>98%) photoisomerization of **5** at each concentration in chloroform.

Table 2 – showing %PSS and % DEQ data for **5**, at concentrations between 5×10^{-6} and 2×10^{-4} M in CHCl_3 .

	%PSS	%DEQ
5×10^{-6} M	99.4%	89.6%
1×10^{-5} M	99.6%	99.6%
1×10^{-4} M	99.8%	99.4%
2×10^{-4} M	99.3%	39.5%

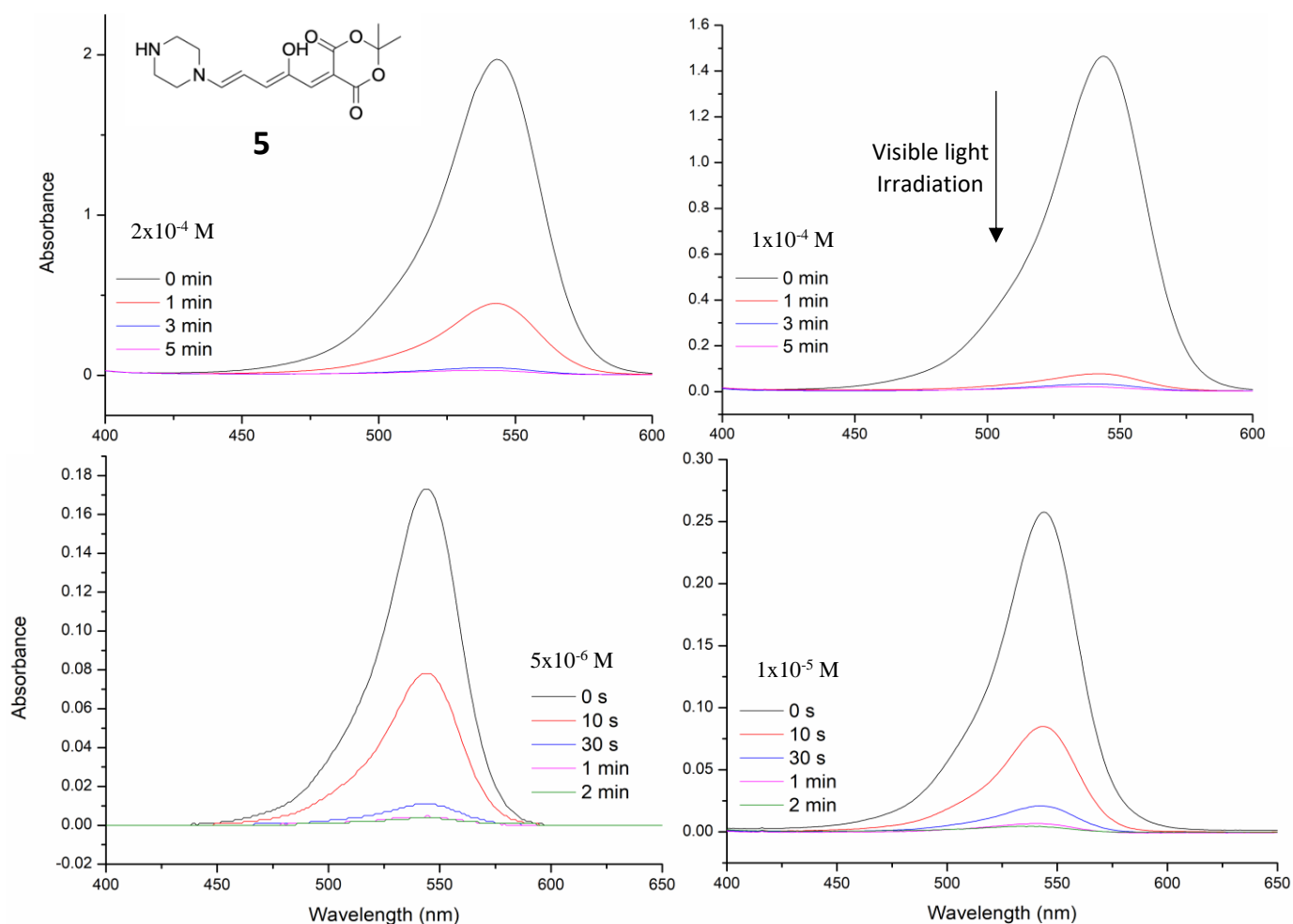
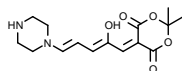


Figure 46. UV-Vis spectra of **5** in chloroform at varying concentrations showing the decrease in absorbance upon irradiation with visible light.

The synthesis of **5** is discussed in chapter 2, see section 2.3.6. The results from testing the photo-switching properties of **5** at concentrations up to 2×10^{-4} M show that the degree of photo-switching (%PSS) does not appear to be affected by photochrome concentration. The %PSS values show nearly all molecules undergo photoisomerisation and cyclization from the coloured to the colourless form. This data suggests that the concentration dependence affecting other DASA molecules does not occur in DASA **5**. Furthermore, the %DEQ values show that in chloroform at lower concentrations **5** appears to have a dark equilibrium where most of molecules exist as the open, coloured isomer shown in Figure 47. This is important as it maximises the photo-switching properties upon illumination, by ensuring the maximum absorbance change is achieved when stimulated with light

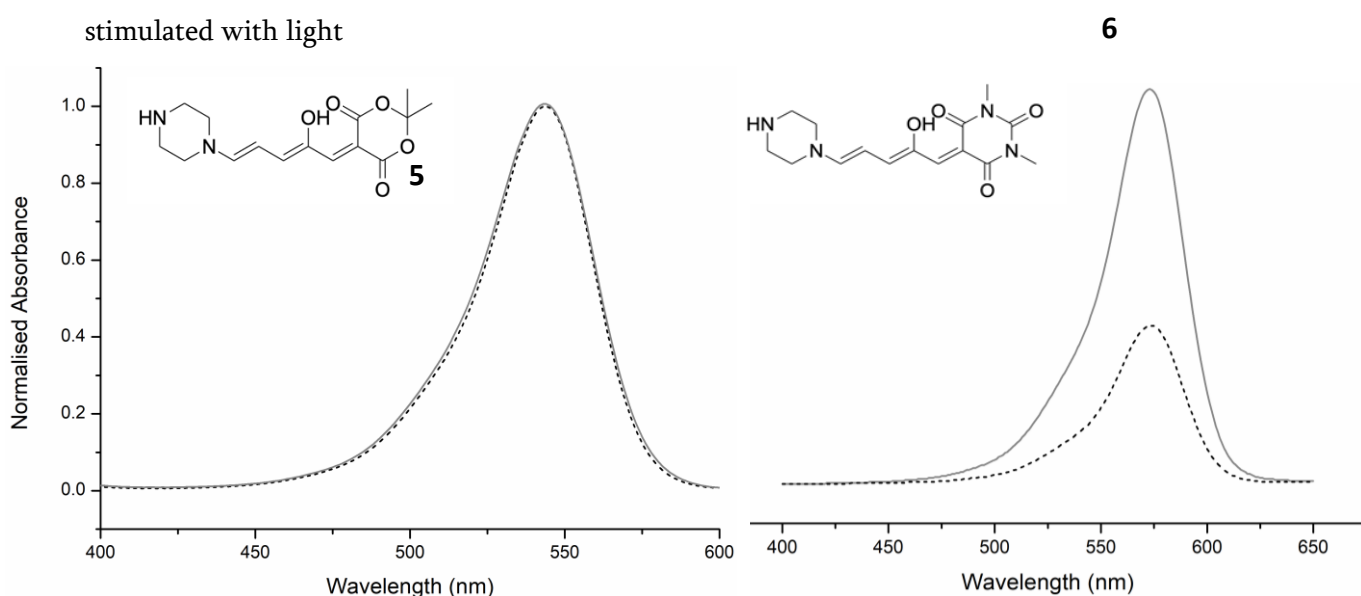


Figure 47. UV-Vis spectra for DASA **5** and **6** showing the Abs_{max} (—) and Abs_{DEQ} (---) at 1×10^{-5} M.

3.3.5 Switching Fatigue of 5. The switching fatigue was tested though exposing samples to multiple cycles of photo-switching stimuli as described in the experimental section. For DASA **5** the high %DEQ values meant that after reaching the PSS under irradiation the reverse isomerisation occurred in the dark without additional heating necessary. Application of heat increases the rate of the thermal reversion substantially however. As Figure 48 shows, heating a 1×10^{-5} M solution of **5** to 50 °C decreases the time of the reverse process by a factor of almost 5

During 6 cycles of sequential irradiation followed by dark at 50 °C, DASA **1** displayed a fatigue of less than 5% permanent photobleaching, shown in figure 49, shown in the same format as the literature.²¹ This is comparable to other first¹ and second generation³ DASAs encouraging the idea that DASAs are fatigue resistant photo-switches. In some cases, extended heating periods would cause minor losses in the absorbance of **5** suggesting that thermal break-down may have

been occurring, therefore it is inconclusive whether **5** was experiencing photochemical fatigue or small amounts of thermal degradation upon repeated cycling. This could be tested by performing cycles without additional heating as the %DEQ values would allow for this

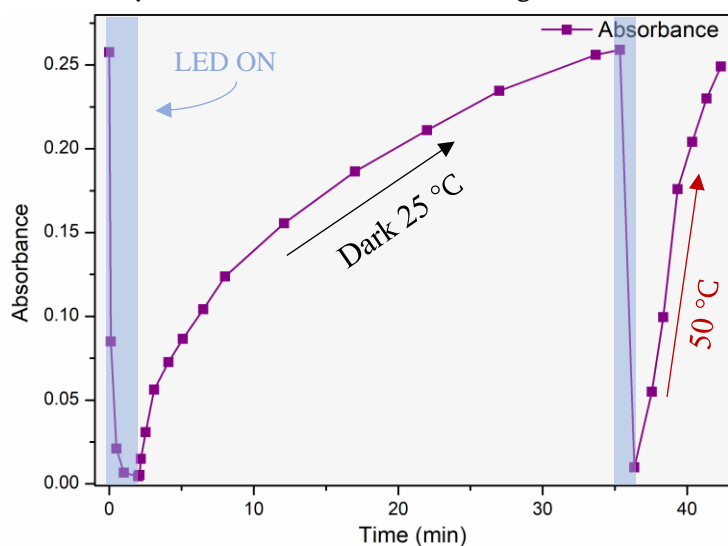


Figure 48. Two switching cycles of **5**, in chloroform (1×10^{-5} M) solution, displayed as absorbance as a function of time. The fully highlighted areas representing periods of irradiation

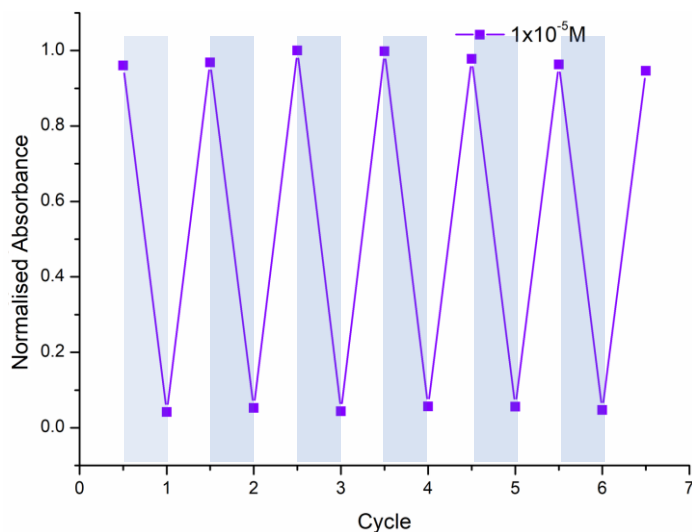


Figure 49. Repeated photo-switching cycles of **5** in chloroform (1×10^{-5} M), the highlighted areas indicate irradiation periods, see experimental section 3.2.2, for full detailed of cycling studies.

3.3.6 Structure Determination of **5 by X-Ray Diffraction.** In addition to the ^1H NMR spectra obtained for compound **5** further structure determination was attained through X-ray diffraction. The crystal structure of the cyclized form was determined, as shown in Figure 50. The structure revealed that for DASA **5** in the solid state, the proton transfers not to the tertiary amine of the donor moiety (N1), as has been observed for all other first generation DASAs, but instead resides on the unreacted secondary amine (N2). The protons were located and clearly visible from the residual electron density in the difference map, attempts to model the proton at the N1 position led to an inferior refinement.

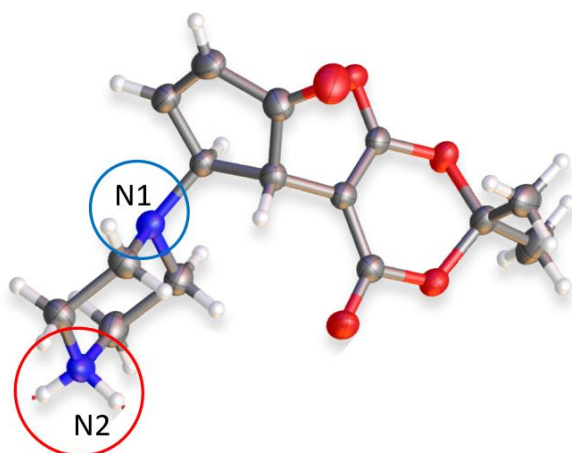
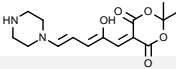


Figure 50. Crystal structure of **5** as the cyclized form, crystallised from H_2O . Red circle (bottom) indicating the position of the transferred proton. Blue circle (top) showing the unprotonated bonding nitrogen.

3.3.7 Photo-switching efficiency of 6. The photo-switching efficiency of **6** was investigated through measuring both the %PSS and %DEQ. The calculated results of the UV-Vis spectroscopy are displayed in table 3. The %PSS was >95% at concentrations up to 1×10^{-3} M/ 1 mM showing the impressive photo-switching efficiency of DASA **6**. Determination of the dark equilibrium resulted in a lot of variance in the %DEQ values obtained, reasons for this are discussed below. The rate of switching was also rapid, to the naked eye, the colour change from coloured to near colourless occurs within 1 minute in chloroform at concentrations up to 1×10^{-4} M. Figure 51 shows the fast and complete photo-switching of **6** up to 1×10^{-4} M. Notably at 1×10^{-3} M the rate of switching slows considerably although the %PSS is still >99%.

Table 3 – showing %PSS and % DEQ data for **6**, at concentrations between 5×10^{-6} and 2×10^{-4} M in CHCl_3 .

		
	%PSS	%DEQ
5×10^{-6} M	95.1%	61.9%
1×10^{-5} M	98.9%	38.9%
1×10^{-4} M	99.4%	46.9%
2×10^{-4} M	99.5%	-

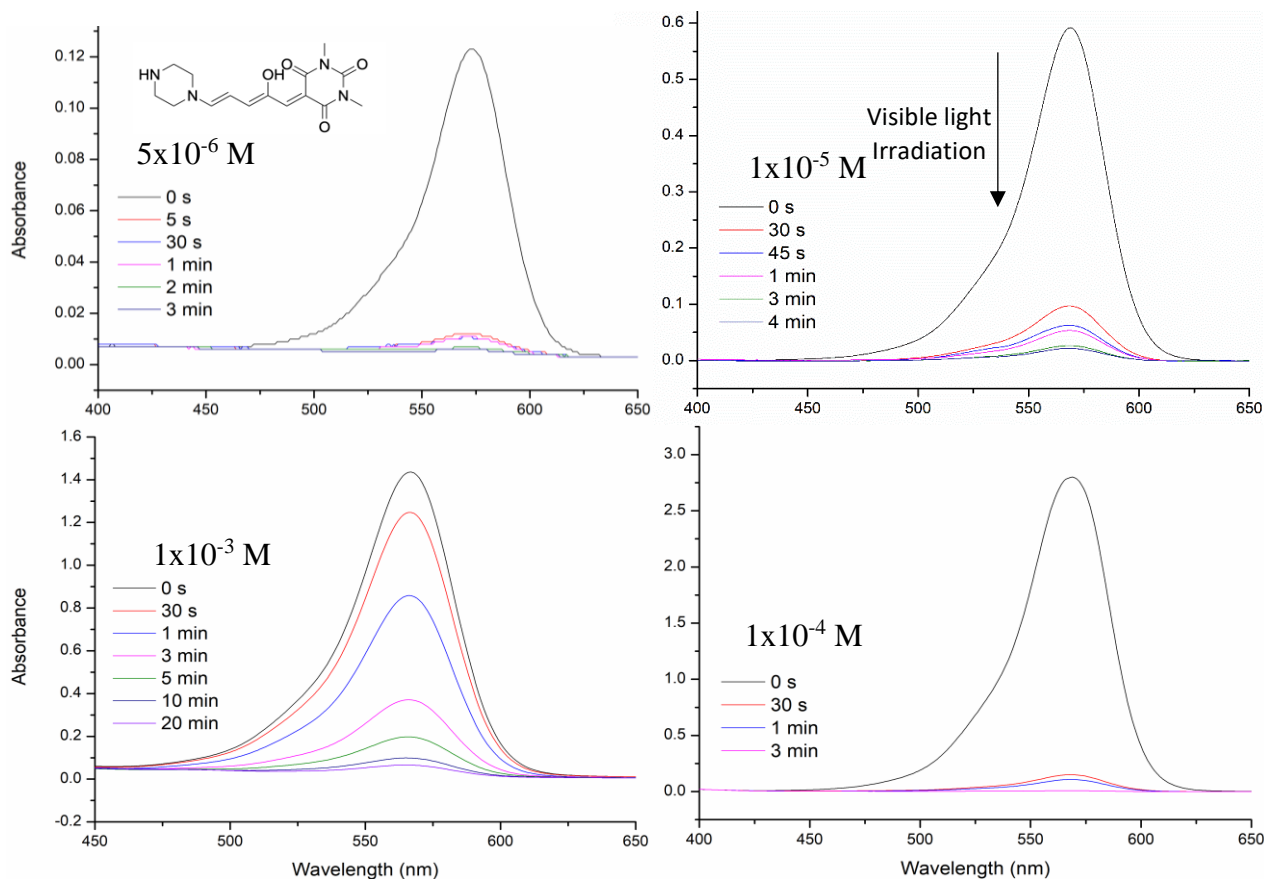


Figure 51. UV-Vis spectra of **6** in chloroform at varying concentrations showing the decrease in absorbance upon irradiation with visible light.

The synthesis of **6** is discussed in chapter 2, see section 2.3.7. The results from testing the photo-switching properties of **6** at concentrations up to 1×10^{-3} M show that the degree of photo-switching (%PSS) does not appear to be affected by photochrome concentration. The high %PSS values at each concentration mean nearly all molecules undergo photoisomerisation and cyclization from the coloured to the colourless form. This data suggests that, consistent with **5**, the concentration dependence affecting other DASA molecules does not inhibit the photo-switching of DASA **6**. However, unlike **5**, the %DEQ values for DASA **6** are less than optimal, see fig. 47, with the equilibrium values being in a range between 30 and 62%, meaning that the ratio of open to cyclized molecules in solution in the dark at approximately 23 °C is undefined. The sensitivity of the thermodynamic equilibrium of DASAs is highly dependent on temperature,⁴ both the dark equilibrium and at the PSS. DASA **6** is especially sensitive to changes in temperature, even $<5^\circ\text{C}$, which may explain why the %DEQ values lacked consistency.

3.3.8 Switching Fatigue of 6. The switching fatigue was tested though exposing samples to multiple cycles of photo-switching stimuli as described in the experimental section. For DASA **6** the %DEQ values meant that after reaching the PSS under irradiation, the reverse isomerisation in the dark required heating to 50 °C fully recover the absorbance. DASA **6** does not appear to have the fatigue resistance shown by **5**, with over 50% of the molecules permanently bleaching over 9

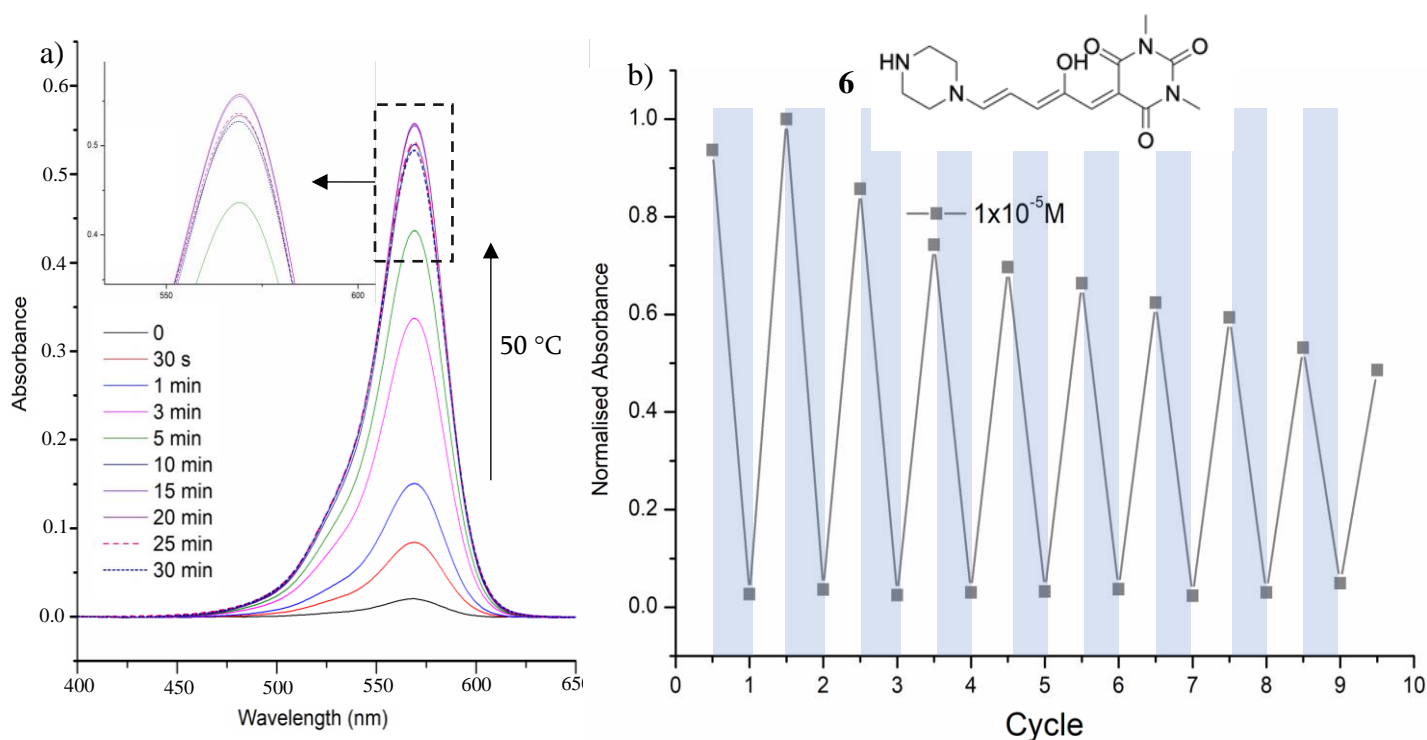


Figure 52. a) UV-Vis spectrum of a 1×10^{-5} M solution of **6** in chloroform illustrating the thermal reversion process. b) Structure of DASA **6** and repeated photo-switching cycles in chloroform (1×10^{-5} M), highlighted areas indicate irradiation periods.

cycles, shown in Figure 52b. During the cycling it was found that on prolonged heating there was a decrease in the absorbance recorded for solutions of **6**, shown in Figure 50a, suggesting thermal breakdown.

The temperature sensitivity of **6** is speculated to be a major factor in the undesirable fatigue observed from the cycling studies. The 50% loss in the recovered absorbance over nine switching cycles could be due to the thermal instability of **6** and not photochemical fatigue. As shown additional heating caused a decrease in the absorbance after a given time, Figure 52a, suggesting the thermal breakdown of **6** at 50°C. Unfortunately, this complicates the situation as it is inconclusive whether permanent bleaching or thermal degradation is occurring. Although, we can conclude that either thermal degradation or permanent bleaching does occur for **6** in solutions of chloroform. To further investigate this, cycling studies could be performed at lower temperatures to limit the potential for thermal breakdown, and focus the testing on photochemical fatigue.

3.3.9 Computational Studies. The minimum energy conformations were calculated for the cyclized form of DASAs **5** and **7** in order to help give some information into the behaviour of the molecules in CHCl₃. Figure 53 shows the lowest energy conformations modelled at the semi-empirical PM7 level. Notably the calculations modelled the unreacted amine as being the site for the proton transfer on DASA **5** without intervention and models are slightly varied in their conformations, due to the changes in the proton transfer. For **7** the intramolecular hydrogen bond is between the protonated bonding amine and one of the carbonyl moieties on the acceptor, whereas for **5** this interaction occurs between the unreacted amine on the piperazine moiety and the acceptor and indicated in figure 53. The conformations shown for **5** and **7** had a calculated heat of formation of -846.60 kJ mol⁻¹ and -834.76 kJ mol⁻¹ respectively.

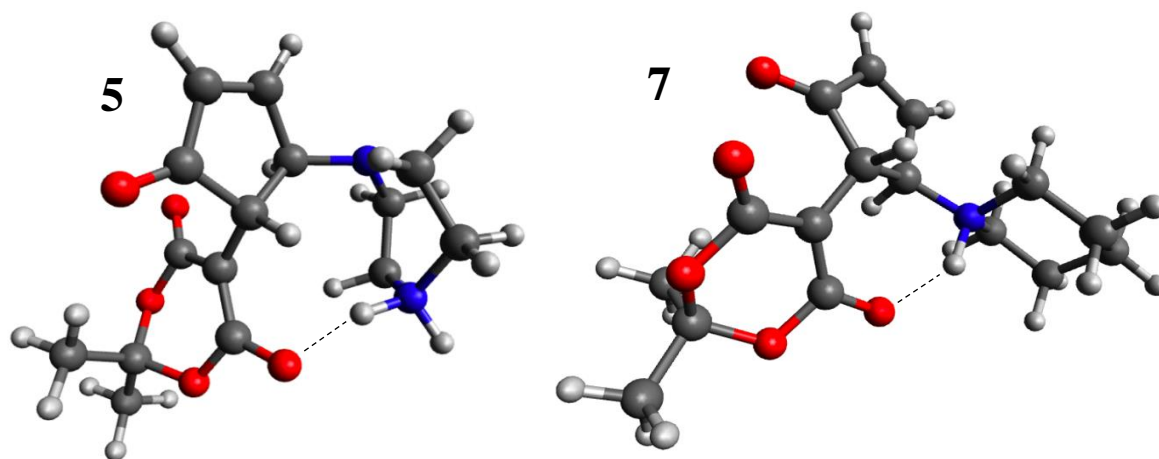


Figure 53. Computational models of the cyclized forms of DASA **5** (left) and **7** (right), the dotted line indicating the intramolecular hydrogen bond.

3.4 Comparisons

The previously unreported mono-substituted piperazine DASAs **5** and **6**, have shown impressive photo-switching properties which do not follow the trends seen in other DASA molecules.¹⁶ DASAs **7** and **8** were synthesised in order to compare photo-switching properties with **5** and **6** and to illustrate the differences in terms of the reported concentration dependence of DASA molecules. Not only the photochemical properties differed, some physical properties varied also. **5** and **6** are less soluble in non-polar solvents such as chloroform, dichloromethane and toluene than **7** and **8**, likely due to the increased polarity from the unreacted amine. The colour of the powdered samples was also drastically different between **5** and **7**, being a dark purple and bright red respectively, although solutions of either molecule were more similar in colour. Knowing this, a slight bathochromic shift in the absorption band would be expected, which there was although very minor at only a few nm, seen in Figure 54. DASA **6** and **8** were very similar in colour, both shades of purple and the same bathochromic shift in absorption from the piperidine to the piperazine variant was observed, shown in Figure 54.

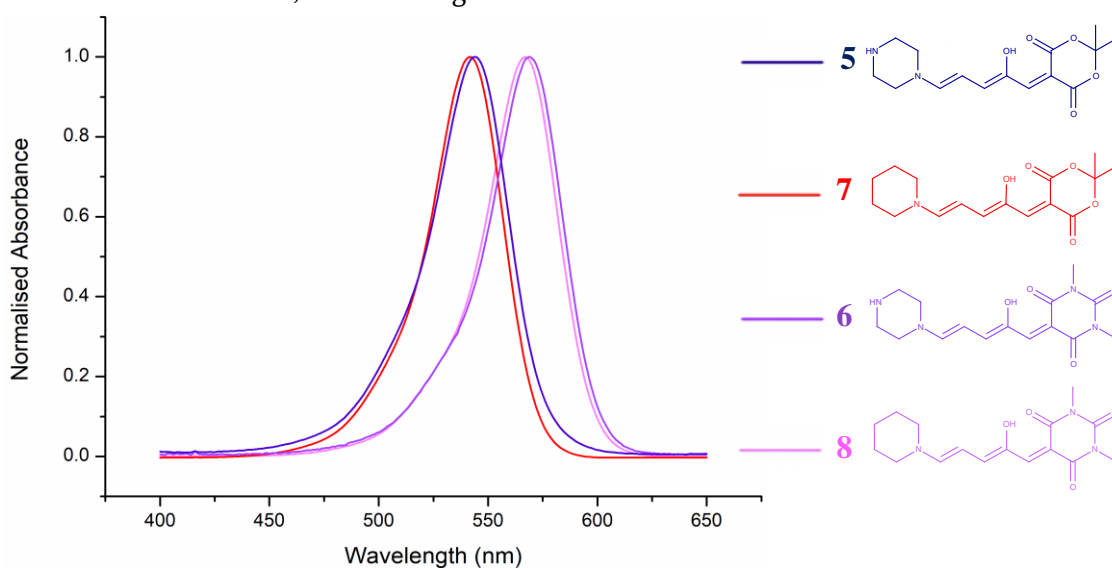


Figure 54. Absorption spectra of DASAs **5**, **6**, **7**, and **8** displaying the minor bathochromic shift in absorbance moving from the piperidine to the piperazine donor. The DASA structures (right side) are coloured according to physical colour of powdered samples.

There was a visual difference in the photo-switching properties as solutions of **7** and **8** did not completely decolourise, however solutions of **5** and **6** at the same concentrations would become completely colourless after irradiation. The %PSS was determined at a variety of concentrations in chloroform, shown in Tables 1, 2, and 3. Figure 55 shows the results of the measurements with the recorded absorbance plotted as a function of time. From the plotted data it is clear to see that **5** and **6** have high %PSS with >95% of the molecules cyclized once the PSS is reached, whereas for **8** even

at the lowest concentrations the %PSS is only 66.43%. As the concentration increases this value decreases further with barely any isomerisation occurring at 2×10^{-4} M. Similarly, the maximum %PSS observed for **7** is <90% with values decreasing further as concentration increases.

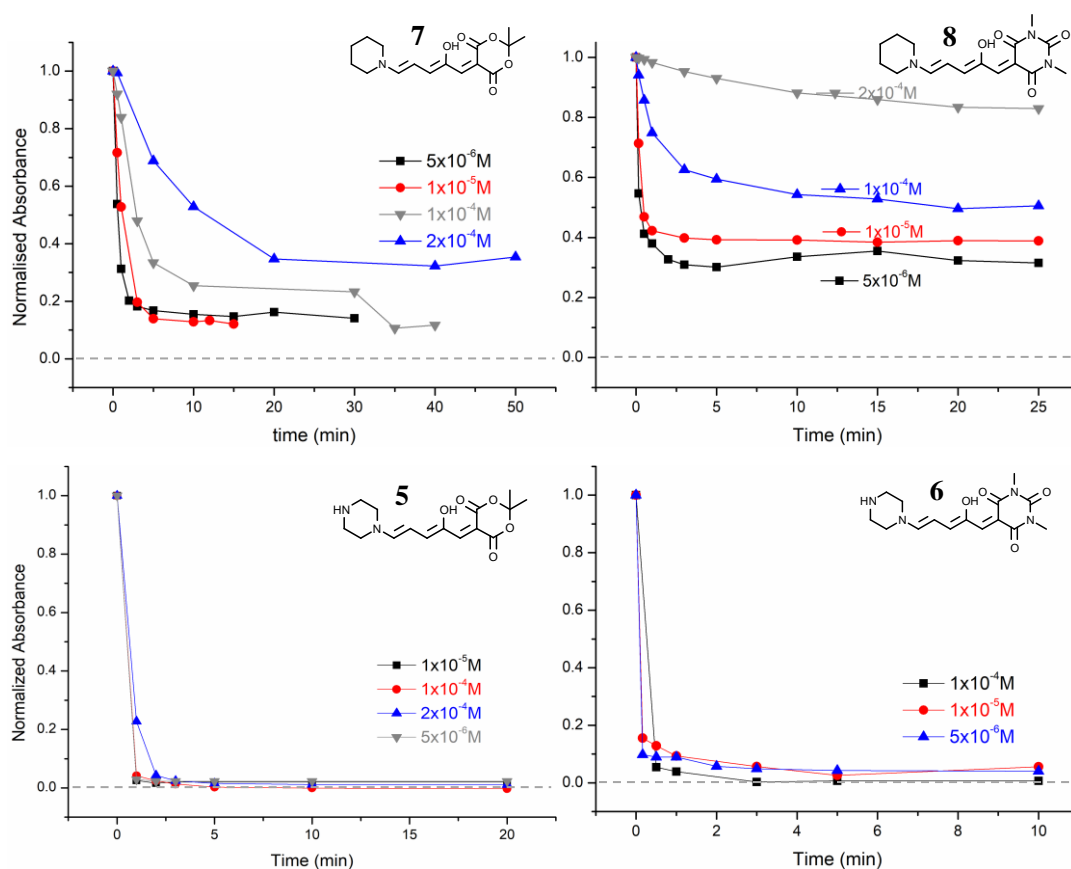


Figure 55. Absorption data for DASAs **5**, **6**, **7** and **8** showing absorption as a function of time illustrating the different %PSS achieved by each DASA molecule. Dotted line indicates zero absorbance.

Consistent with other DASAs published previously the photo-switching rate and %PSS of the piperidine DASAs are concentration dependent; switching rate and %PSS decrease with increasing photochrome concentration. Conversely, the piperazine DASAs **5** and **6** show no clear relationship between %PSS and concentration up to that which was tested. Only the photo-switching rate changed, decreasing with increased concentration. The effect is observed at higher concentrations, as Figure 56 shows the 1×10^{-3} M solution of **6** takes an additional 7 minutes of irradiation, but a similar %PSS is achieved as the lower concentrations, as Table 2 and Figure 46 in the results showed. A 1×10^{-3} M solution of **7** on the other hand showed essentially no isomerisation or colour change, shown in Figure 56. It is also important to note that this is reaching the concentration limit for solutions of **5** and **6** in chloroform, therefore it may be possible to assume that at all possible concentrations >90% %PSS can be achieved. From the data acquired it is obvious that there is a difference in the photo-switching ability of **5** and **6** when compared to **7** and **8**. The

only difference between the molecular structures is the unreacted amine on the piperazine DASAs, therefore the variation in the properties must be due to this and how it affects the photo-switching and the behaviour of the molecules in solution

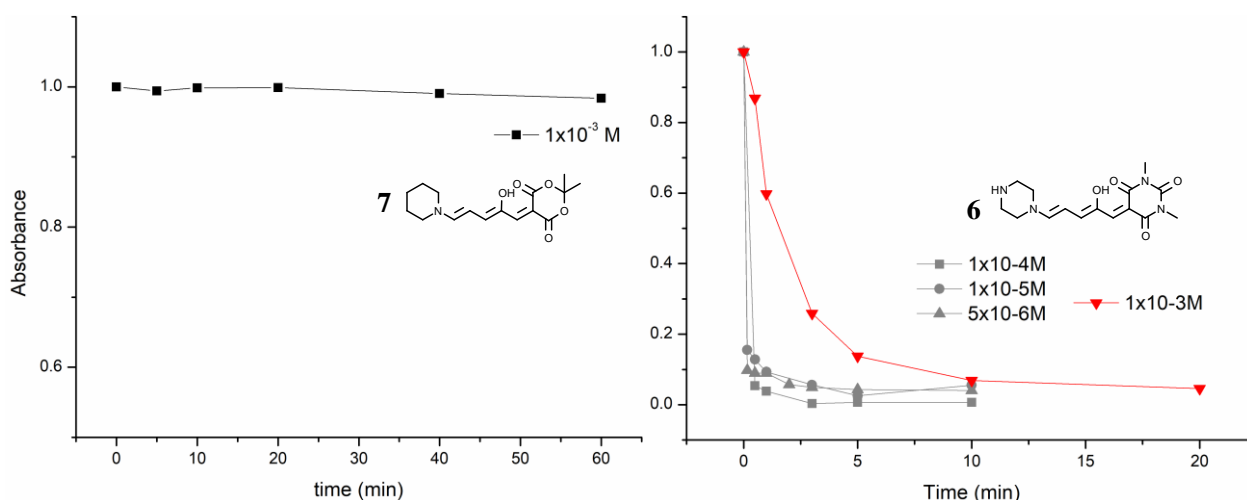


Figure 56. Absorption data for DASAs **2** and **4** showing in absorption as a function of time illustrating the different %PSS achieved by the each DASA molecule.

From the X-ray diffraction data the cyclized structure of **5** was determined, and as shown in Figures 50 and 57a, the unreacted amine becomes protonated in the proton transfer steps of the photo-switching mechanism. In contrast to all other first generation DASA molecules where this proton transfers onto the bonding amine, shown in Figure 57b in the crystal structure of **7** taken from the literature.² The report which highlighted the concentration dependence of DASA molecules¹⁶ suggested that the reason for the phenomenon was “long-range Coulombic interactions” which interfere with the electrocyclization steps of the isomerisation. Considering that polarization of the triene is necessary for a successful cyclization, long range coulombic

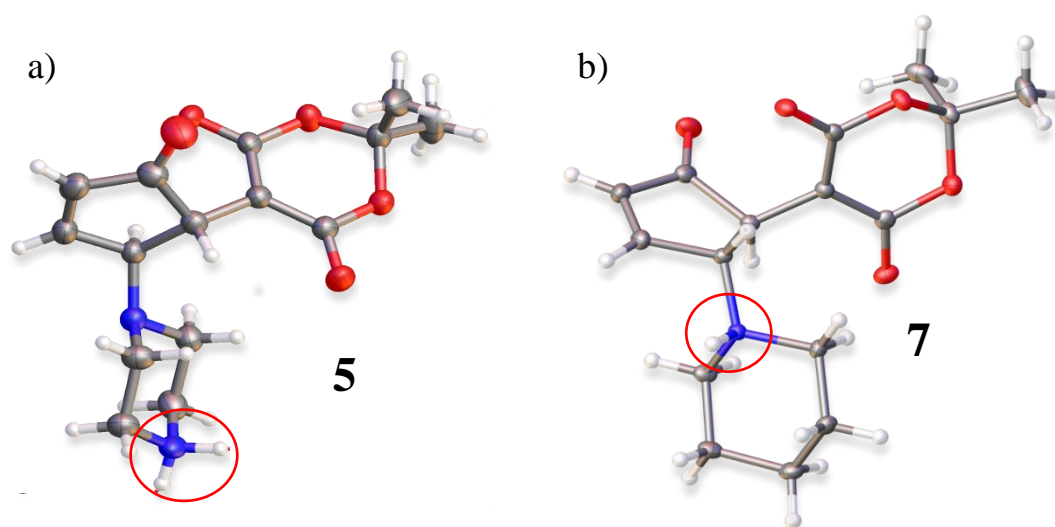


Figure 57. a) Crystal structure of **5** obtained through single crystal X-ray diffraction. b) Crystal structure of **7**. Reprinted with permission from ref. 22. Copyright© 2014, American Chemical Society.

interactions could indeed become a hinderance. If the hydroxyl group or carbonyl moieties of an uncyclized molecule interact with the charges on a neighbouring cyclized molecule the polarization of the triene could be interrupted, stopping the isomerisation moving past the photo-induced steps, which are not affected by concentration.¹⁶

The differences in the proton transfer and cyclised structured could allow for stronger intramolecular interactions between the zwitterionic components on the donor and acceptor moieties. The increased separation of the charges compared with other DASAs, could be eliminating some steric hindrance allowing for a stronger interaction. This stronger interaction could in turn limit the strength of intermolecular coulombic interactions affecting the electrocyclization steps. This is further supported by the semiempirical calculation performed, the computational models showed slight differences in the conformations of **5** and **7** shown in Figure 53. Visually the models suggest a stronger hydrogen bonding interaction for **5** due to the increased conformational freedom of the interaction. The computationally modelled conformation was not found in any crystallography data, however the crystals were grown in water and the photo-switching data was recorded in chloroform, additionally the solid state structures do not represent the behaviour of molecules in solution. The computational data also showed the cyclized conformation of **5** to be lower in energy than the linear form in chloroform, which could be a factor in the lack of concentration dependence as the equilibrium will favour the lowest energy form.

3.5 Conclusions

In part one of this project the attempted synthesis of isolated bi-functional symmetric DASAs was not successful, reactions between the activated furfural intermediates (**M-Int** and **B-Int**) and the selected di-amine donors (**PZ** and **TBP**) resulted in either the mono-substituted product alone or mixtures of the mono- and di-substituted products. After repeated attempts only the mono-substituted piperazine DASAs **5** and **6** could be synthesised in isolation, full conclusions for this can be found in chapter 2.

Although the photochromic properties of bi-functional DASA molecules could not be tested, investigating the properties of the previously undiscovered DASAs **5** and **6** revealed excellent photo-switching efficiency in terms of the %PSS and the rate of photo-switching. There appears to be no degradation caused by the unreacted amine present for **5**, furthermore DASA **5** shows minor fatigue across multiple switching cycles. DASA **6** showed signs of thermal instability and does not share the same fatigue resistance as **5**, with only 50% of the absorbance recovered over

9 switching cycles. The concentration dependence of **5** and **6** was investigated through comparisons with DASAs **7** and **8** and it was found that the new DASA molecules do not exhibit the same photo-switching properties. **5** and **6** demonstrate no concentration dependence in regard to %PSS in contrast to **7** and **8** where the %PSS is highly concentration dependent. The rate of photo-switching was found to be concentration dependent for all compounds, decreasing switching speeds as concentration increased.

The structural changes to the molecules caused by the unreacted amine are speculated to be the reason for the differences in the properties of **5** and **6** when compared to **7** and **8**. X-ray crystallography determined that the free amine effects the cyclized structure of the molecules, through changing where the proton transfers to during the electrocyclization. The changed structure could allow for different conformations which could limit intermolecular interactions that have been speculated as the cause of the concentration dependence. DASA **5** and **6** show that the DASA family of photo-switches is still not fully understood and that there are still ways the molecular design could be optimised to generate the most desirable properties for photo-switching.

The intermolecular interactions are still not fully understood, and the reasons for the concentration dependence are still unclear but the results of this investigation suggest that the balance between intra- and intermolecular interactions likely do play a role in the phenomenon. This could be further investigated computationally with higher level modelling of the molecules and the intermolecular interactions, or synthetically by designing additional DASA molecules with other potential sites for proton transfer, through using donors such as imidazolines and other heterocyclic compounds containing two nitrogen atoms.

The uniqueness of the unreacted amine's ability to produce the advantageous photochromic properties could be investigated through comparisons with a DASA synthesised using morpholine as the donor group. Comparing the photo-switching properties of the DASAs will indicate if the unreacted amine is a necessity, or if the changes in the distribution of electron density on the donor alone can eliminate the concentration dependence that is observed for other DASA molecules.

Chapter 4 – Solid-State Photo-Switching

4.1 Introduction

As noted in chapter 1, the solid-state properties of DASAs are the least studied aspect of the family of photochromes and no solid-state photo-switching has been reported for DASA molecules to date. During synthesis, reported in chapters 2 and 3, a number of crystals were isolated and the structures determined; preliminary investigations into the crystals revealed some interesting switching properties. Furthermore, powdered samples exposed to light gave some indications that solid-state switching could occur. While a full study of solid-state switching is beyond the scope of the present work, the following investigation into the solid-state observations made of DASA **8** are a preliminary study in the area that has the potential to make a substantial impact in the field of DASA materials.

4.2 Experimental

The procedure for the synthesis of compound **8** is presented in chapter 3. Solvent evaporation and vapour diffusion crystallisation were the techniques used to isolate crystals, as detailed below.

Powdered X-ray Diffraction (PXRD). Powder X-ray diffraction patterns were recorded using a Rigaku miniflex 600 X-ray diffractometer, using Cu K α radiation ($\lambda = 1.54413 \text{ \AA}$) operating at 40 kV and 15 mA (2θ range $5^\circ - 40^\circ$).

Single crystal X-ray diffraction (SCXRD). Single crystal diffraction data were collected using an Oxford Diffraction SuperNova, using Cu K α radiation ($\lambda = 1.54413 \text{ \AA}$) with an AtlasS2 detector. Crystals were kept at 100 K during data collection. Using Olex2,⁷² the structure was solved with the ShelXT⁷³ structure solution program using Direct Methods and refined with the ShelXL⁷⁴ refinement package using Least Squares minimisation.

Fourier Transform Infrared Spectroscopy (FT-IR). FT-IR spectroscopy was recorded using a Shimadzu IRAfinity-1 FT-IR spectrometer.

4.3 Results and Discussion

4.3.1 Single Crystals.

4.3.1.1 Dichloromethane Solvate. Three crystal structures were determined for compound **8**, crystallised from 3 different solvents. Crystals were isolated in dichloromethane (DCM) without extensive efforts, and the DCM solvated structure in Figure 58a was determined, full crystallographic data are presented in Appendix 2.3. The structure is of the cyclised DASA form, and the crystals were highly crystalline and appeared purple as shown in Figure 58b. Over 72 hours in ambient conditions discoloration occurred in addition to a loss of crystallinity as shown in Figure 58c; then when heat was applied some recolouration occurred, seen in Figure 58d.

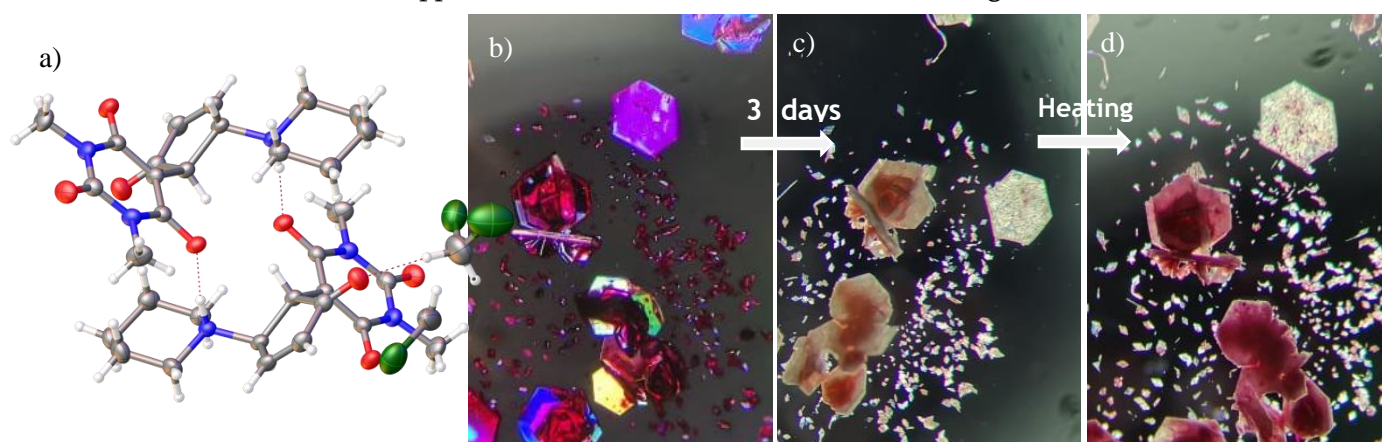


Figure 58. a) Crystal structure of the DCM solvated form of **8**. b) Image of crystals upon discovery soon after removal of solvent, appearing coloured and crystalline. c) Image of crystals after 3 days under ambient conditions, appearing colourless and having lost crystallinity. d) Image of crystals after heating applied via a heat gun.

No further characterisation was possible through X-ray diffraction after the discolouration due to the loss in crystallinity, suggesting some amount of internal strain was generated with the colour change. The photo- and thermochromic behaviour imply that the DASAs may be switching in the solid-state, such solid-state switching would generate significant strain within the crystal, which may be the source of the loss of crystallinity. The loss in crystallinity may also be associated with loss of DCM from the crystal lattice.

However, considering the crystal structure obtained is the cyclised colourless form one would expect the crystals to be colourless, not purple. Closer inspection, using the microscope, revealed the purple colour was due to solvent residues present on the surfaces of the crystal rather than any intrinsic colour. The recolouration upon heating is speculated to be due to remaining solvent within the crystals dissolving small amounts of the crystal as it evaporates causing the colour to appear, as the coloured form of the molecule is favoured in solutions of DCM, especially when

heated. Moreover, the smaller crystals did not recolour to the same extent as larger crystals, possibly because it was easier for any DMC to escape without heating applied.

4.3.1.2 Water Solvate. Large, good quality single crystals, seen in Figure 59a, were easily obtained from solution in water, due to the relatively high solubility and slow evaporation rates. The crystals isolated were water solvates, depicted in Figure 59b. Consistent with the DCM solvate, the crystals contained the cyclized form of **8**, as expected due to the favourability of the zwitterion form in polar protic solvents. No changes were observed from the crystals when left under ambient conditions.

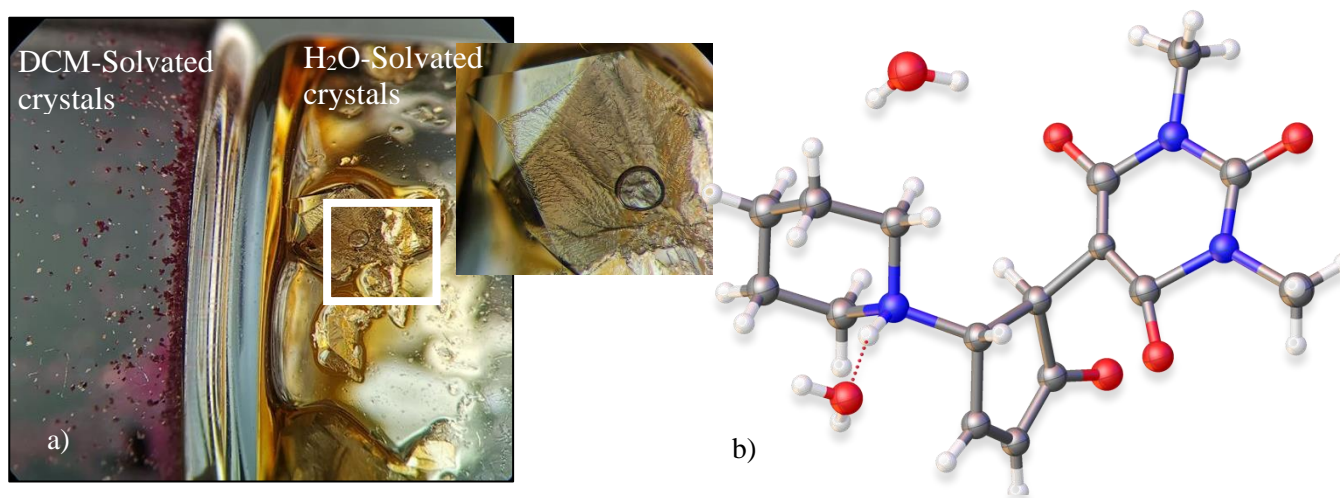


Figure 59. a) Images depicting DCM-solvated crystals (left) and water solvated crystals (right). b) Crystal structure of water solvated form of **8**.

However, when heating the crystals there was an obvious colour change from yellow-colourless to a pink-purple, shown in Figure 60, as the images show this was not an isolated event. Notably, the crystal in Figure 60a fractured and lengthened slightly as the colour change occurred, suggestive of DASA switching, although this motion was isolated to that particular crystal. Similarly with the DCM solvate structure determination was not possible after the colour change, attempts to run variable temperature X-ray diffraction experiments to probe the structure as the colour change occurred were prevented by cracking of the crystal. This meant no further diffraction data could be obtained for the crystals. The colour would fade over time in leaving the crystals in ambient conditions in the light, shown in Figure 61, then upon reheating the colour would appear again.

Unlike the DCM-solvated crystals it is less likely that solvent molecules evaporating from within the crystal are causing the colour to appear as water favours the colourless form, and

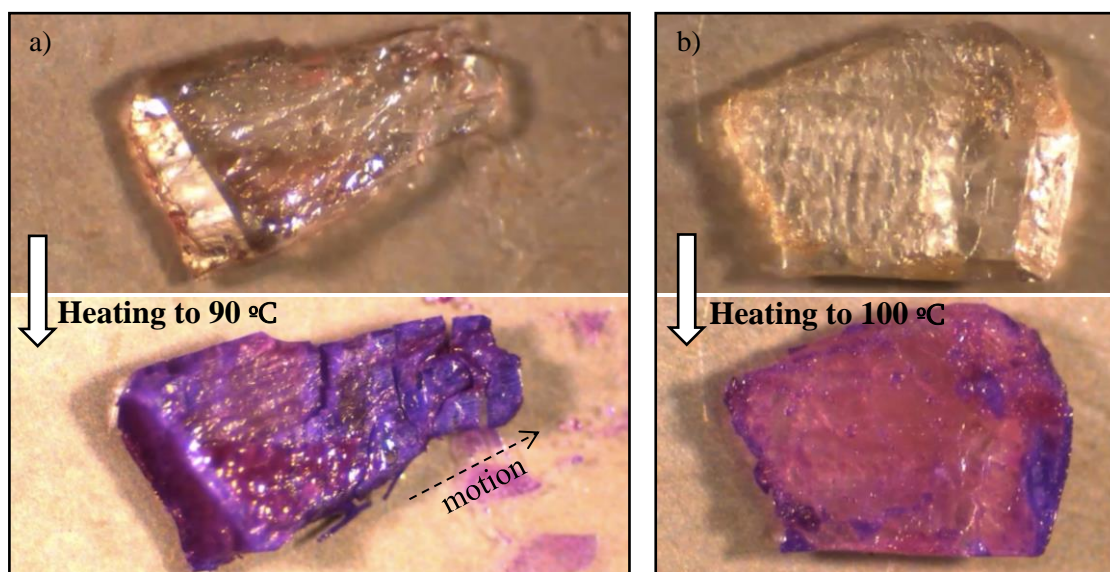


Figure 60. Images of the H_2O -solvate crystals of **8**, showing the colour change from near colourless to purple upon heating

solutions in water are not coloured, even when heated. Furthermore, the slight change in the shape of the crystal, shown in Figure 60a, indicates some amount of internal strain within the crystal, especially as the long axis of the crystal lengthens and the cracks form along the short axis. This motion and cracking could be due to the elongation of the DASA molecules as they isomerise from the compact cyclized form to the elongated triene form although no clear crystallographic or spectroscopic data yet exists to support that analysis.

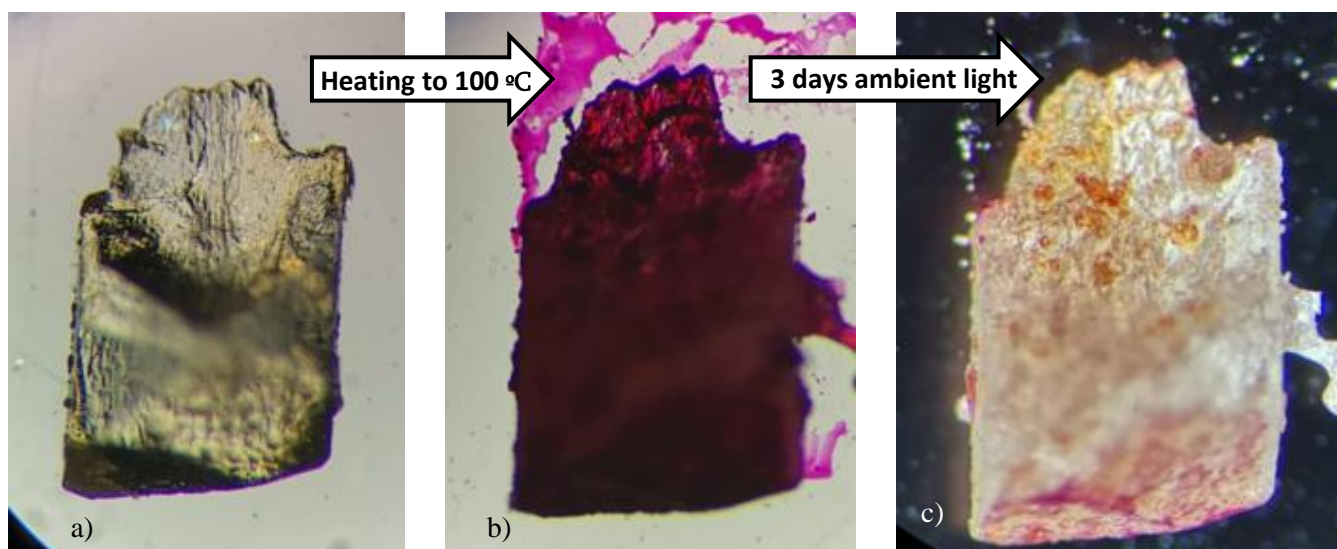


Figure 61. Images of single crystal of the water solvate, a) after isolation, b) After heating, c) after 3 days in ambient lighting conditions.

4.3.1.3 Un-Solvated Form. Single crystals were isolated from solutions in methanol after the solutions became colourless. The structure was determined with no solvate molecules found, shown in Figure 62a, full crystallographic data are presented in Appendix 2.2. Consistent with the DCM and water solvated forms, the DASA was crystallised as the cyclized form. The crystals were

colourless, shown in Figure 62b (blue colour present from microscope polarizer) although when heated a pink colour was observed, shown in Figure 62c. The crystals did not completely colourise and the colouration was inconsistent, appearing more as a surface covering, moreover it appeared that where the crystals overlap residual solvent was trapped and the colour seemed visibly darker there. This suggests the colour arises from residual methanol around and in-between the crystals causing a solution-based colour change as the area is heated. However, in solutions of methanol DASA photo-switching is irreversible, the colour cannot be recovered in solution through heating, so this is unlikely to be the case, further investigation is necessary.

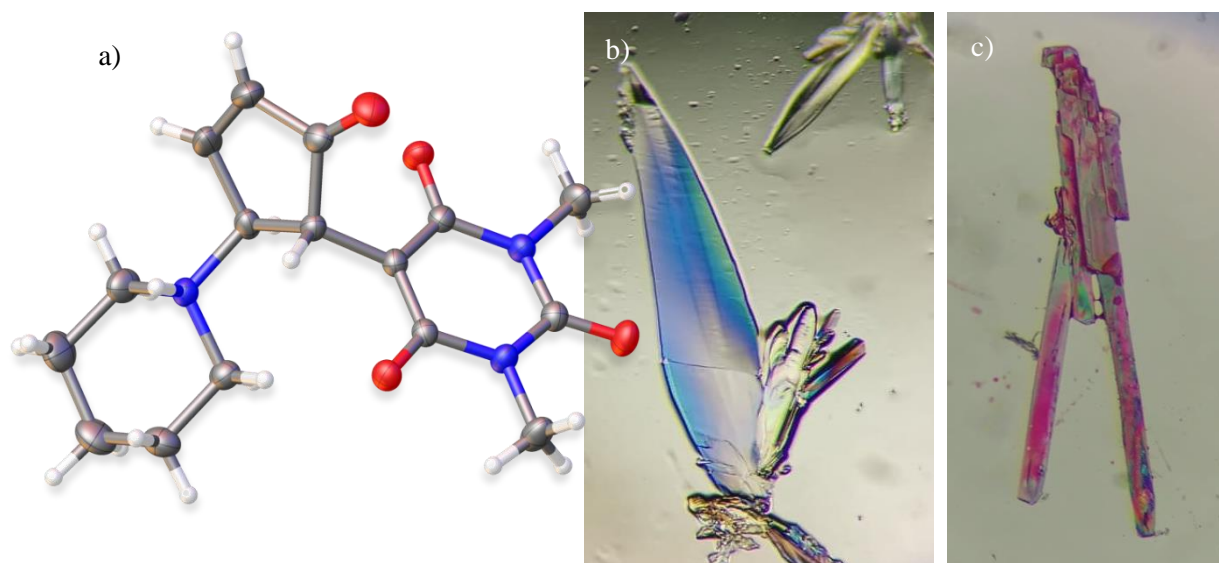


Figure 62. a) Crystal structure of the un-solvated form of **8**. b) Image of crystals after growth, blue colour is due to light polarization effects. c) Image of crystals after being heated

4.3.2 Powdered samples. In addition to possible solid-state switching of single crystals the powdered samples of **8**, produced from reactions in THF with no post reaction crystallisation demonstrated what seemed to be solid-state photo-switching. As seen in Figure 63a the powder tended toward colourless from purple under ambient lighting. Upon the addition of heating with a heat gun at 450 °C for a few seconds, the purple colour returned in a reversible manner, as shown in Figure 63b. Assuming complete discoloration of the powder was occurring, rather than just the surface suggested that loss of solvent was the causing the discoloration and not DASA photochromism, as light cannot penetrate through the powder and illuminate the inside. However, if this was the case recolouration upon heating should not have been possible. Clearly further work is needed to understand the origin of the visible colour change in these materials.

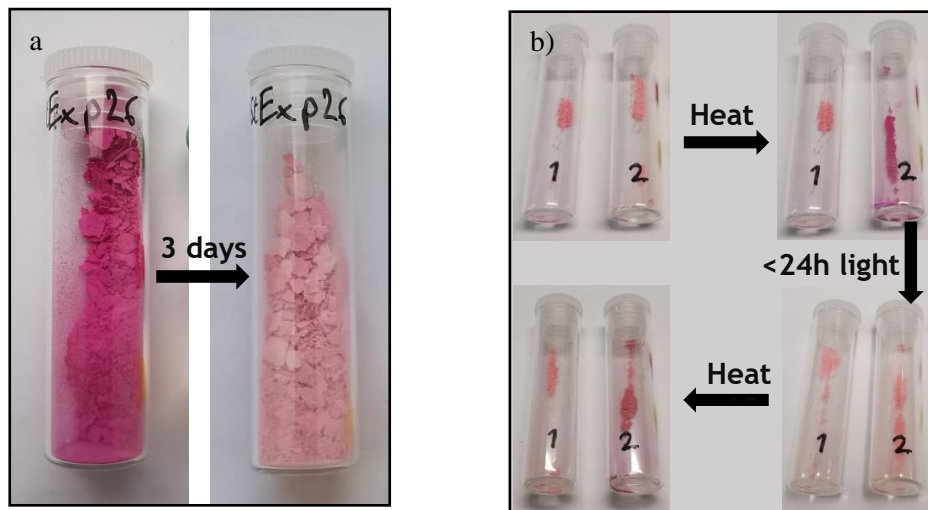


Figure 63. a) Images of powdered samples of **8** undergoing colour change from purple to light pink, in ambient conditions. b) Images of powdered samples of **8** after heating and illumination showing both the reversibility and repeatability of the colour change. Vial 1 represents a reference sample that was left in ambient light and not heated, for comparison with 2.

The ^1H NMR shown in chapter 3, contained a broad peak with a chemical shift indicative of water, this was also speculated to be causing the colour change as water heavily favours the colourless form. To test this, desiccation experiments were performed in the dark and under illumination to assess the effect of removing atmospheric water. Figure 64 shows the results, and it is clear that the desiccated sample in the dark exhibited little or no colour change (Fig. 64a), whereas the desiccated sample that was under illumination demonstrated a large colour change to the pale pink seen in Figure 64b. These results indicate that when removing atmospheric water visible light

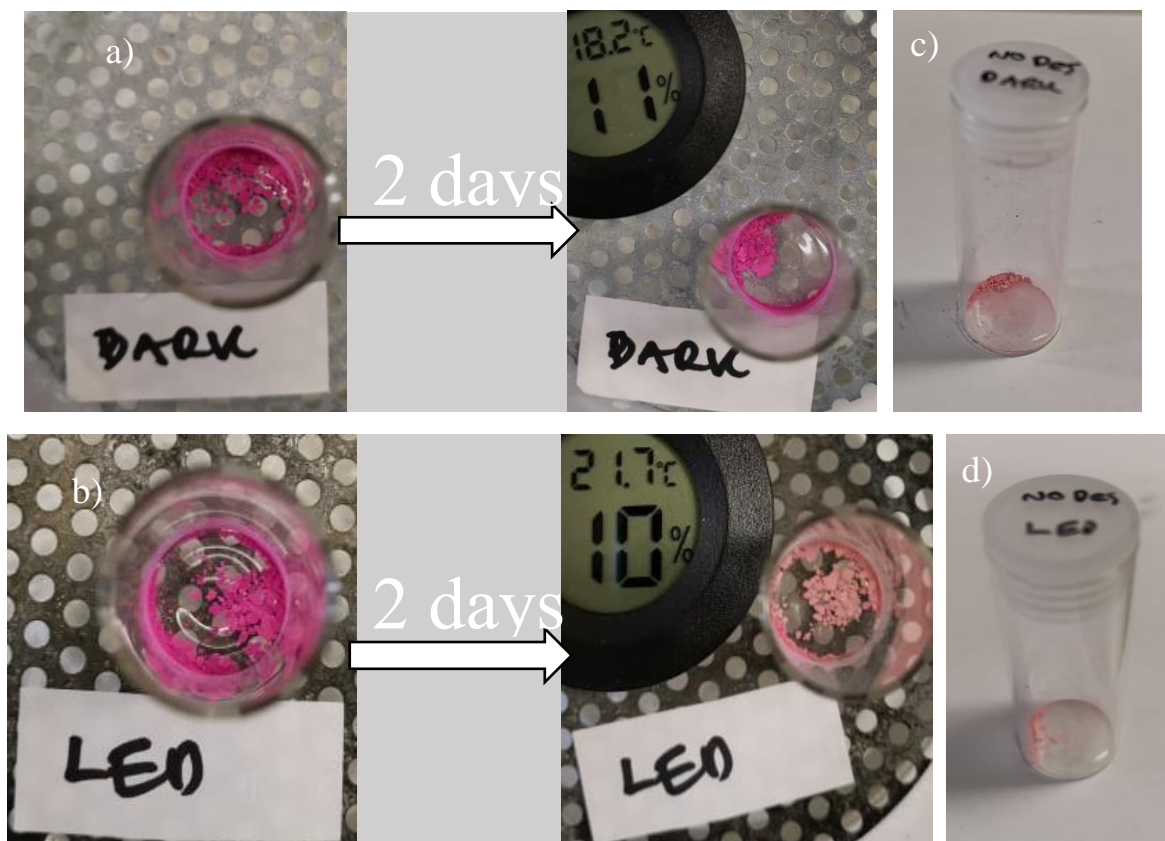


Figure 64. a) Desiccated sample which was placed in a dark cupboard. b) Desiccated sample that was placed under LED illumination. c) Non-desiccated control sample placed in a dark cupboard. d) Non-desiccated control sample placed under LED illumination.

irradiation causes a colour change to occur, and no colour change is observed in the dark, suggesting that DASA photochromism is responsible. However, non-desiccated control samples left in the same environment as the desiccated samples both became pale in colour, seen in Figure 64c,d. This suggests that water trapped within the powder can also cause some colour change to occur both illuminated and in the dark. These results indicate there are multiple factors affecting the colour changing properties of these materials and both lattice water, light irradiation and temperature play a significant role.

Infrared spectra for the pale and purple powders are shown in Figure 65, along with stacked X-ray diffraction powder patterns. Neither technique was able to form strong distinctions between the purple and pale powders. The patterns obtained are essentially identical with the only obvious changes being to the intensity of peaks of the IR spectrum, and an additional peak, highlighted in Figure 65a, appeared in the PXRD when heating the powder from pale to purple. If DASA photo-switching is responsible for the colour change, then the lack of changes seen in the XRD could be explained by only one form being crystalline, in that case XRD measurements would only ever identify this form as the non-crystalline form would not interact with the X-rays. However, the IR spectra should illustrate changes between a DASAs open, and cyclised forms as multiple IR active bands are changed during photoisomerisation including an increase in the number of carbonyl bonds, which one would imagine to be clearly visible through IR spectroscopy. Further investigation is necessary to determine the exact cause of the colour change observed.

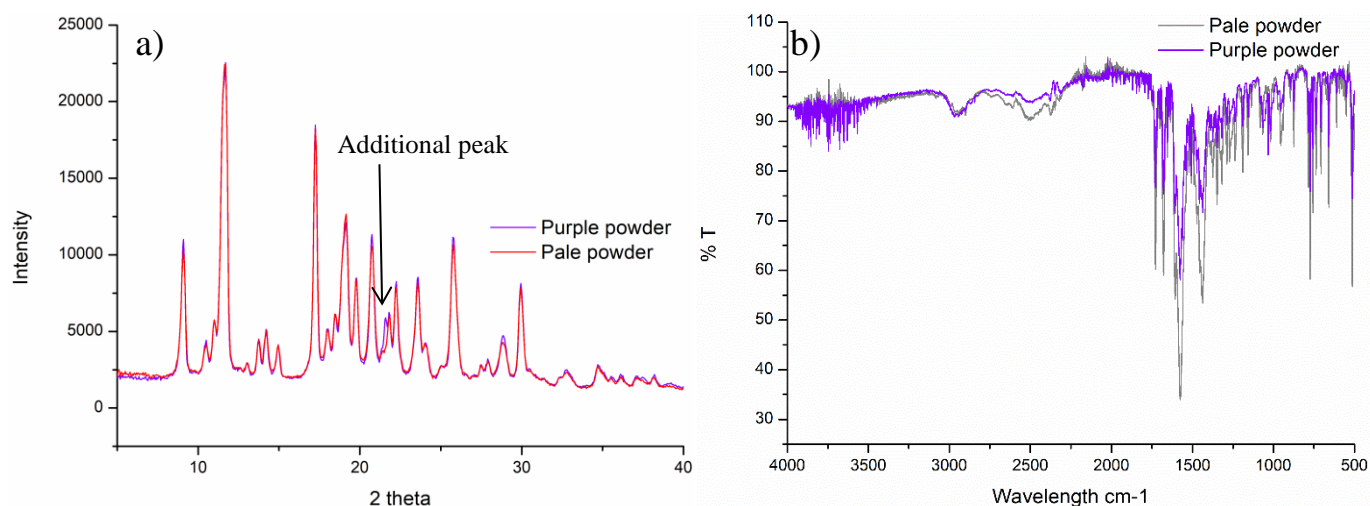


Figure 65. a) Powder X-ray diffraction patterns of the pale and purple powders. b) FT-IR spectra of the purple and pale powders.

4.4 Conclusion

Single crystals and powdered samples of DASA **8** displayed signs of solid-state photo-switching, through changes in colour on irradiation and subsequent heating in the dark. Three crystal structures were determined, and crystals isolated showed the ability to become coloured with heating in the dark, although the process could not be probed through X-ray diffraction due to complications involving the reduction in crystal quality. Analysis of the powdered samples revealed no clear spectroscopic or crystallographic information that directly relates to the change in colour observed, therefore it is inconclusive whether this phenomenon is due to the photochemical reactions of DASA molecules in the solid-state, at the surface or as a result of solvent loss. Further investigation is needed to confirm definitively that solid-state photo-switching is possible for DASA molecules, but the results above clearly merit further work.

Further experimentation could involve temperature dependent Powder X-ray diffraction so that a constant temperature can be maintained throughout the measurement, in addition to experiments probing the effect of humidity on the rate of the colour change, which would give more insight into water's role in the process.

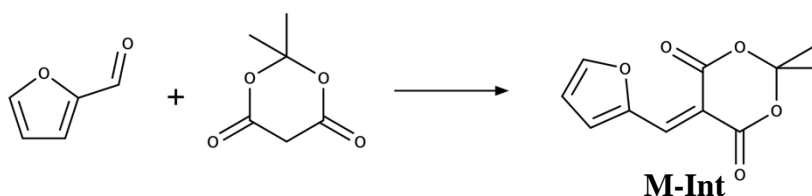
Chapter 5 - Experimental Chapter

5.1 Synthesis

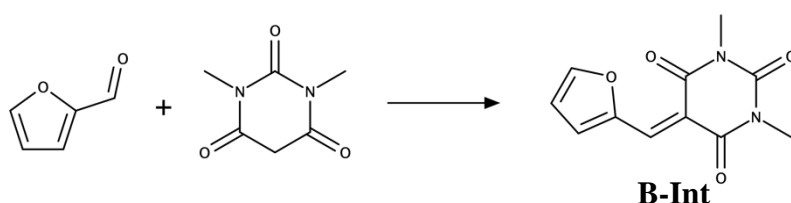
General methods. Unless stated otherwise all reactions were performed in oven dried glass ware in an atmosphere of air using reagent or analytical grade solvents. All reagents obtained from commercial suppliers were used as received. Reaction temperatures were controlled through automated heating plates with oil or aluminium bead baths, and unless explicitly stated reaction were performed at room temperature (approximately 23 °C). Data for ¹H NMR spectra are reported as follows: chemical shift (δ ppm), multiplicity, coupling constant (Hz), and integration;

Procedure A. Activated furfural intermediate (1 equiv) was dissolved in minimal THF, to this solution the amine (0.5 equiv) dissolved in minimal THF was added. The reaction mixture was stirred at room temperature for no less than 2 h, followed by cooling to 0 °C for 20 min. The mixture was then filtered and the resultant solid was washed with ether and further dried under vacuum.

Procedure B. Piperazine (0.3 mmol, 25.8 mg) and **M-Int** (1 mmol, 0.2222g) were dissolved in a solution of THF (4 mL) and Methanol (1 mL). Added to this was a solution of K₂CO₃ (0.003 mmol, 4.2 mg) in water (0.3 mL), methanol (0.5 mL), and THF (0.1 mL). The mixture was left to stir at room temperature (23 °C) for 20 h, followed by cooling to 0 °C for 20 min. The mixture was then filtered and the resultant solid was washed with ether and further dried under vacuum.



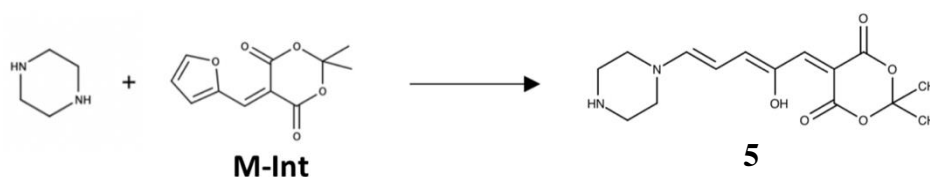
5-[(furan-2-yl)methylidene]-2,2-dimethyl-1,3-dioxane-4,6-dione (**M-Int**). **M-Int** was prepared by literature procedure². Meldrum's acid (10 mmol, 1.44 g) and furfural (10 mmol, 0.961 g) were mixed in water (30 mL) followed by heating to 75 °C and stirring for 2 hours. The solid obtained was filtered, vacuum dried and dissolved in dichloromethane (30 mL) followed by washing sequentially with saturated NaHSO₃ (30 mL), water (30 mL), NaHCO₃ (30 mL), and brine solution (30 mL). The organic layer was then dried over MgSO₄, filtered, and the solvent removed via rotary evaporation, yielding a yellow powder (0.969 g, 43%): ¹H NMR (600 MHz, CDCl₃) δ 8.46



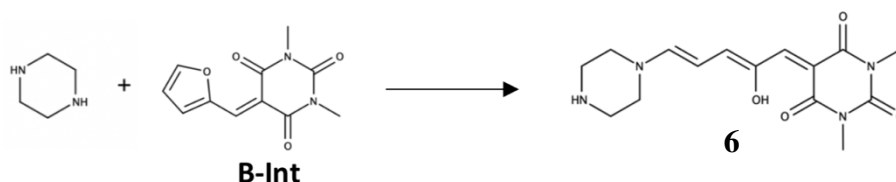
(d, $J = 3.9$ Hz, 1H), 8.36 (s, 1H), 7.85 (dd, $J = 0.5, 1.1$ Hz, 1H) 6.75 (dq, $J = 3.9, 0.7$ Hz, 1H) 1.77 (s, 6H).

5-[(cyclopenta-1,3-dien-1-yl)methylidene]-1,3-dimethyl-1,3-diazinane-2,4,6-trione (B-Int). 1,3-Dimethylbarbituric acid (10 mmol, 1.56 g) and furfural (10 mmol, 0.961 g) were mixed in water (40 mL) and stirred for 12 hours at room temperature. The solid obtained was filtered, vacuum dried and dissolved in dichloromethane (60 mL) followed by washing sequentially with saturated NaHSO₃ (30 mL), water (30 mL), NaHCO₃ (30 mL), and brine solution (30 mL). The organic layer was then dried over MgSO₄, filtered, and the solvent removed via rotary evaporation, yielding a yellow powder (1.67 g, 71%); ¹H NMR (600 MHz CDCl₃) δ 8.65 (d, $J = 3.9$ Hz, 1H), 8.45 (s, 1H), 7.86 (d, $J = 1.4$ Hz, 1H), 6.75 (dq, $J = 3.9, 0.7$ Hz, 1H), 3.41 (d, $J = 3.29$ Hz, 6H).

Compounds 1, 2, 3, 4. The attempted synthesis of **1, 2, 3, and 4** all followed procedure A. Reaction temperatures, durations and reagent ratios were varied across multiple reactions, the details of which are discussed in chapter 2.

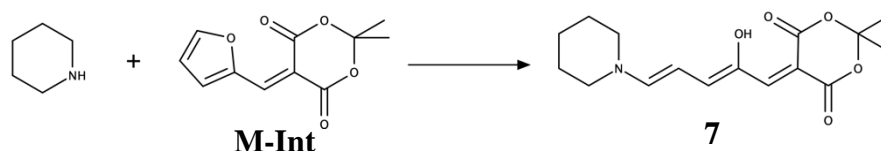


5-[(2Z,4E)-2-hydroxy-5-(piperazin-1-yl)penta-2,4-dien-1-ylidene]-2,2-dimethyl-1,3-dioxane-4,6- (5). Meldrum's acid intermediate **M-int** (0.555 g, 2.5 mmol) was dissolved in THF (5 mL). To this solution piperazine (0.189 g, 2.19 mmol) dissolved in THF (5 mL) was added. The reaction mixture was stirred for 2 h, followed by cooling to 0 °C for 20 min. The mixture was filtered and the resultant solid was washed with diethyl ether and further dried under vacuum yielding a dark purple powder (0.583 g, 86%). ¹H NMR (600 MHz d₆ – DMSO) δ 8.52 (s, 2H), 7.50 (dd, $J = 5.77, 1.95$ Hz, 1H), 6.20 (dd, $J = 5.97, 1.83$ Hz, 1H), 3.91 (d, $J = 2.43$ Hz, 1H), 3.15 (d, $J = 2.9$ Hz, 1H), 3.08 (t, $J = 4.5$ Hz, 4H), 2.68 – 2.79 (m, 4H), 1.48 (s, 6H).

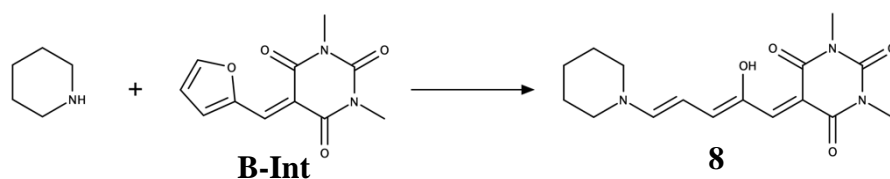


5-[(2Z,4E)-2-hydroxy-5-(piperazin-1-yl)penta-2,4-dien-1-ylidene]-1,3-dimethyl-1,3-diazinane-2,4,6-trione (6). Barbituric acid intermediate **B-int** (0.234 g, 1 mmol) was dissolved in THF (15 mL). To this solution piperazine (0.0689 g, 0.8 mmol) dissolved in THF (5 mL) was added.

The reaction mixture was stirred at room temperature (23 °C) for 17 h, followed by cooling to 0 °C for 20 min. The mixture was filtered and the resultant solid was washed with diethyl ether and further dried under vacuum yielding a purple powder (0.0783 g, 25%). ¹H NMR (600 MHz d₄ – MeOD) δ 7.50 (dd, *J* = 5.97, 2.07 Hz, 1H), 6.26 (dd, *J* = 5.97, 2.07 Hz, 1H), 4.10 (dt, *J* = 3.04, 2.07 Hz, 1H) 3.59 (d, *J* = 3.17 Hz, 1H), 3.13 – 3.19 (m, 3H), 3.08 – 3.11 (m, 7H), 2.75 (m, 4H).



5-[(2Z,4E)-2-hydroxy-5-(piperidin-1-yl)penta-2,4-dien-1-ylidene]-2,2-dimethyl-1,3-dioxane-4,6-dione (**7**). Compound **7** was prepared by literature procedure.² Meldrum's acid intermediate **M-int** (0.299 g, 1.35 mmol) was dissolved in THF (5 mL) and left to stir. Piperidine (0.115 g, 1.35 mmol) was added via micropipette, the reaction was left to stir at room temperature (23 °C) for 1 h followed by cooling to 0 °C for 20 min. The mixture was filtered and the resultant solid was washed with diethyl ether and further dried under vacuum yielding a red powder (0.330 g, 79.2%). ¹H NMR (600 MHz CD₂Cl₂) δ 11.31 (s, 1H), 7.25 (d, *J* = 12.17 Hz, 1H), 6.85 (dd, *J* = 1.35, 12.42 Hz, 1H), 6.06 (t, *J* = 12.3 Hz, 1H), 3.41-3.51 (m, 4H), 1.67(s, 6H), 1.59 (s, 6H).



5-[(2Z,4E)-2-hydroxy-5-(piperidin-1-yl)penta-2,4-dien-1-ylidene]-1,3-dimethyl-1,3-diazinane-2,4,6-trione (**8**). Compound **8** was prepared by literature procedure.² Barbituric acid intermediate **B-int** (0.299 g, 1.28 mmol) was dissolved in THF (20 mL). To this solution piperidine (0.109 g, 1.28 mmol) was added via micropipette. The reaction mixture was stirred at room temperature (23 °C) for 2.5 h, followed by cooling to 0 °C for 20 min. The mixture was filtered and the resultant solid was washed with diethyl ether and further dried under vacuum yielding a purple powder (0.221 g, 54%). ¹H NMR (600 MHz D₂O) δ 7.8 (dd, *J* = 6.2, 2.07 Hz, 1H), 6.61 (dd, *J* = 6.1, 1.8 Hz, 1H), 4.48 (q, *J* = 1.8 Hz, 1H), 3.81 (d, *J* = 3.5 Hz, 1H) 3.10 – 3.19 (m, 10H), 1.58-1.81 (m, 6H).

5.2 UV-Vis spectroscopy

General methods. The UV-Vis absorption spectra were recorded using a Shimadzu UV-1800 spectrometer. Each spectrum recorded was over a range of 400 – 650 nm. The samples were

irradiated from all directions using a 50 W, 650 K, full spectrum LED flood light, illuminating a container lined with reflective mylar sheeting, room temperature was maintained by allowing a current of air to flow through the container. Samples were continuously irradiated in between each measurement and sequential measurements of the UV-Vis absorbance were taken until no notable changes in the spectra were observed, at which point the thermal reversion was recorded through the same procedure, heating samples in a dark oven at 50 °C. In-situ irradiation of samples was not possible due to the apparatus available, as the illumination would interfere with the incident beams and detector of the spectrometer. Therefore samples were quickly moved from the illumination container to the spectrometer to take measurements and placed back inside once the measurement was finished, the scan rate of the spectrometer was increased to the max in order to limit the time samples were left unirradiated. Similarly, when performing the thermal reversion measurements samples were moved between the oven and spectrometer, wrapped in foil to avoid light contamination while transporting.

Instrumentation

High performance liquid chromatography (HPLC)

HPLC was performed using an Agilent technologies 1260 Infinity HPLC. Reverse phase HPLC was run using a gradient eluent starting at 98% water and 2% methanol (0.1% NH₃) ramping up to 50% methanol. Temperature was controlled at 23 °C. and flow rate of 4 mL/min was maintained. 50 µL injections were injected from a 3.6 mg/mL solution. An Agilent 5 Prep-C₁₈, 50 x 10 mm column was used.

Liquid Chromatography - Mass spectroscopy (LC-MS)

LC-MS was performed using the Thermo Scientific Dionex UltiMate 3000 HPLC and Thermo MSQ Plus Quadrupole Mass Spectrometer. Reverse phase HPLC was run using an isocratic eluent of 50% H₂O and 50% methanol (0.1% NH₃), and flow rate of 4 mL/min. The column used was a Thermo Acclaim RSLC 120 C₁₈, 3 µm, 3.0 x 75 mm. Negative ion electrospray ionisation was used for the mass spectroscopy.

¹H NMR spectroscopy

¹H NMR spectroscopy was recorded using a 600 MHz five channel Bruker Avance III. Unless stated otherwise spectra were recorded at room temperature (approximately 20 °C).

Powdered X-ray Diffraction (PXRD). Powder X-ray diffraction patterns were recorded using a Rigaku miniflex 600 X-ray diffractometer, using Cu K α radiation ($\lambda = 1.54413 \text{ \AA}$) operating at 40 kV and 15 mA (2θ range 5 θ - 40 θ).

Single crystal X-ray diffraction (SCXRD). Single crystal diffraction data were collected using an Oxford Diffraction SuperNova, using Cu K α radiation ($\lambda = 1.54413 \text{ \AA}$) with an AtlasS2 detector. Crystals were kept at 100 K during data collection. Using Olex2,⁷² the structure was solved with the ShelXT⁷³ structure solution program using Direct Methods and refined with the ShelXL⁷⁴ refinement package using Least Squares minimisation.

Computational experiments. The initial minimum energy conformations of all molecules were assessed following conformational searches and energy minimisations using the intrinsic molecular dynamics MM2 force field intrinsic to Chem3D, v15.0 (Perkin Elmer). All final conformations were modelled at the semi-empirical PM7 level (in CHCl₃, $\epsilon=4.81$, COSMO) using MOPAC 2016⁽⁶⁶⁾ through the MOPAC Interface with Chem3D, v15.0 (Perkin Elmer).

Fourier Transform Infrared Spectroscopy (FT-IR). FT-IR spectroscopy was recorded using a Shimadzu IRAfinity-1 FT-IR spectrometer.

References

1. (a) H. Bouas-Laurent, H. Dürr, *Pure and Appl. Chem.*, 2007, **73**(4), 639–665. (b) S. Aiken, R. J. L. Edgar, C. D. Gabbutt, B. M. Heron and P. A. Hobson, *Dye. Pigment.*, 2018, **149**, 92–121.
2. S. Kobatake, M. Irie, *Annu. Rep. Prog. of Chem.*, 2003, **99**(8), 277–313.
3. M. Irie, *Chem. Rev.*, 2000, **100**(5), 1683–1684.
4. J. Fritzsche. *Comptes Rendus Acad. Sci.*, Paris, 1867, **69**, 1035.
5. Havinga, E. Meijer, *Polym.*, 1987, **18**, 277–281.
6. Y. Hirshberg, *Compt. Rend. Acad. Sci.*, Paris, 1950, **231**, 903.
7. Z. L. Pianowski, *Chem. Eur. J.*, 2019, **25**(20), 5128–5144.
8. Robert c. Bertelson, *Mol. Cryst. Liq. Cyst.* 1994, **246**, 1–8.
9. J. Griffiths, *Chem. Soc. Rev.*, 1972, **1**, 481–493
10. A. A. Beharry, G. A. Woolley, *Chem. Soc. Rev.*, 2011, **40**(8), 4422–4437.
11. S. Sporlein, H. Carstens, H. Satzger, C. Renner, R. Behrendt, L. Moroder, P. Tavan, W. Zinth and J. Wachtveitl, *Proc. Natl. Acad. Sci. U. S. A.*, 2002, **99**, 7998–8002.
12. H. Rau, *Angew. Chem., Int. Ed. Engl.*, 1973, **12**, 224–235.
13. Z. L. Pianowski, *Chem. Eur. J.*, 2019, **25**(20), 5128–5144.
14. M. Irie, (2000). *Chem. Rev.*, 2000, **100**, 1685–1716.
15. Richard M. Kellogg, M. B. Groen, H. Wynberg, *J. Org. Chem.*, 1967, **32**(10), 3093–3100.
16. C. Petermayer, H. Dube, *Acc. Chem. Res.*, 2018, **51**(5), 1153–1163.
17. D. J. Van Dijken, P. Kovaříček, S. P. Ihrig, & S. Hecht, *J. Am. Chem. Soc.*, 2015, **137**(47), 14982–14991.
18. H. Qian, S. Pramanik, and I. Aprahamian, *J. Am. Chem. Soc.*, 2017, **139**(27), 9140–9143.
19. Y. Yokoyama, *Chem. Rev.*, 2000, **100**(5), 1717–1739.
20. V. P. Rybalkin, S. Y. Pluzhnikova, L. L. Popova, Y. V. Revinskii, K. S. Tikhomirova, O. A. Komissarova, V. I. Minkin, *Mendeleev Commun.*, 2016, **26**(1), 21–23.
21. S. Helmy, F. A. Leibfarth, S. Oh, J. E. Poelma, C. J. Hawker, and J. Read De Alaniz, (2014). *J. Am. Chem. Soc.*, 2014, **136**(23), 8169–8172.
22. S. Helmy, S. Oh, F. A. Leibfarth, C. J. Hawker, and J. Read De Alaniz, *J. Org. Chem.*, 2014, **79**(23), 11316–11329.
23. S. O. Poelma, S. S. Oh, S. Helmy, A. S. Knight, G. L. Burnett, H. T. Soh, and J. Read De Alaniz, *Chem. Comm.*, 2016, **52**(69), 10525–10528.

24. Q. Chen, Y. J. Diaz, M. C. Hawker, M. R. Martinez, Z. A. Page, S. Xiao-An Zhang, and J. Read de Alaniz, *Macromolecules*, 2019, **52**, 4370–4375.
25. Mason, B. P., Whittaker, M., Hemmer, J., Arora, S., Harper, A., Alnemrat, S., and Hooper, J. P. *App. Phys. Lett.*, 2016, **108**(4), 041906.
26. H. Zhao, D. Wang, Y. Fan, M. Ren, S. Dong and Y. Zheng, *Langmuir*, 2018, **34**(50), 15537–15543.
27. M. Nau, D. Seelinger and M. Biesalski, *Adv. Mater. Interface.*, 2019, **6**(17), 1900378.
28. O. Rifaie-Graham, S. Ulrich, N. F. B. Galensowske, S. Balog, M. Chami, D. Rentsch, and N. Bruns, *J. Am. Chem. Soc.*, 2018, **140**(25), 8027–8036.
29. M. M. Lerch, S. J. Wezenberg, W. Szymanski, and B. L. Feringa, *J. Am. Chem. Soc.*, 2016, **138**(20), 6344–6347.
30. J. R. Hemmer, S. O. Poelma, N. Treat, Z. A. Page, N. D. Dolinski, Y. J. Diaz, and J. Read De Alaniz, *J. Am. Chem. Soc.*, 2016, **138**(42), 13960–13966.
31. N. Mallo, P.T. Brown, H. Iranmanesh, T. S. C. MacDonald, M. J. Teusner, J. B. Harper, and J. E. Beves, *Chem. Comm.*, 2016, **52**(93), 13576–13579.
32. J. R. Hemmer, Z. A. Page, K.D. Clark, F. Stricker, N. D. Dolinski, C. J. Hawker, and J. Read De Alaniz, *J. Am. Chem. Soc.*, 2018, **140**(33), 10425–10429.
33. M. M. Lerch, W. Szymański, and B. L. Feringa, *Chem. Soc. Rev.*, 2018, **47**(6), 1910–1937.
34. M. Di Donato, A. Lapini, A. D. Laurent, A. Iagatti, L. Bussotti, and B. L. Feringa, *J. Am. Chem. Soc.*, 2017, **139**(44), 15596–15599.
35. M. M. Lerch, M. Medved, A. Lapini, A. D. Laurent, A. Iagatti, L. Bussotti, and B. L. Feringa, *J. Phys. Chem. A*, 2018, **122**(4), 955–964.
36. M. M. Lerch, M. Di Donato, A. D. Laurent, M. Medved', A. Iagatti, L. Bussotti, and B. L. Feringa, *Angew. Chem.*, 2018, **57**(27), 8063–8068.
37. (H. Zulfikri, M. A. J. Koenis, M. M. Lerch, M. Di Donato, W. Szymański, C. Filippi, and W. J. Buma, *J. Am. Chem. Soc.*, 2019, **141**(18), 7376–7384.
38. O. Nieto Faza, C. Silva López, R. Álvarez and Á. R. De Lera, *Chem. Eur. J.*, 2004, **10**(17), 4324–4333.
39. M. J. Riveira, L. A. Marsili and M. P. Mischne, *OBC.*, 2017, **15**(44), 9255–9274.
40. J. N. Bull, E. Carrascosa, N. Mallo, M S. Scholz, G. Da Silva, J. E. Beves, and E. J. Bieske, *J. Phys. Chem. Lett.*, 2018, **9**(3), 665–671.

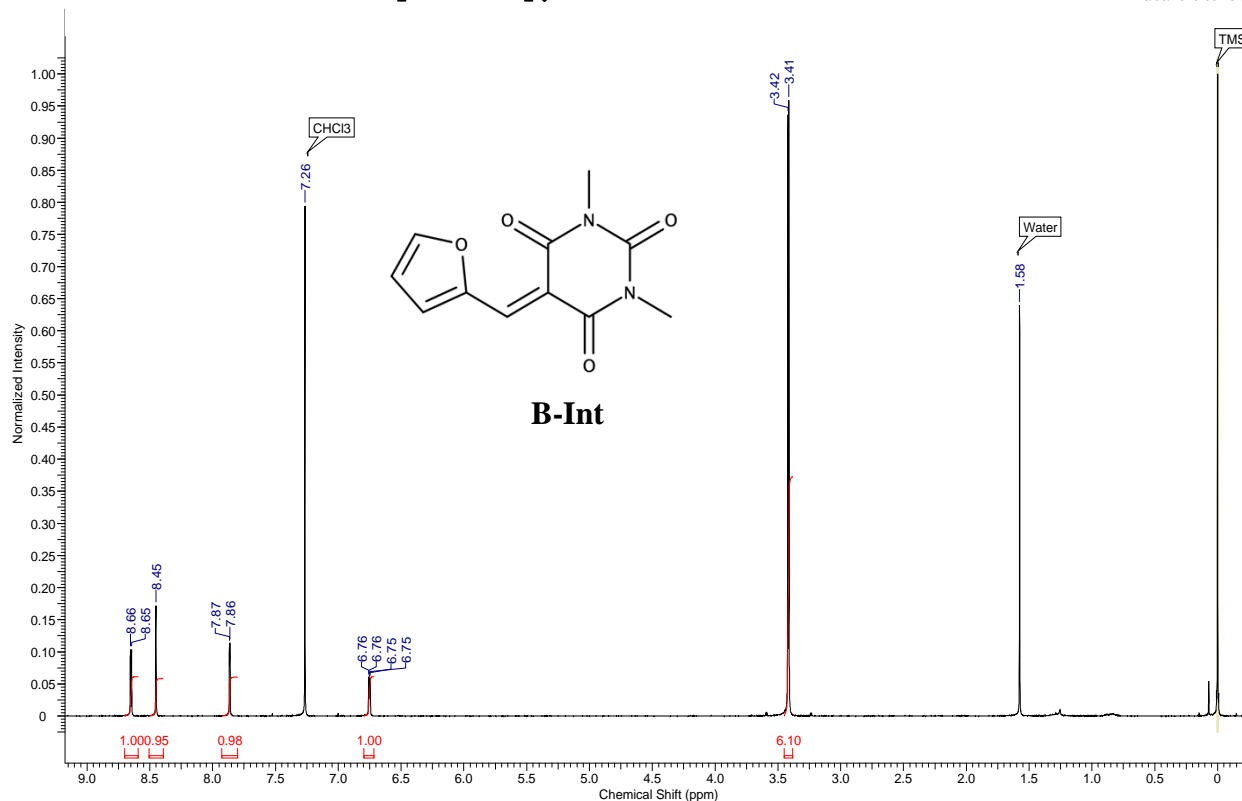
41. M. M. Lerch, M. J. Hansen, W. A. Velema, W. Szymanski and B. L. Feringa, *Nat. Commun.*, 2016, **7**, 12054.
42. B. F. Lui, N. T. Tierce, F. Tong, M. M. Sroda, H. Luo, J. Read de Alaniz, and C. J. Bardeen, *Photochem. Photobiol. Sci.*, 2019, **18**, 1587-1595.
43. K. Amimoto, and T. Kawato, *JPPC.*, 2005, **6**(4), 207–226.
44. S. Bénard and Y. Pei, *Chem. Comm.*, 2000, **1**, 65–56.
45. S. Bénard, and P. Yu, *Adv. Mater.*, 2000, **12**(1), 48–50.
46. J. Ahrens, T. Bian, T. Vexler, and R. Klajn, *ChemPhotoChem*, 2017, **1**(5), 230–236.
47. F. Y. Tang, J. N. Hou, K. X. Liang, Y. Liu, L. Deng and Y. N. Liu, *New. J. Chem.*, 2017, **41**(14), 6071–6075.
48. S. Ulrich, J. R. Hemmer, Z. A. Page, N. D. Dolinski, O. Rifaie-Graham, N. Bruns, and J. Read De Alaniz, *ACS Macro Lett.*, 2017, **6**(7), 738–742.
49. S. Singh, K. Friedel, M. Himmerlich, Y. Lei, G. Schlingloff, and A. Schober, *ACS Macro Lett.*, 2015, **4**(11), 1273–1277.
50. G. Sinawang, B. Wu, J. Wang, S. Li, and Y. He, *Macromol. Chem. Phys.*, 2016, **217**(21), 2409–2414.
51. E. Lee, D. Kim, H. Kim, and J. Yoon, *Sci. Rep.*, 2015, **5**(June), 1–8.
52. E. Wang, M. S. Desai, and S. W. Lee, *Nano Lett.*, 2013, **13**(6), 2826–2830.
53. Wani, O. M., Zeng, H., & Priimagi, A. (2017). *Nat. Commun.*, 2017, **8**(May), 1–7.
54. O. M. Wani, R. Verpaalen, H. Zeng, A. Priimagi, and A. P. H. J. Schenning, *Adv. Mater.*, 2019, **31**(2), 1–6.
55. O. M. Wani, H. Zeng, P. Wasylczyk, and A. Priimagi, *Adv. Opt. Mater.*, 2018, **6**(1), 2–7.
56. M. Bi, Y. He, Y. Wang, W. Yang, B. Qin, J. Xu, and C. Li, *Polymers*, 2019, **11**(4), 735.
57. M. Yamada, M. Kondo, J. I. Mamiya, Y. Yu, M. Kinoshita, C. J. Barrett and T. Ikeda, *Angew. Chem.*, 2008, **47**(27), 4986–4988.
58. M. Yamada, M. Kondo, R. Miyasato, Y. Naka, J. I. Mamiya, M. Kinoshita, and T. Ikeda, *J. Mater. Chem.*, 2009, **19**(1), 60–62.
59. F. Cheng, R. Yin, Y. Zhang, C. C. Yen, and Y. Yu, *Soft Matter*, 2010, **6**(15), 3447–3449.
60. J. A. Lv, W. Wang, J. Xu, T. Ikeda, and Y. Yu, *Macromol. Rapid Commun.*, 2014, **35**(14), 1266–1272.
61. C. J. Barrett, J. I. Mamiya, K. G. Yager, and T. Ikeda, *Soft Matter*, 2007, **3**(10), 1249–1261.

62. M. Moniruzzaman, G. F. Fernando, C. Sabey, D. Winter, R. A. Badcock, J. Akhavan, and E. Krofli, *SPIE - Organic Optoelectronics and Photonics*, 2004, 5464,
63. A. Ryabchun, Q. Li, F. Lancia, I. Aprahamian, and N. Katsonis, *J. Am. Chem. Soc.*, 2019, **141**(3), 1196–1200.
64. M. Morimoto, and M. Irie, *J. Am. Chem. Soc.*, 2010, **132**(40), 14172–14178.
65. R. Tiwari, S.W. Connolly, S. J. Holder, H. J. Shepherd, In preparation
66. S. Helmy, PhD thesis, *UC Santa Barbara*, 2015. <https://escholarship.org/uc/item/1zv1q6vn>
67. IUPAC. Compendium of Chemical Terminology, 2nd ed. (the "Gold Book"). Compiled by A. D. McNaught and A. Wilkinson. Blackwell Scientific Publications, Oxford (1997)
68. M. Irie, *Photochem. Photobiol. Sci.*, 2010, **9**, 1535–1542.
69. M. Morimoto and M. Irie, *Chem. Commun.*, 2005, 3895–3905.
70. Y. Funasako, M. Ason, J. I. Takebayashi and M. Inokuchi, *Cryst. Growth Des.*, 2019, **19**, 7308–7314.
71. Y. Funasako, H. Miyazaki, T. Sasaki, K. Goshima and M. Inokuchi, *J. Phys. Chem. B*, 2020, **124**, 7251–7257.
72. G.M Sheldrick, *Acta Cryst.*, 2015, A71, 3-8
73. O. V. Dolomanov, L. J. Bourhis, R. J. Gildea, J. A. K. Howard and H. J. Puschmann, *Appl. Cryst.* 2009, **42**, 339-341.
74. G. M. Sheldrick, *Acta Cryst.*, 2015, C71, 3-8
75. rMOPAC2016, James J. P. Stewart, Stewart Computational Chemistry, Colorado Springs, CO, USA, [HTTP://OpenMOPAC.net](http://OpenMOPAC.net) (2016)

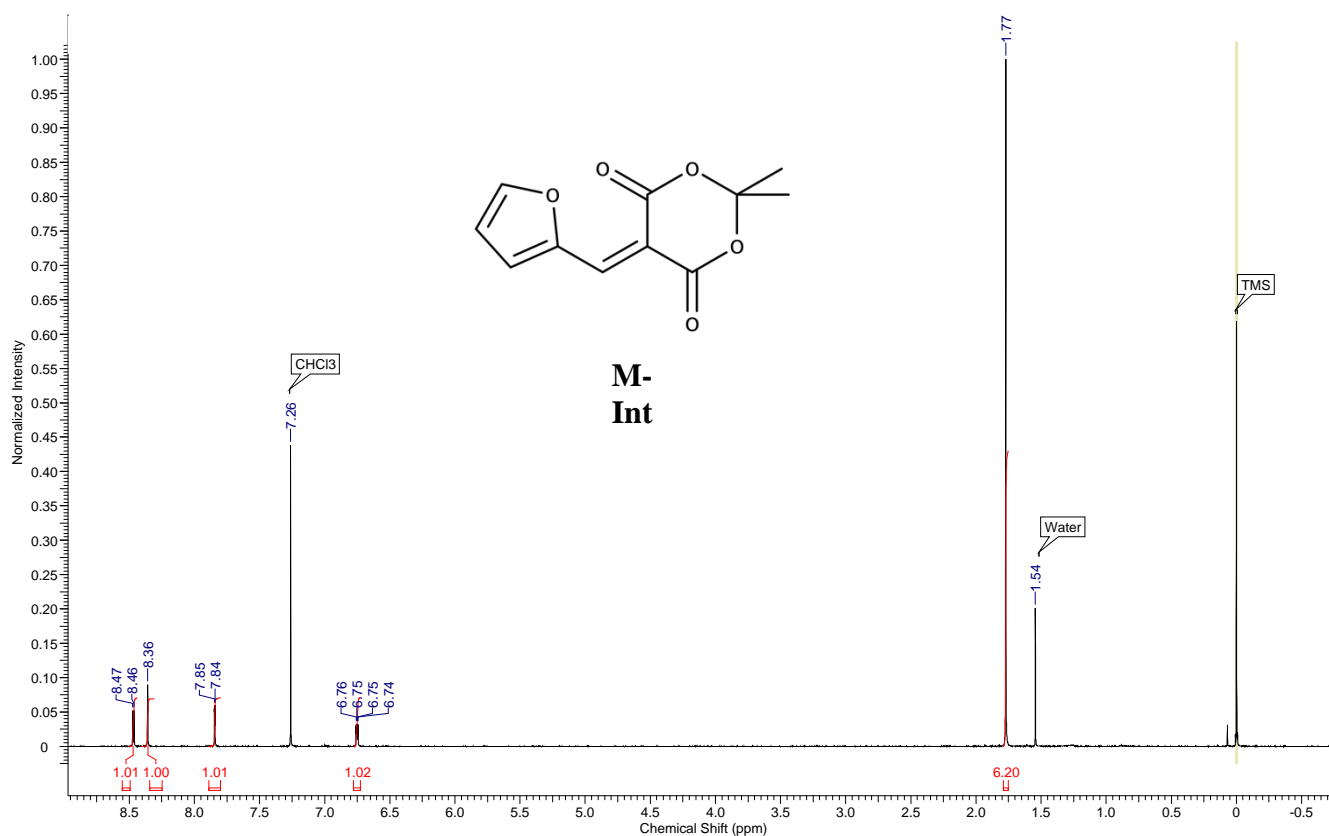
Appendix

- 1- NMR Spectra
- 2- X-ray Diffraction Crystal structures
- 3- UV-Vis Spectroscopy Spectra
- 4- (Aza-) Piancatelli Rearrangement & Iso Nararov Reaction

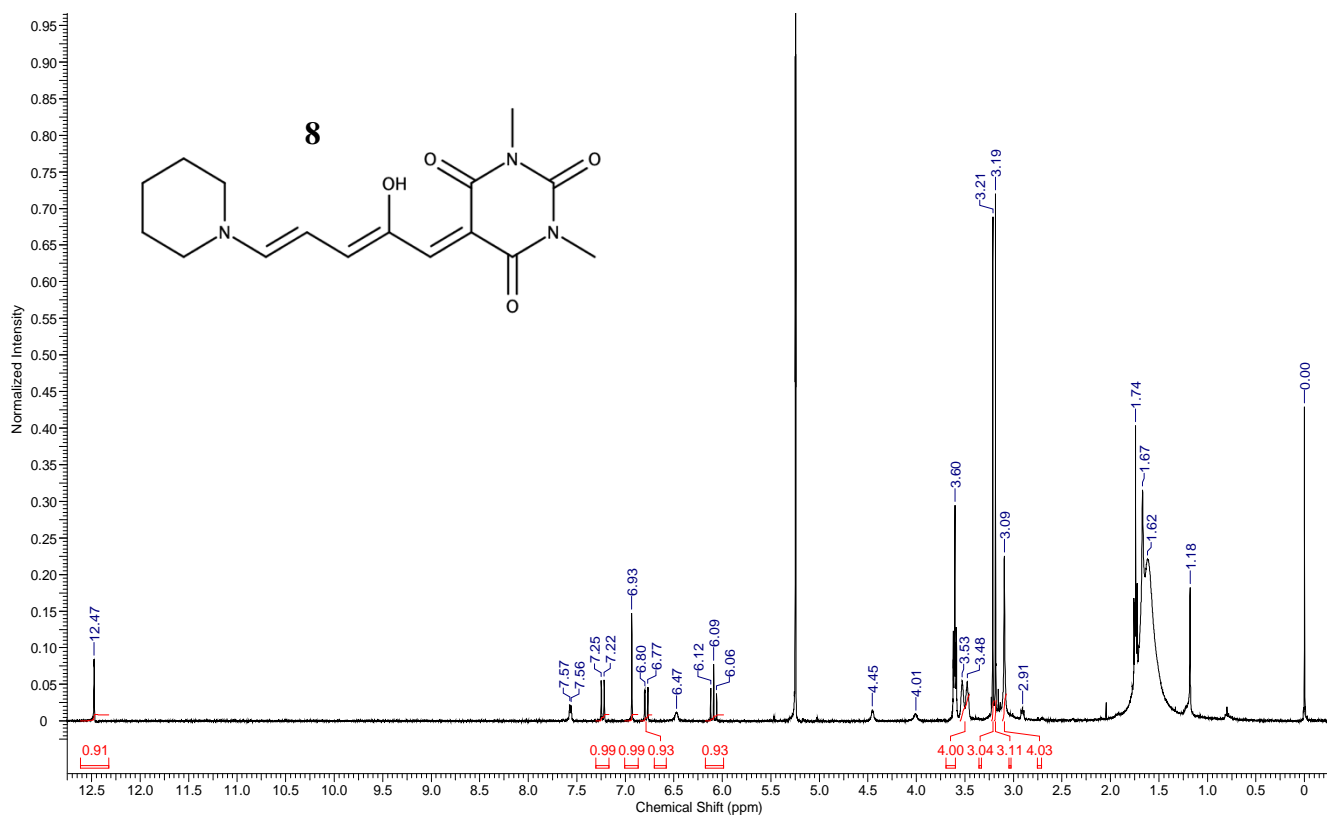
Appendix 1 – NMR Spectroscopy



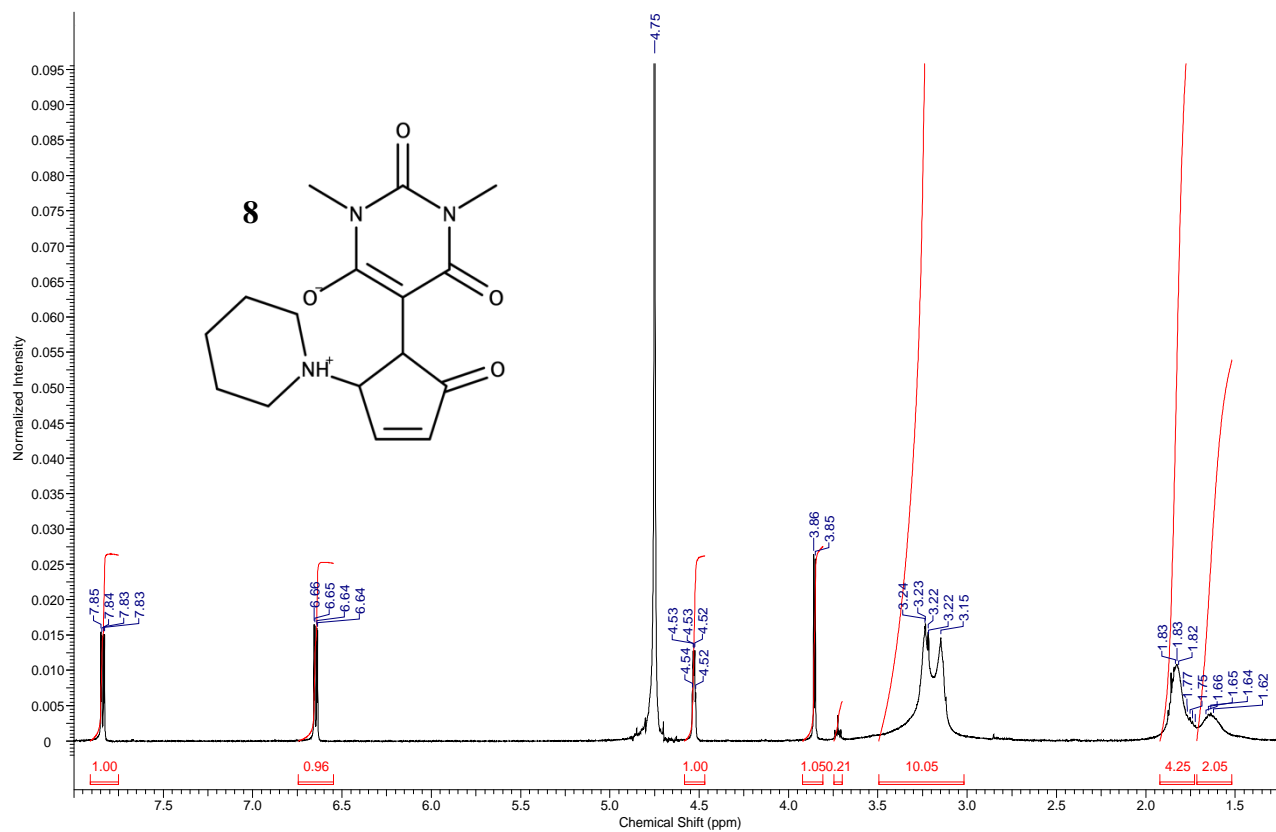
Appendix 1.1. NMR of 5-[(cyclopenta-1,3-dien-1-yl)methylidene]-1,3-dimethyl-1,3-diazinane-2,4,6-trione, B-Int. (600 MHz, CDCl₃)



Appendix 1.2. NMR of 5-[(furan-2-yl)methylidene]-2,2-dimethyl-1,3-dioxane-4,6-dione, M-Int. (600 MHz, CDCl₃)



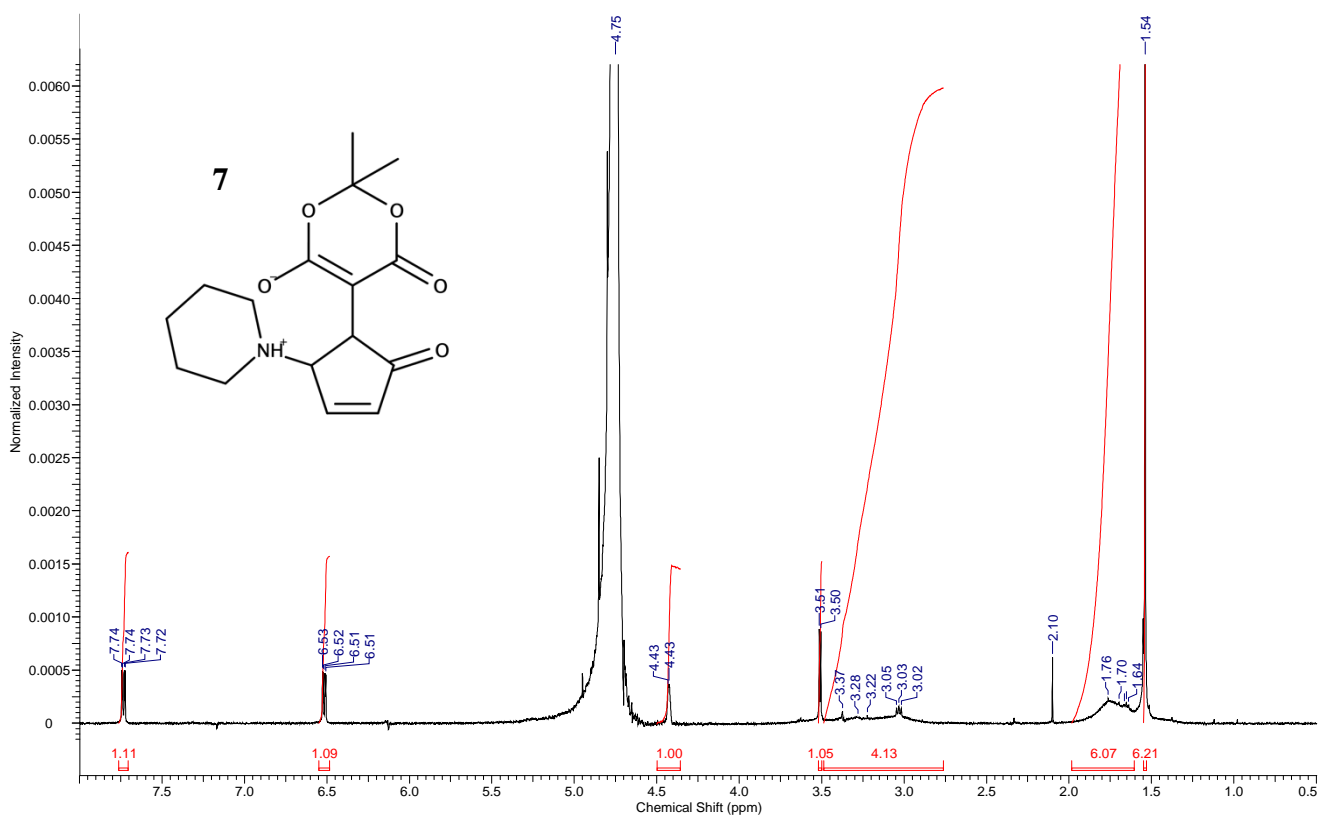
Appendix 1.3. NMR of 5-[(2Z,4E)-2-hydroxy-5-(piperidin-1-yl)penta-2,4-dien-1-ylidene]-1,3-dimethyl-1,3-diazinane-2,4,6-trione (8), (600 MHz, CD₂Cl₂)



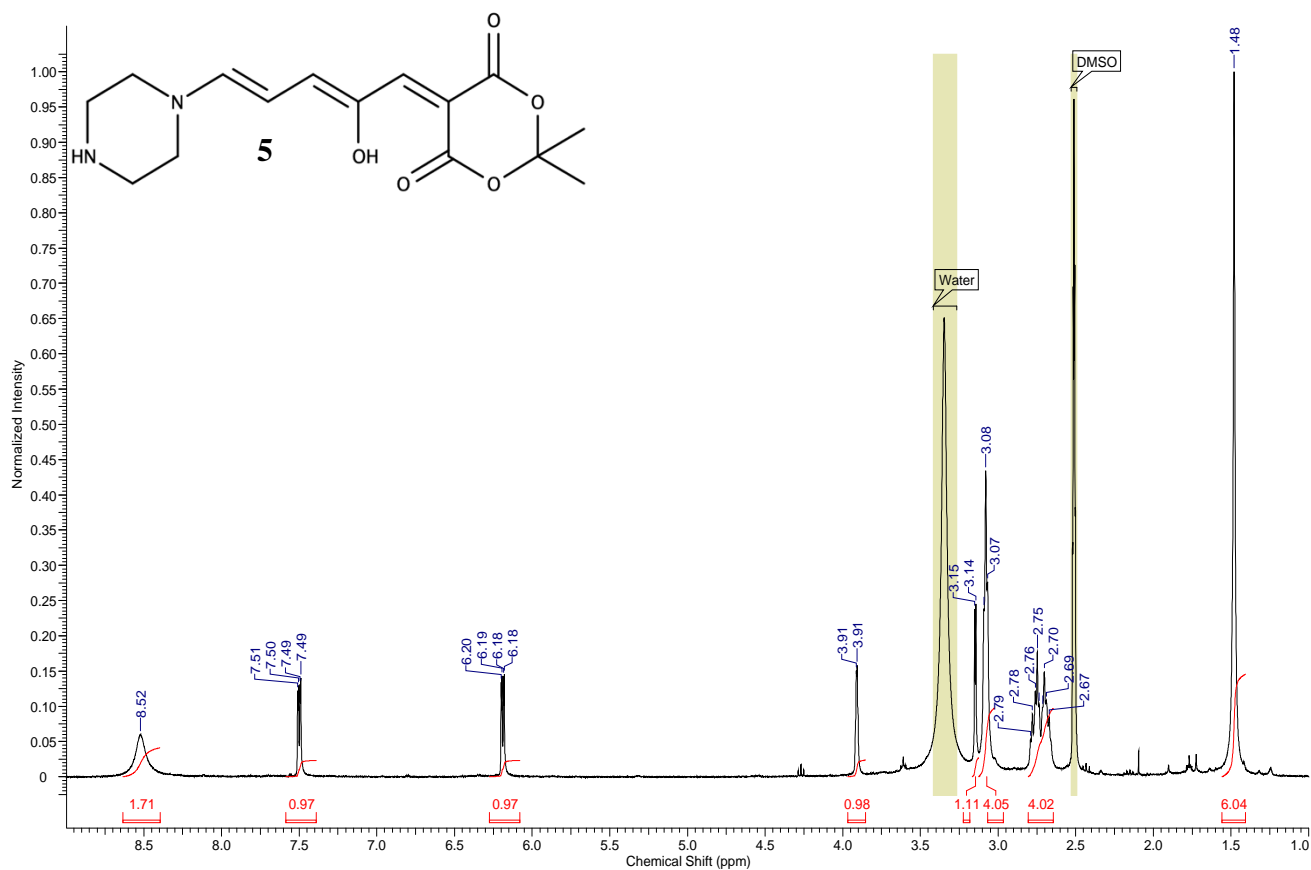
Appendix 1.4. NMR of 5-[(2Z,4E)-2-hydroxy-5-(piperidin-1-yl)penta-2,4-dien-1-ylidene]-1,3-dimethyl-1,3-diazinane-2,4,6-trione (8), (600 MHz, D₂O)



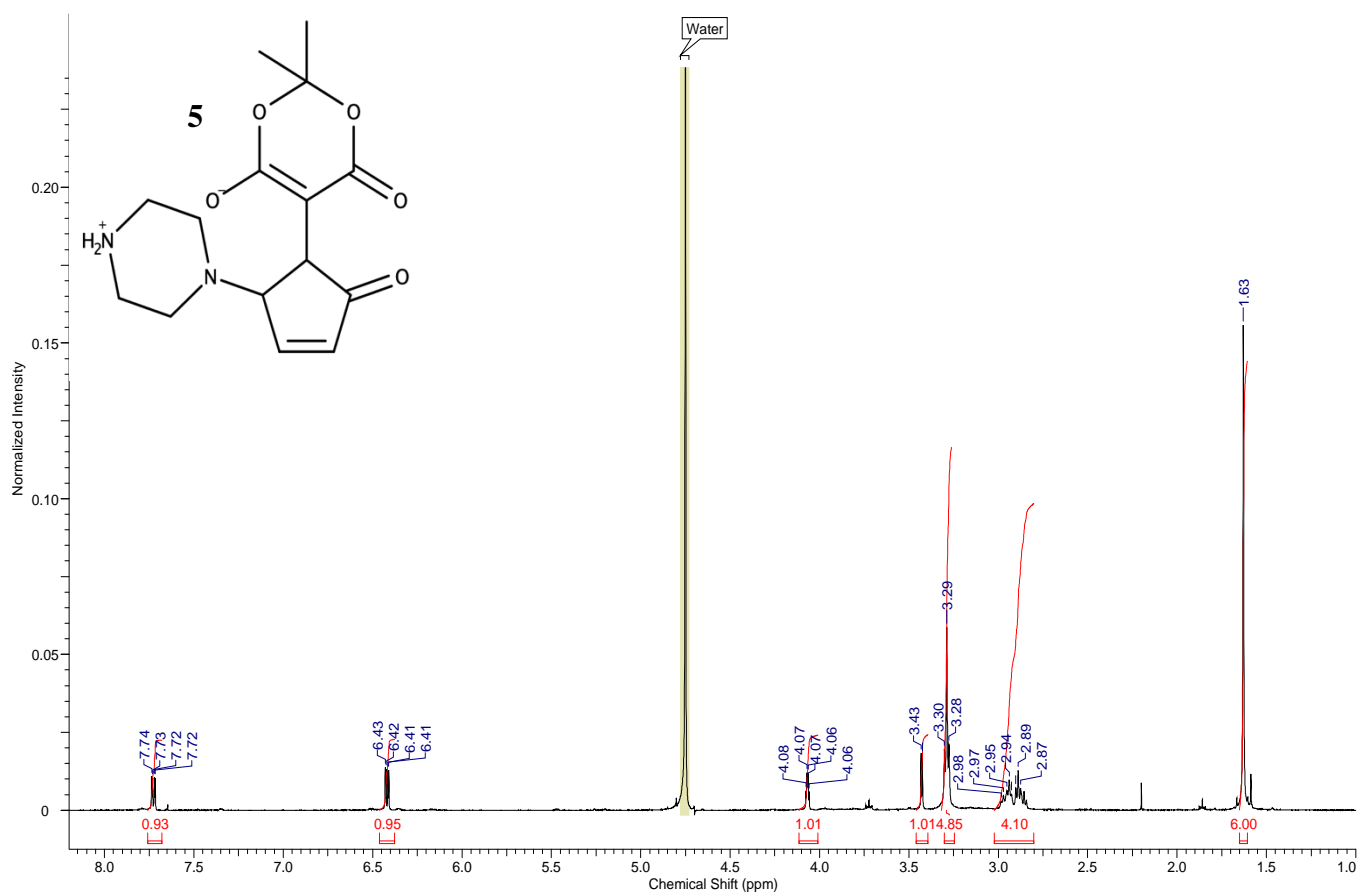
Appendix 1.5. NMR of 5-[(2Z,4E)-2-hydroxy-5-(piperidin-1-yl)penta-2,4-dien-1-ylidene]-2,2-dimethyl-1,3-dioxane-4,6-dione (7). (600 MHz, CD₂Cl₂)



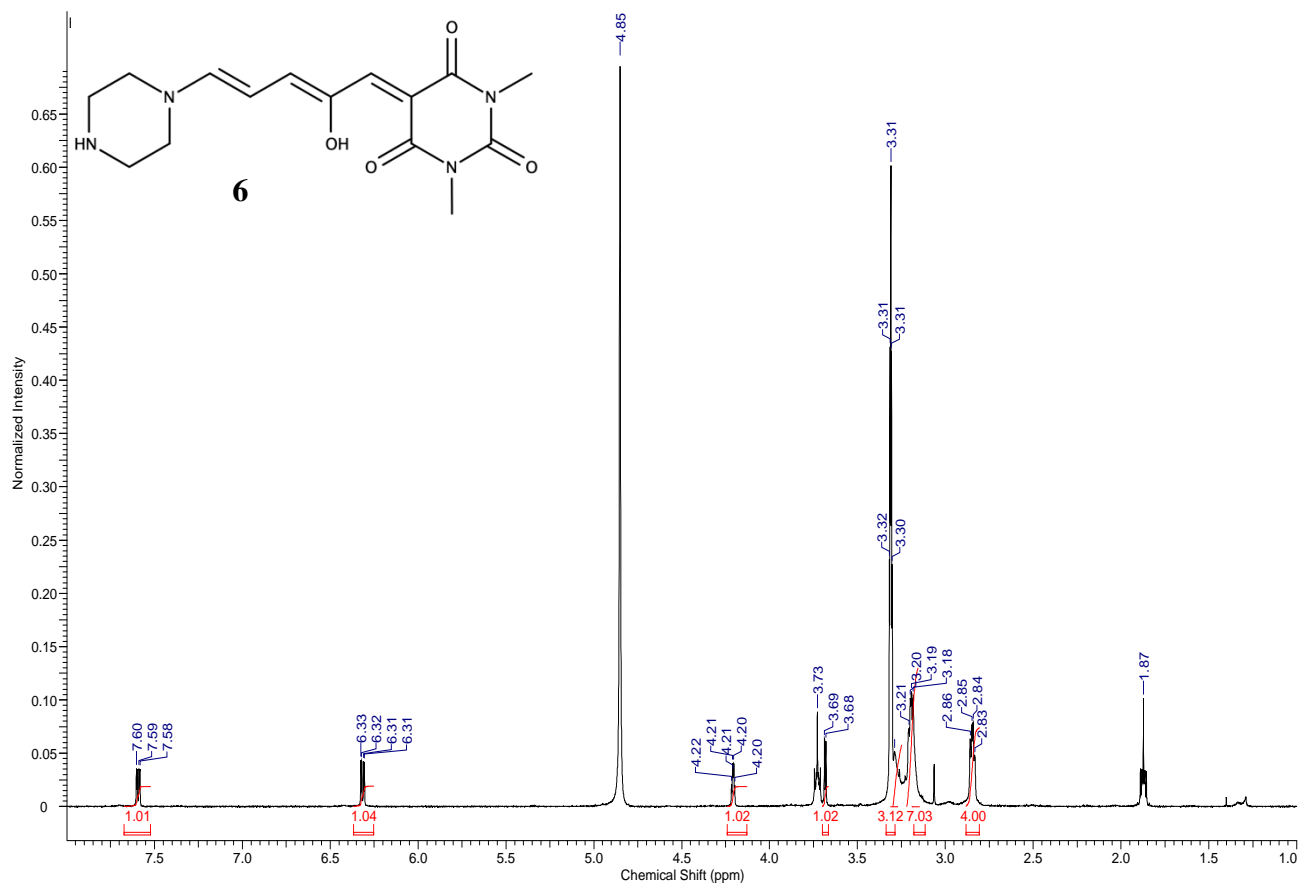
Appendix 1.6. NMR of 5-[(2Z,4E)-2-hydroxy-5-(piperidin-1-yl)penta-2,4-dien-1-ylidene]-2,2-dimethyl-1,3-dioxane-4,6-dione (7). (600 MHz, D₂O)



Appendix 1.7. NMR of -[(2Z,4E)-2-hydroxy-5-(piperazin-1-yl)penta-2,4-dien-1-ylidene]-2,2-dimethyl-1,3-dioxane-4,6- (5). (600 MHz, d₆ DMSO)

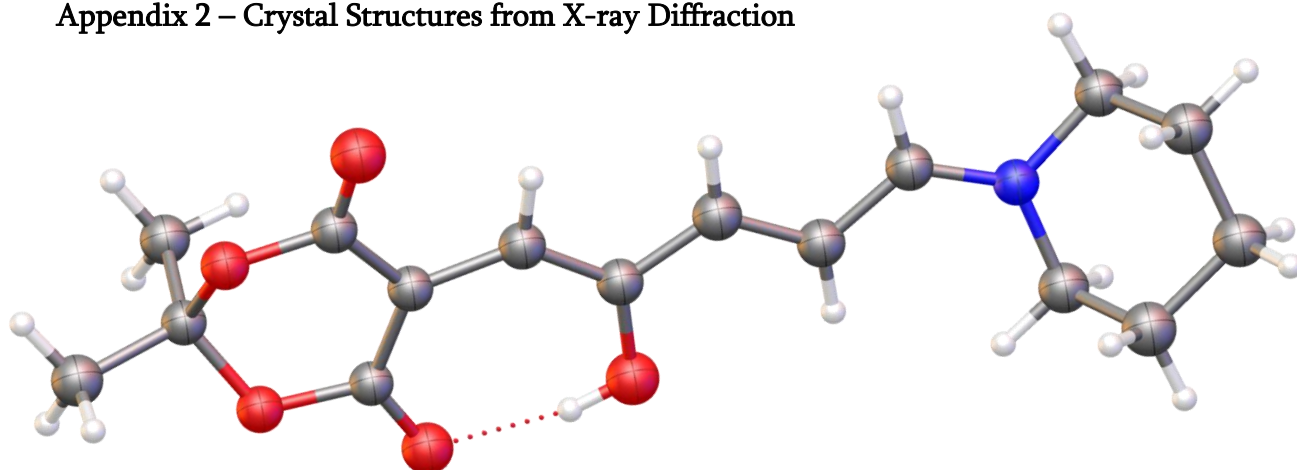


Appendix 1.8. NMR of 5-[(2Z,4E)-2-hydroxy-5-(piperazin-1-yl)penta-2,4-dien-1-ylidene]-2,2-dimethyl-1,3-dioxane-4,6- (5). (600 MHz, d₆ D₂O)



Appendix 1.9. NMR of 5-[(2Z,4E)-2-hydroxy-5-(piperazin-1-yl)penta-2,4-dien-1-ylidene]-1,3-dimethyl-1,3-diazinane-2,4,6-trione (6). (600 MHz, d_6 D₂O)

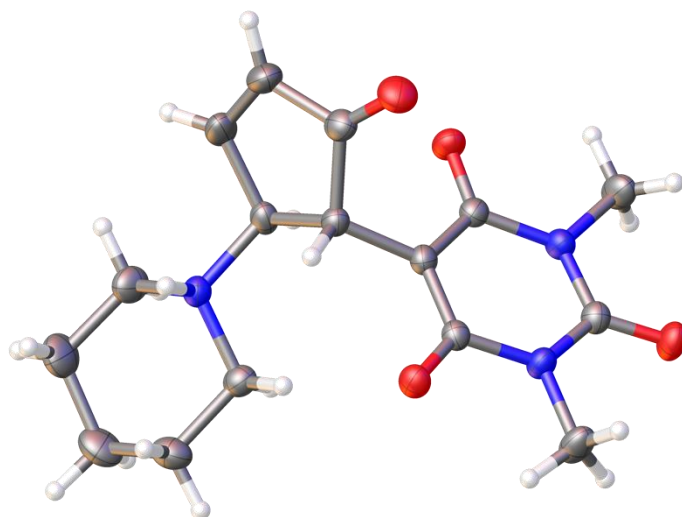
Appendix 2 – Crystal Structures from X-ray Diffraction



Appendix 2.1. Crystal structure of 5-[(2Z,4E)-2-hydroxy-5-(piperidin-1-yl)penta-2,4-dien-1-ylidene]-2,2-dimethyl-1,3-dioxane-4,6-dione (7).

Table 1 Crystal data and structure refinement for DASA 7.

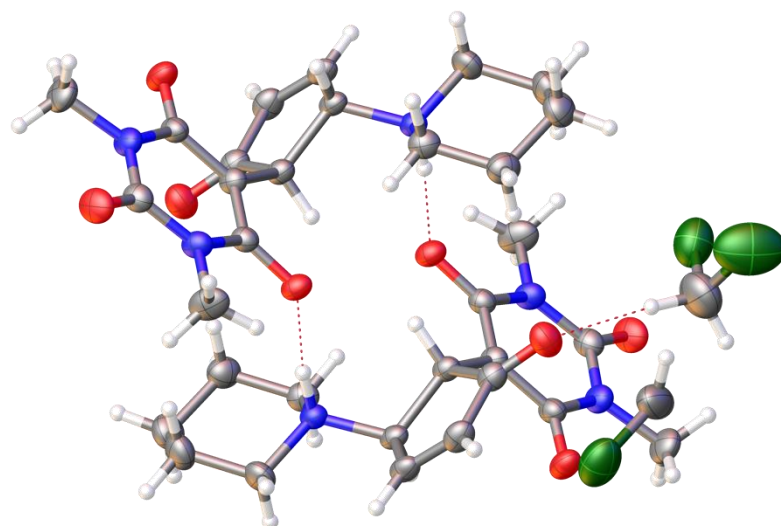
Identification code	Sc-Exp23_2-hjs1-ref
Empirical formula	C ₁₆ NO ₅
Formula weight	286.18
Temperature/K	199.99(10)
Crystal system	monoclinic
Space group	P2 ₁ /n
a/Å	6.26835(10)
b/Å	8.9482(2)
c/Å	27.3236(5)
α/°	90
β/°	90.2079(15)
γ/°	90
Volume/Å ³	1532.58(5)
Z	4
ρ _{calc} /cm ³	1.2402
μ/mm ⁻¹	0.817
F(000)	574.3
Crystal size/mm ³	0.187 × 0.143 × 0.038
Radiation	Cu Kα (λ = 1.54184)
2θ range for data collection/°	10.4 to 146.38
Index ranges	-7 ≤ h ≤ 7, -10 ≤ k ≤ 10, -33 ≤ l ≤ 33
Reflections collected	36131
Independent reflections	3049 [R _{int} = 0.0419, R _{sigma} = 0.0161]
Data/restraints/parameters	3049/0/88
Goodness-of-fit on F ²	3.667
Final R indexes [I ≥ 2σ (I)]	R ₁ = 0.1183, wR ₂ = 0.3904
Final R indexes [all data]	R ₁ = 0.1268, wR ₂ = 0.4100
Largest diff. peak/hole / e Å ⁻³	0.97/-0.75



Appendix 2.2. Crystal structure of 5-[(2Z,4E)-2-hydroxy-5-(piperidin-1-yl)penta-2,4-dien-1-ylidene]-1,3-dimethyl-1,3-diazinane-2,4,6-trione (8).

Table 2 Crystal data and structure refinement for **7** (un-solvated).

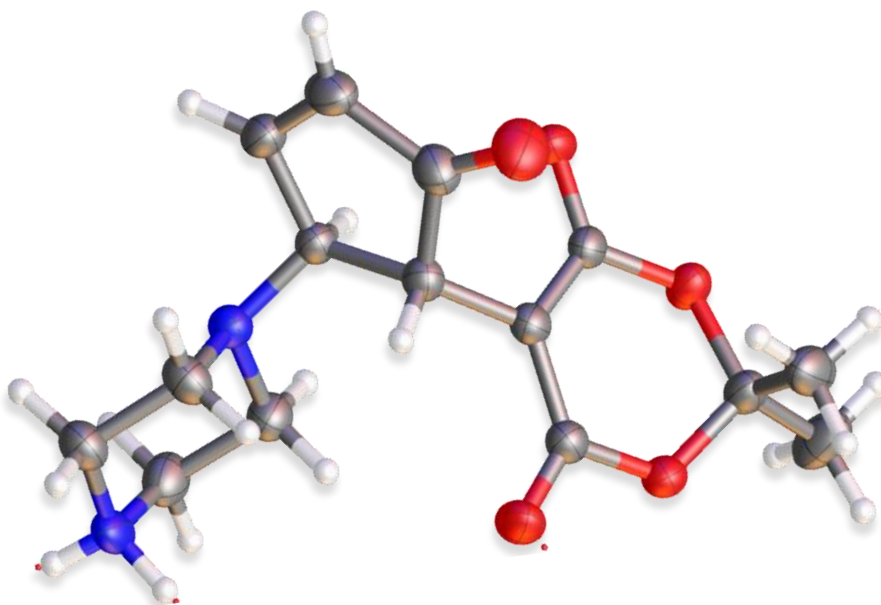
Identification code	Sc-Exp-26-6
Empirical formula	C ₁₇ H ₂₁ N ₂ O ₄
Formula weight	317.36
Temperature/K	200.00(10)
Crystal system	monoclinic
Space group	P2 ₁ /n
a/Å	10.27001(19)
b/Å	13.9357(2)
c/Å	12.0223(2)
α/°	90
β/°	114.759(2)
γ/°	90
Volume/Å ³	1562.46(6)
Z	4
ρ _{calc} /cm ³	1.349
μ/mm ⁻¹	0.795
F(000)	676.0
Radiation	CuKα (λ = 1.54184)
2θ range for data collection/°	9.55 to 145.598
Index ranges	-12 ≤ h ≤ 8, -17 ≤ k ≤ 15, -14 ≤ l ≤ 14
Reflections collected	6223
Independent reflections	3038 [R _{int} = 0.0221, R _{sigma} = 0.0288]
Data/restraints/parameters	3038/0/210
Goodness-of-fit on F ²	1.040
Final R indexes [I ≥ 2σ (I)]	R ₁ = 0.0407, wR ₂ = 0.1089
Final R indexes [all data]	R ₁ = 0.0458, wR ₂ = 0.1156
Largest diff. peak/hole / e Å ⁻³	0.26/-0.22



Appendix 2.3. Crystal structure of DCM solvate of 5-[(2Z,4E)-2-hydroxy-5-(piperidin-1-yl)penta-2,4-dien-1-ylidene]-1,3-dimethyl-1,3-diazinane-2,4,6-trione (8).

Table 3 Crystal data and structure refinement for **7** (DCM solvate).

Identification code	ov_SC-Exp26-1
Empirical formula	C ₁₉ H ₂₇ N ₁₀ O ₄ Cl _{0.13}
Formula weight	463.94
Temperature/K	293(2)
Crystal system	monoclinic
Space group	C2/c
a/Å	18.4548(6)
b/Å	10.3999(3)
c/Å	22.0770(7)
α/°	90
β/°	99.120(3)
γ/°	90
Volume/Å ³	4183.6(2)
Z	8
ρ _{calc} /cm ³	1.473
μ/mm ⁻¹	1.042
F(000)	1961.0
Radiation	CuKα (λ = 1.54184)
2θ range for data collection/°	8.112 to 145.72
Index ranges	-22 ≤ h ≤ 18, -12 ≤ k ≤ 6, -20 ≤ l ≤ 27
Reflections collected	7847
Independent reflections	4053 [R _{int} = 0.0296, R _{sigma} = 0.0384]
Data/restraints/parameters	4053/0/255
Goodness-of-fit on F ²	1.035
Final R indexes [I ≥ 2σ (I)]	R ₁ = 0.0592, wR ₂ = 0.1545
Final R indexes [all data]	R ₁ = 0.0732, wR ₂ = 0.1644
Largest diff. peak/hole / e Å ⁻³	0.67/-0.73

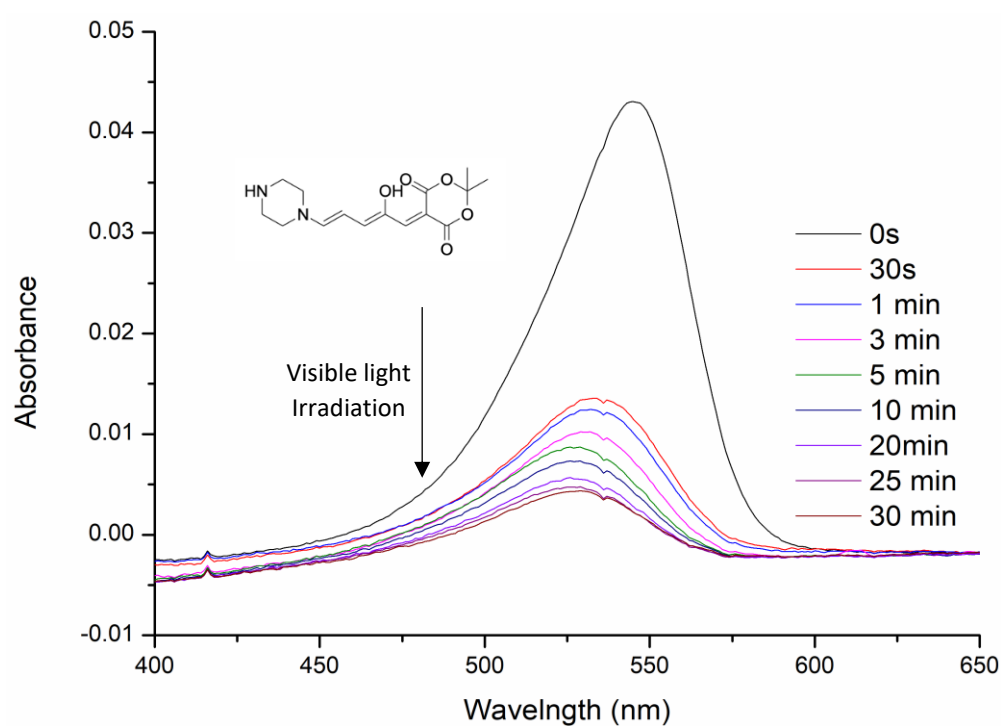


Appendix 2.4 Crystal structure of 5-[(2Z,4E)-2-hydroxy-5-(piperazin-1-yl)penta-2,4-dien-1-ylidene]-2,2-dimethyl-1,3-dioxane-4,6-dione (5), crystallised from water.

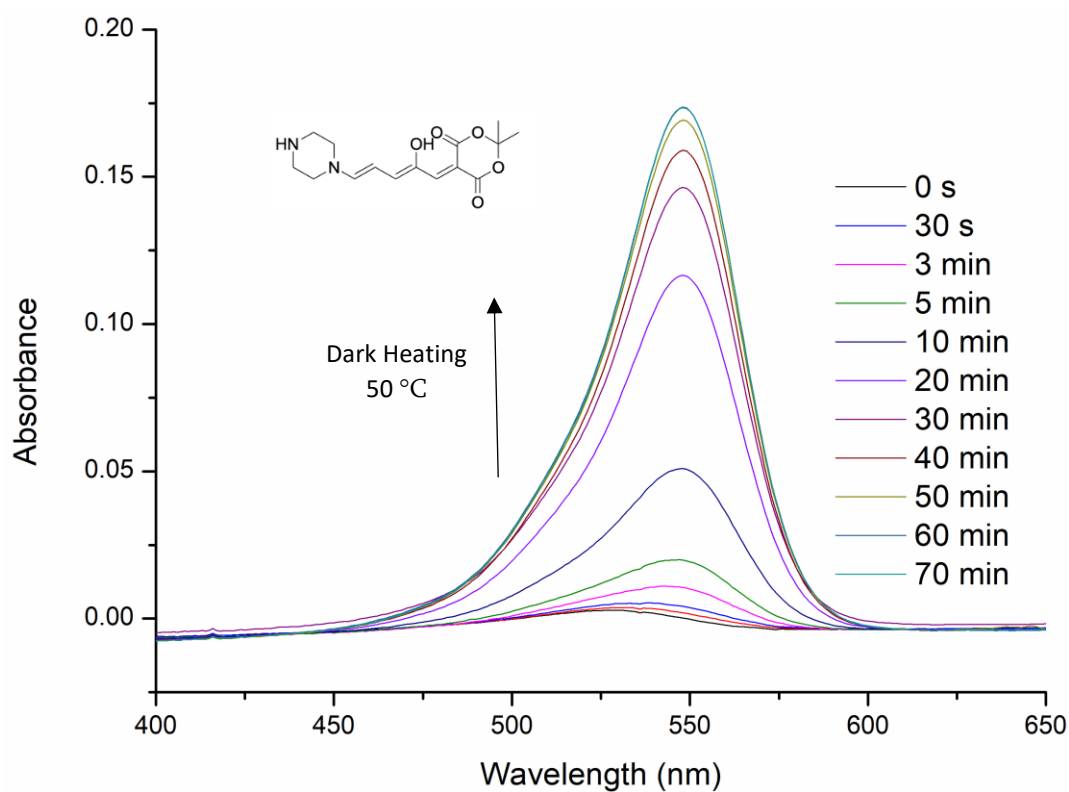
Table 4 Crystal data and structure refinement for 5.

Identification code	SWC_H6_1_mI_hjs1-ref
Empirical formula	$C_{30}H_{46}N_4O_{13.67}$
Formula weight	681.37
Temperature/K	199.99(10)
Crystal system	monoclinic
Space group	I2/a
a/Å	18.9604(2)
b/Å	14.24355(17)
c/Å	25.8806(3)
$\alpha/^\circ$	90
$\beta/^\circ$	90.0229(12)
$\gamma/^\circ$	90
Volume/Å ³	6989.40(15)
Z	8
$\rho_{\text{calc}}/\text{cm}^3$	1.295
μ/mm^{-1}	0.867
F(000)	2907.0
Crystal size/mm ³	0.216 × 0.058 × 0.052
Radiation	CuK α ($\lambda = 1.54184$)
2 θ range for data collection/ $^\circ$	7.084 to 146.778
Index ranges	-23 ≤ h ≤ 14, -17 ≤ k ≤ 17, -25 ≤ l ≤ 31
Reflections collected	25756
Independent reflections	6928 [$R_{\text{int}} = 0.0347$, $R_{\text{sigma}} = 0.0272$]
Data/restraints/parameters	6928/0/459
Goodness-of-fit on F ²	1.054
Final R indexes [$I \geq 2\sigma(I)$]	$R_1 = 0.0506$, $wR_2 = 0.1382$
Final R indexes [all data]	$R_1 = 0.0534$, $wR_2 = 0.1423$
Largest diff. peak/hole / e Å ⁻³	0.95/-0.22

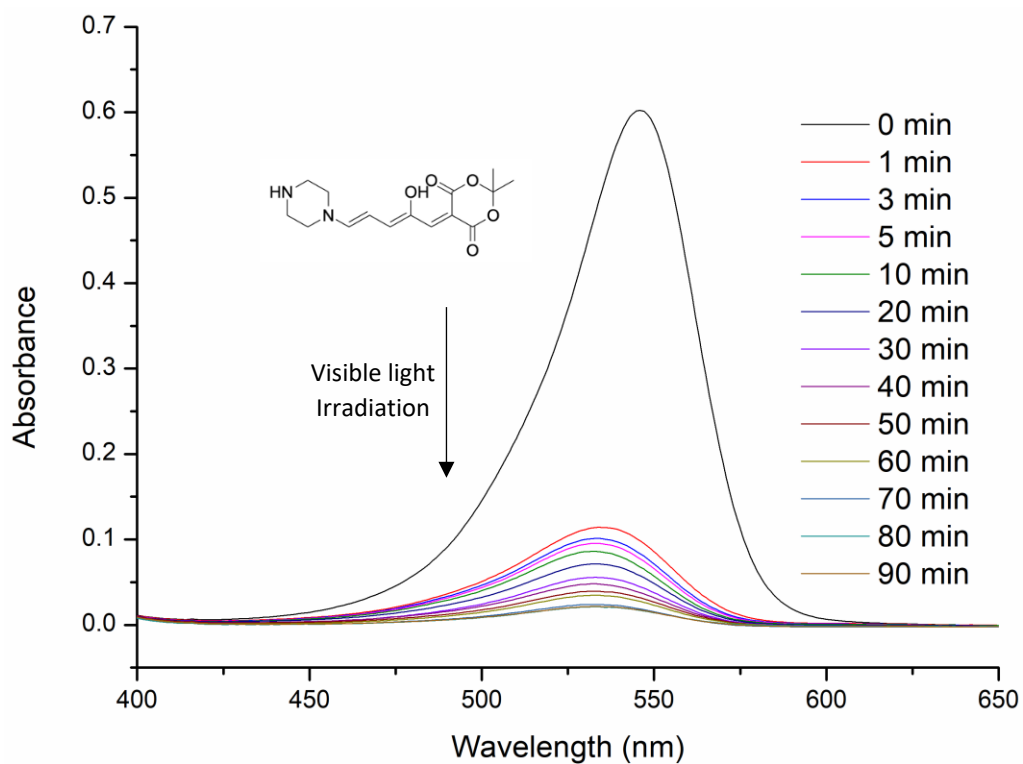
Appendix 3 – UV-Vis Spectroscopy Spectra



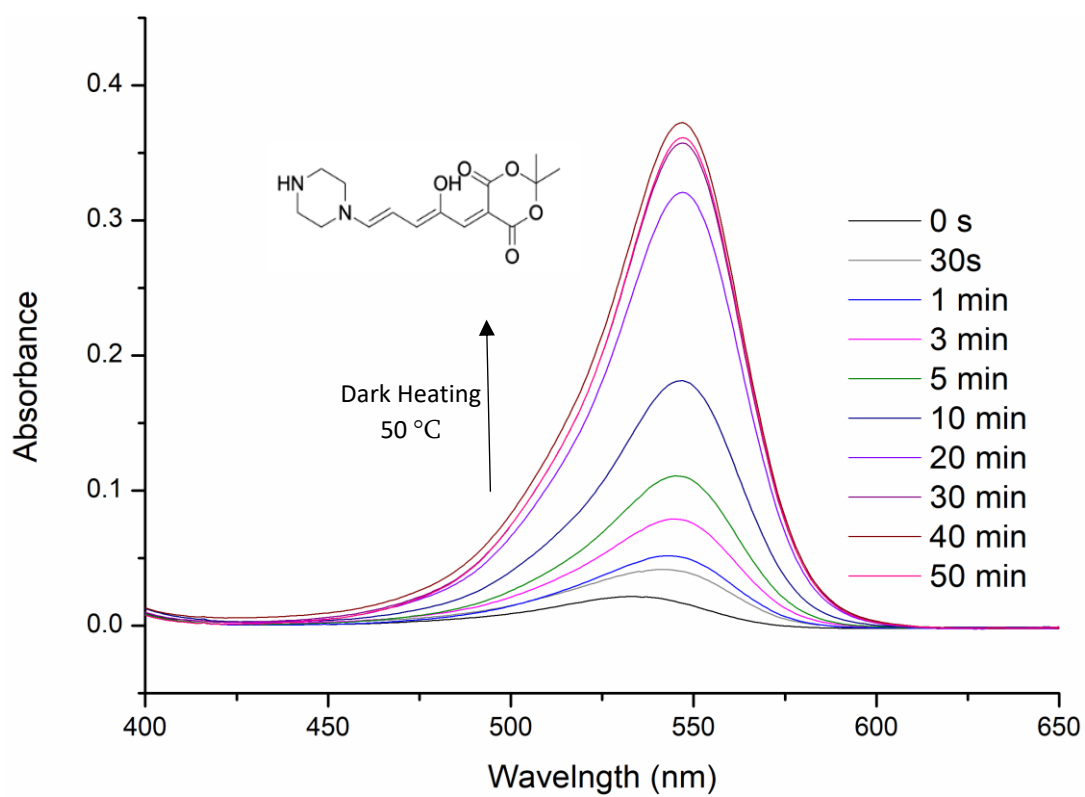
Appendix 3.1. UV-Vis spectrum of a 1×10^{-5} M solution of 5 in chlorobenzene



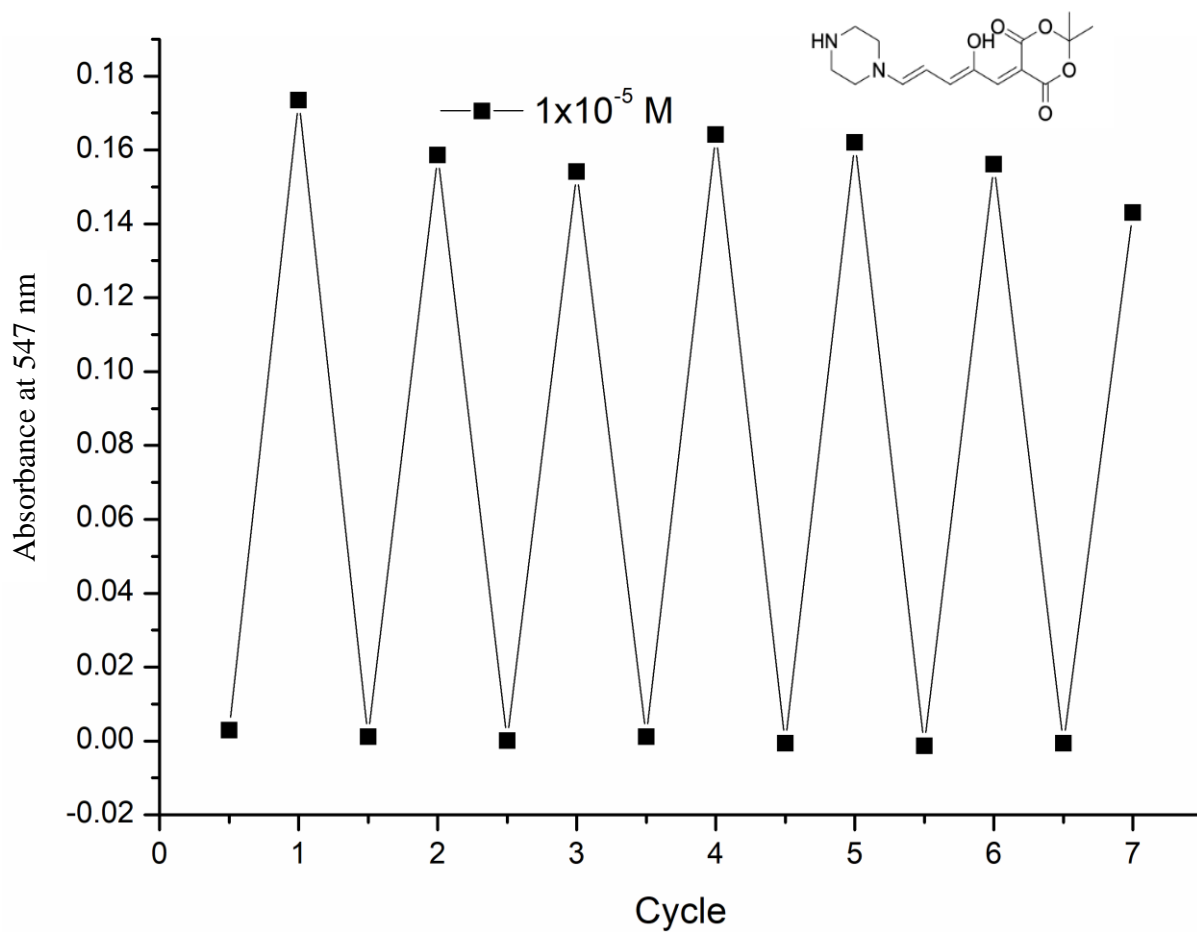
Appendix 3.2. UV-Vis spectrum of a 1×10^{-5} M solution of 5 in chlorobenzene



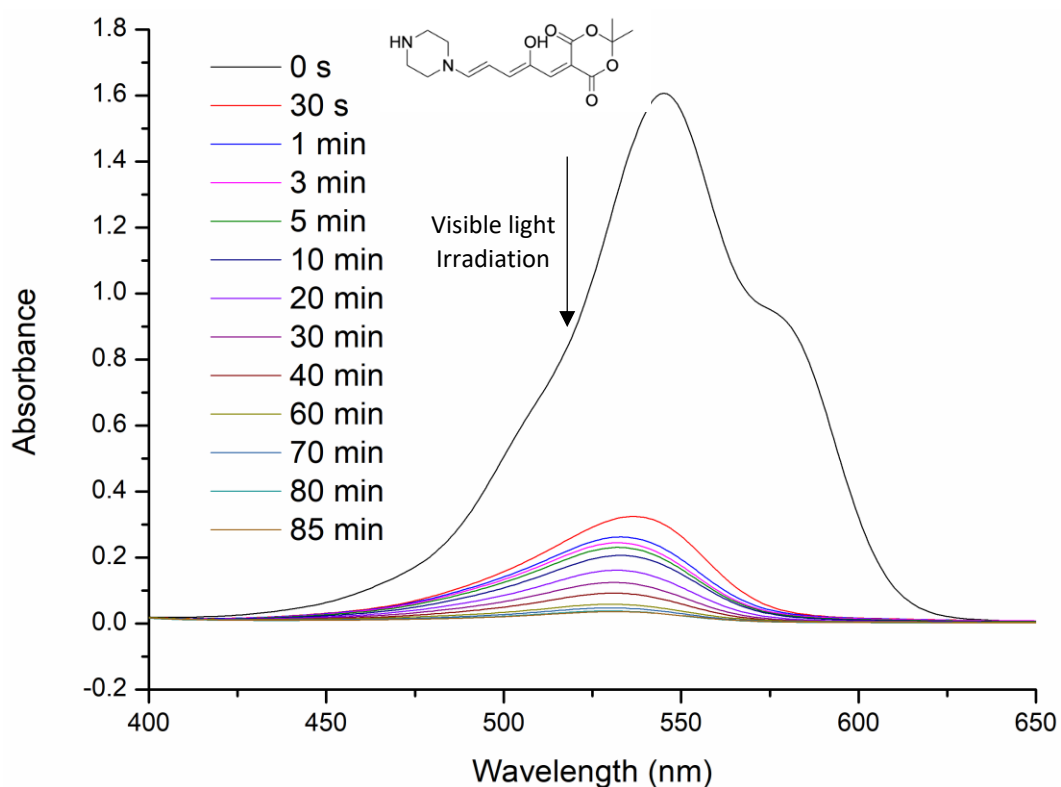
Appendix 3.3. UV-Vis spectrum of a 1×10^{-4} M solution of 5 in chlorobenzene



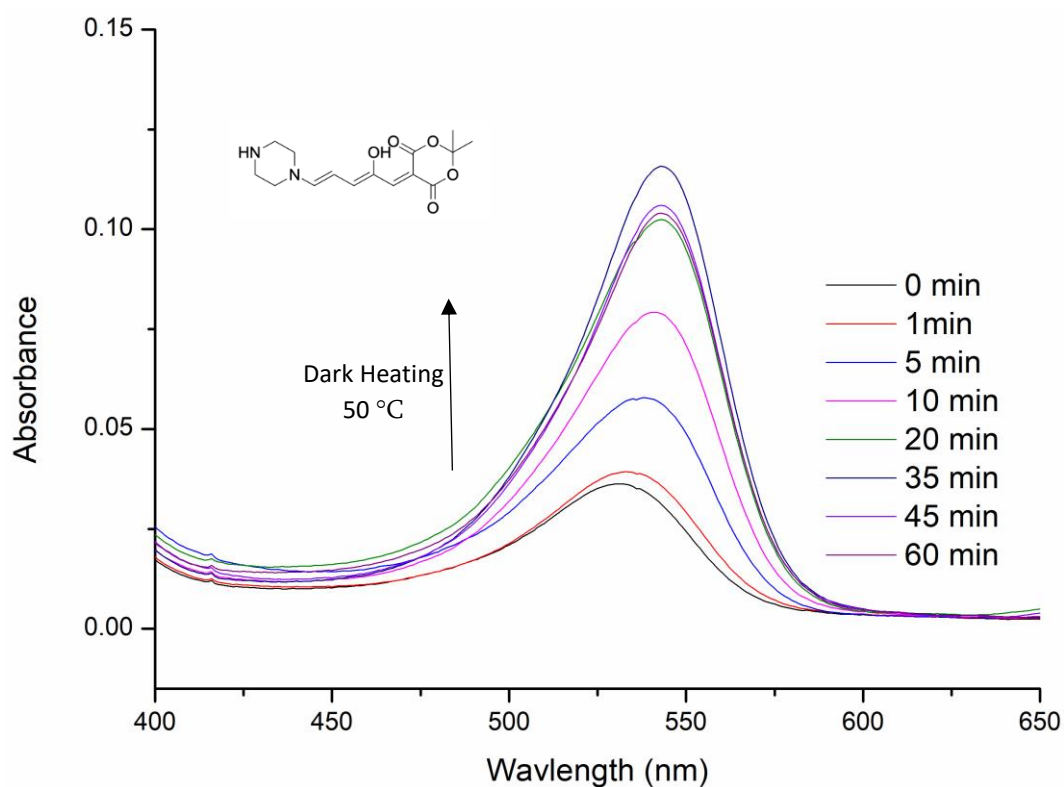
Appendix 3.4. UV-Vis spectrum of a 1×10^{-4} M solution of 5 in chlorobenzene



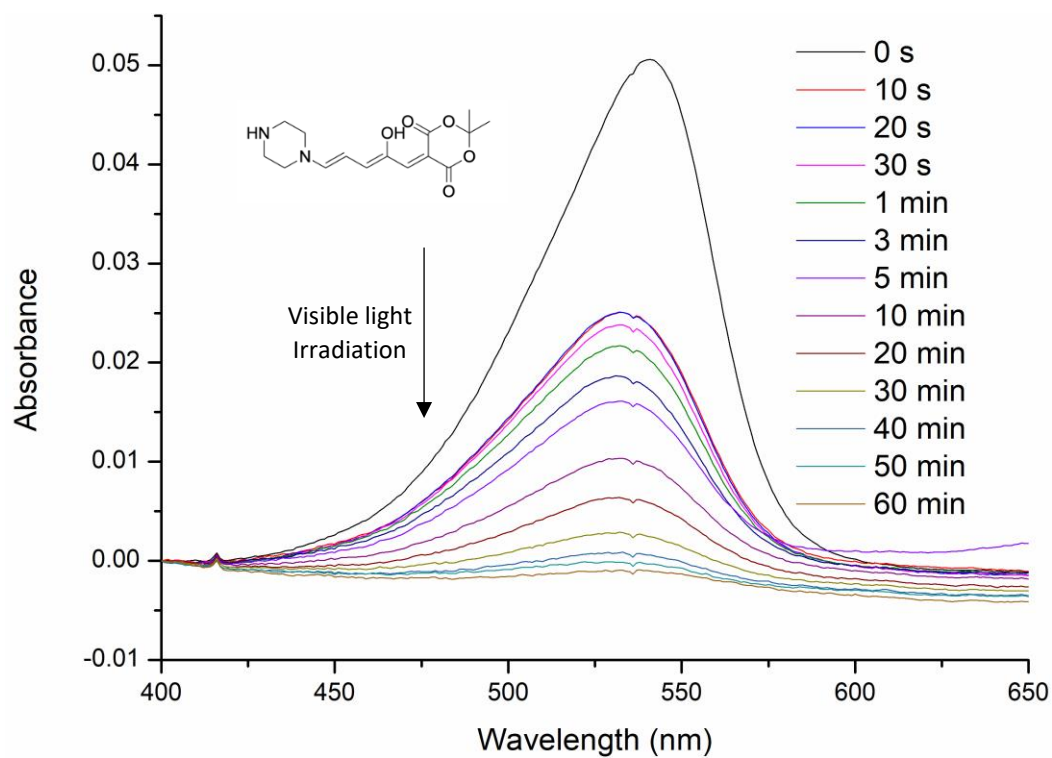
Appendix 3.5. UV-Vis data of a 1×10^{-5} M solution of 5 in chlorobenzene performing multiple switching cycles.



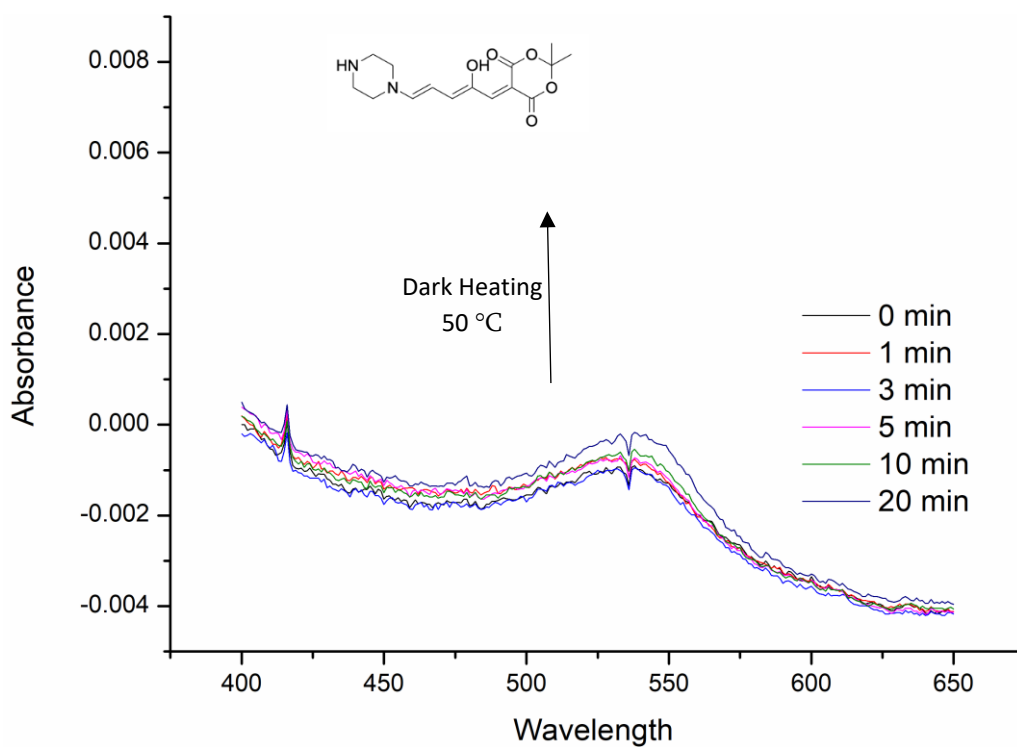
Appendix 3.6. UV-Vis spectrum of a 1×10^{-4} M solution of 5 in Toluene.



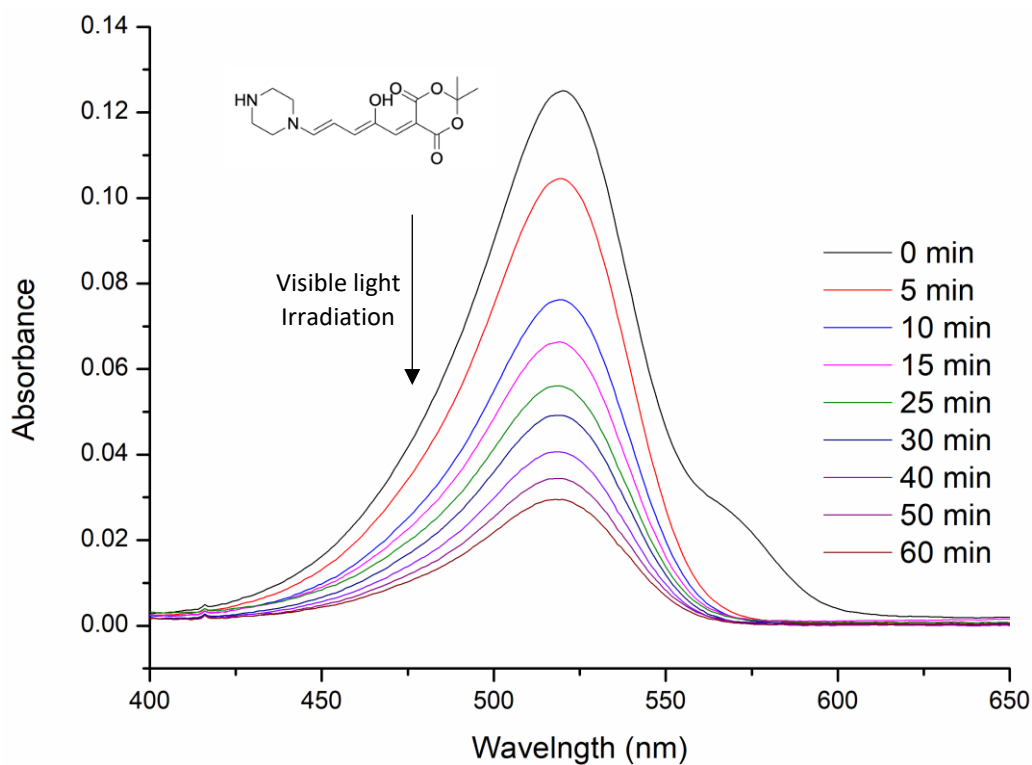
Appendix 3.7. UV-Vis spectrum of a 1×10^{-4} M solution of 5 in Toluene.



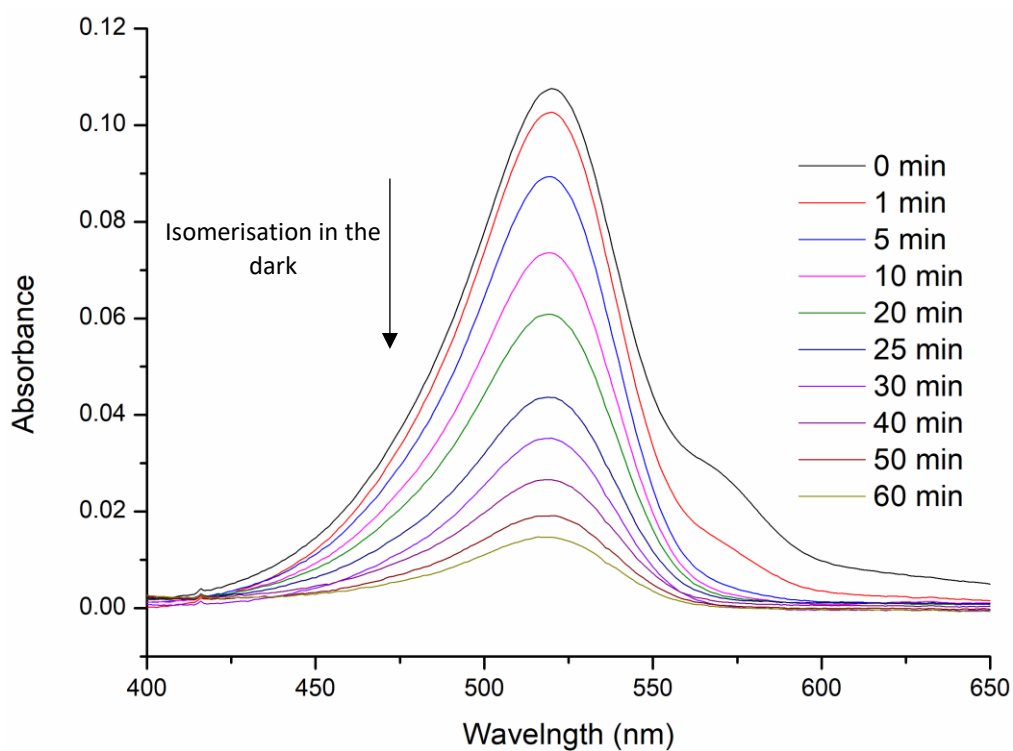
Appendix 3.8. UV-Vis spectrum of a 1×10^{-5} M solution of 5 in Toluene.



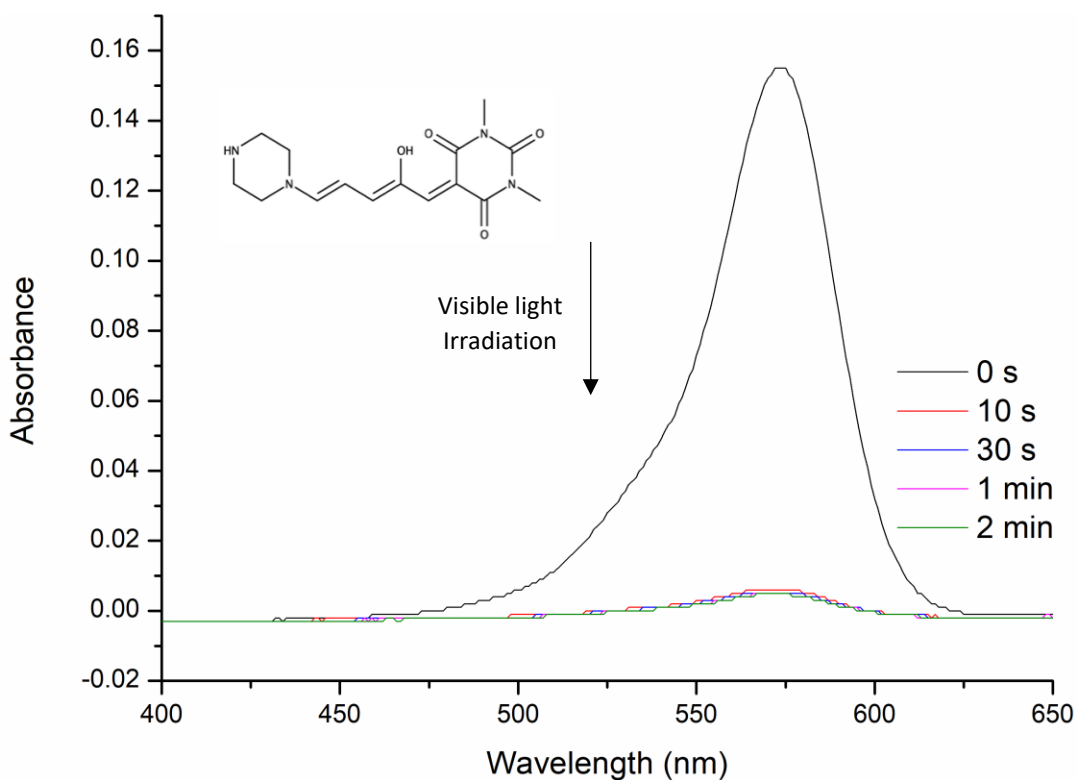
Appendix 3.9. UV-Vis spectrum of a 1×10^{-5} M solution of 5 in Toluene.



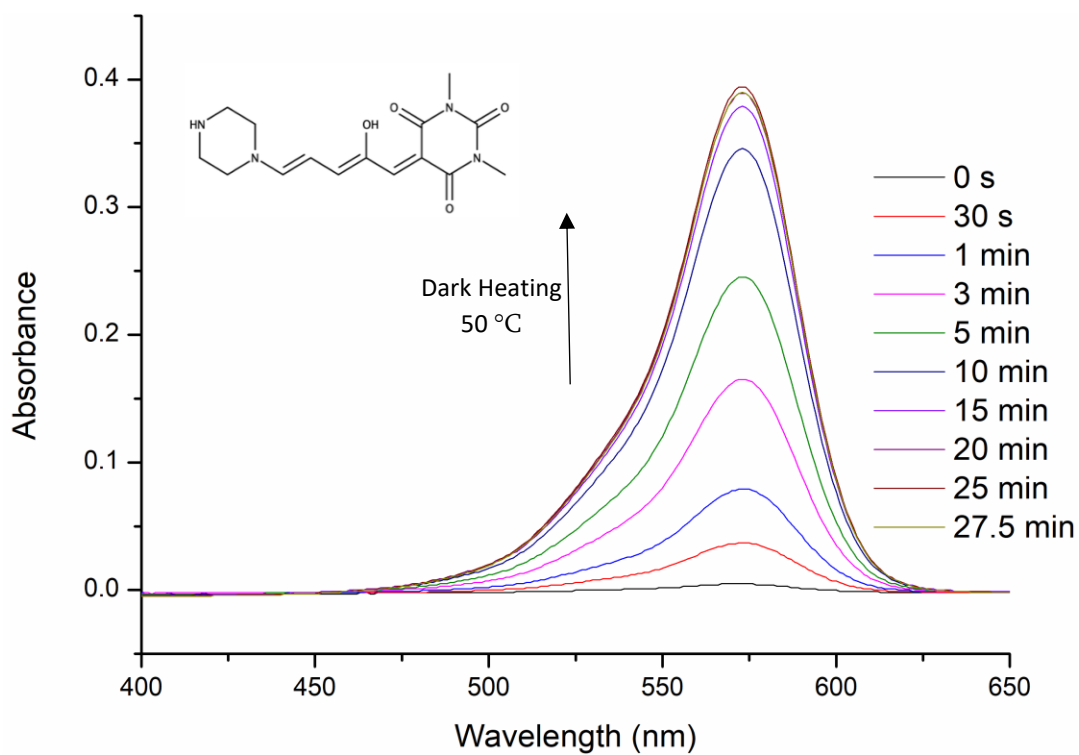
Appendix 3.10. UV-Vis spectrum of a 1×10^{-5} M solution of 5 in Methanol.



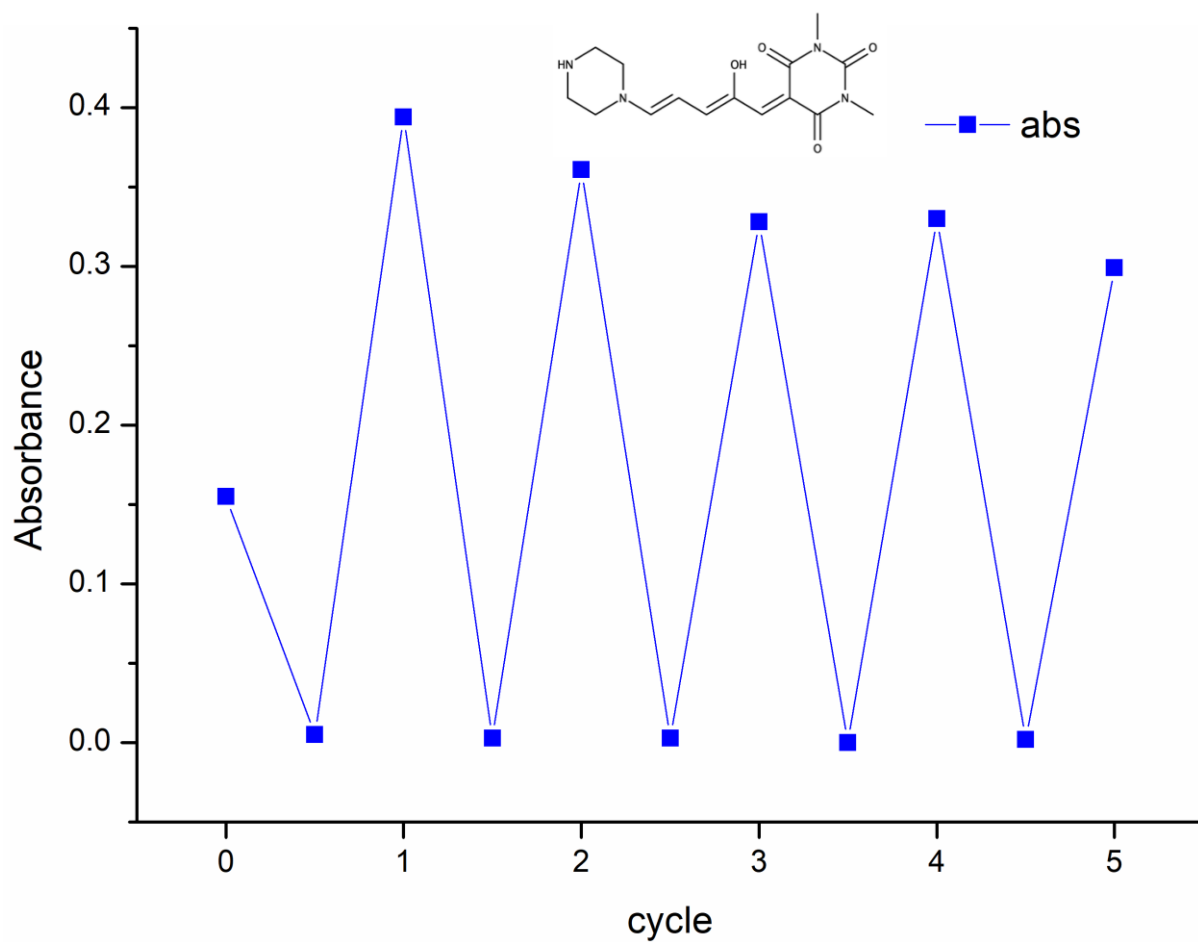
Appendix 3.11. UV-Vis spectrum of a 1×10^{-5} M solution of 5 in Methanol.



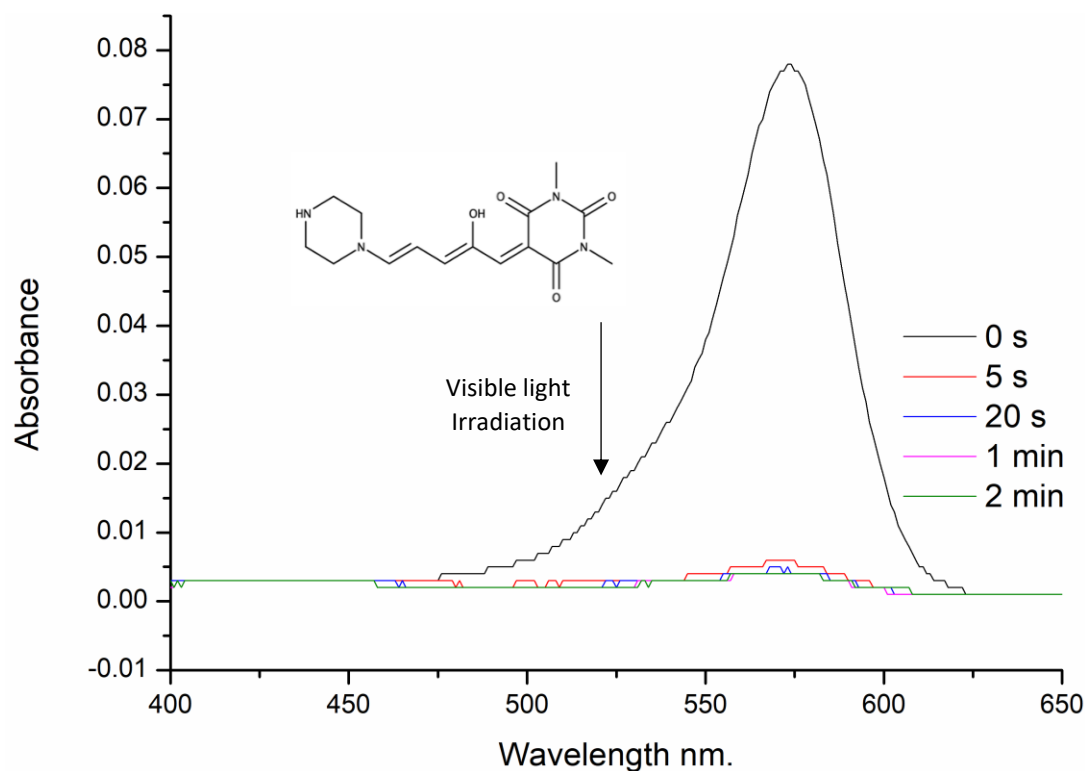
Appendix 3.12. UV-Vis spectrum of a 1×10^{-5} M solution of 6 in chlorobenzene. Using a 1cm cuvette.



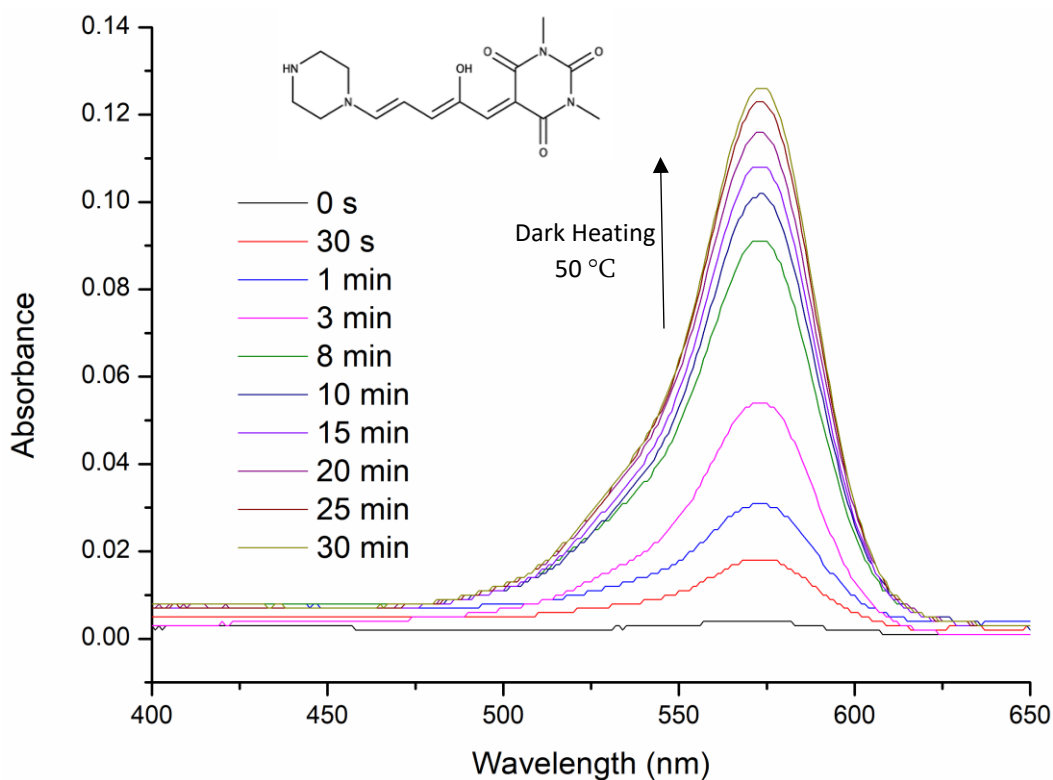
Appendix 3.13. UV-Vis spectrum of a 1×10^{-5} M solution of 6 in chlorobenzene.



Appendix 3.14. UV-Vis data of a 1×10^{-5} M solution of 5 in chlorobenzene performing multiple switching cycles. Cycle time can be inferred from the UV-Vis absorption spectra in appendix 3.12 and 3.13 which show the time to isomerise in both directions.

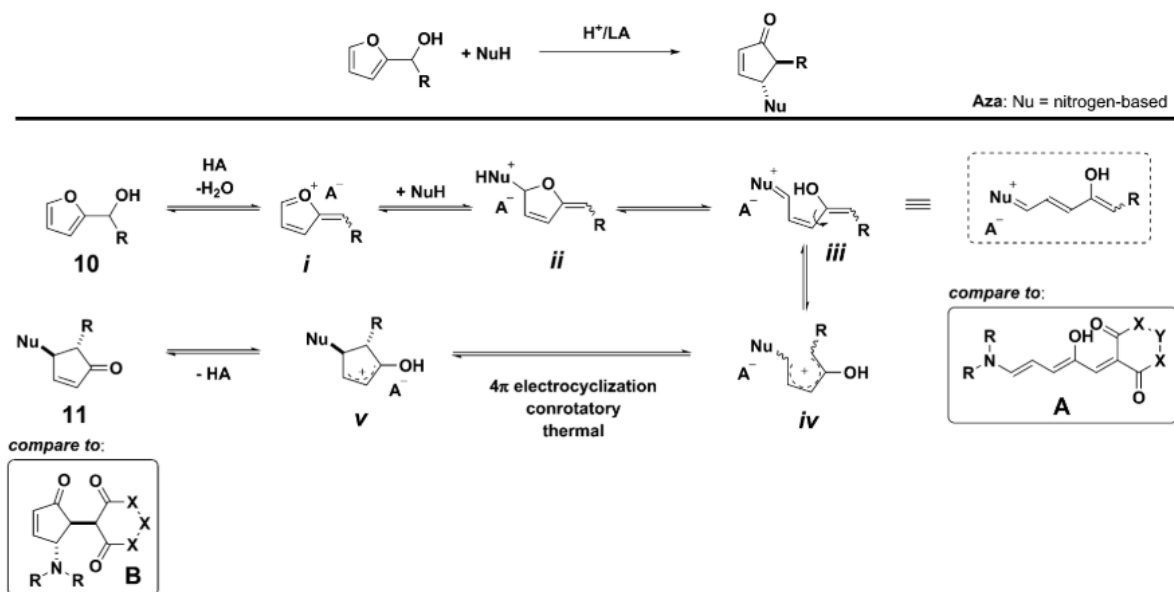


Appendix 3.15. UV-Vis spectrum of a 1×10^{-4} M solution of 6 in chlorobenzene. In a 1 mm cuvette.

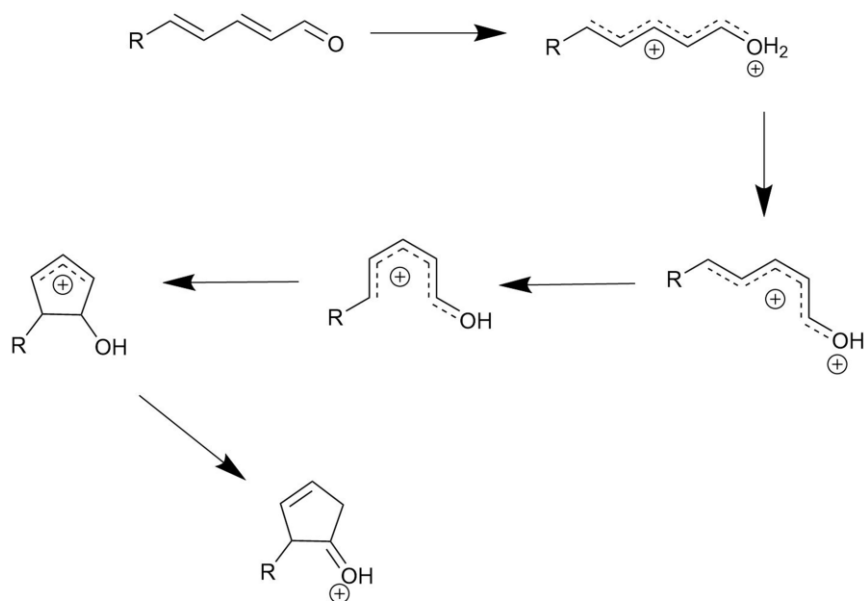


Appendix 3.15. UV-Vis spectrum of a 1×10^{-4} M solution of 6 in chlorobenzene. In a 1 mm cuvette.

The (Aza-)Piancatelli Rearrangement



Appendix 4.1 (Aza-)Piancatelli Rearrangement, Reproduced from ref. 33. with permission from The Royal Society of Chemistry



Appendix 4.2 Schematic representation of the Iso-Nazarov reaction